Determination of the appropriate dosage of Adipose tissue-derived Stem Cell secretome for Spinal Cord Injury Regenerative Medicine Approaches

Tiago André Moreira Gomes

Novembro | 2020

Universidade do Minho
Escola de Medicina

Tiago André Moreira Gomes

Determination of the appropriate dosage of Adipose tissue-derived Stem Cell secretome for Spinal Cord Injury Regenerative Medicine Approaches

Novembro de 2020

Universidade do Minho
Escola de Medicina

Tiago André Moreira Gomes

Determination of the appropriate dosage of Adipose tissue-derived Stem Cell secretome for Spinal Cord Injury Regenerative Medicine Approaches

Dissertação de Mestrado em Ciências da Saúde

Trabalho efetuado sob a orientação do

Doutor António José Braga Osório Gomes Salgado

E do

Doutor Eduardo Domingos Correia Gomes

Novembro de 2020

ACKNOWLEDGMENTS

Aos meus orientadores, António Salgado e Eduardo Gomes, agradeço por terem puxado por mim, pela orientação científica que me têm fornecido desde o início deste projeto e por terem demonstrado confiança nas minhas capacidades. Foi um enorme prazer aprender e crescer convosco!

A todos os membros da Tó Team, agradeço por terem contribuído para o avanço deste projeto. Foi fantástico trabalhar com um grupo multidisciplinar com um enorme espírito de equipa.

Aos meus amigos do lab (Gi, Ju, João e Bruna) e às minhas amigas (Joana, Sofia e Carla), agradeço pelo apoio constante, pelas gargalhadas e pela partilha de momentos inesquecíveis.

À minha família, aos meus pais e à minha irmã, agradeço pelo amor incondicional, por terem acreditado sempre em mim e por me terem ajudado a atingir os meus objetivos da melhor forma.

Ao Doutor Nuno Sousa, Presidente da Escola de Medicina, Doutor Jorge Correia-Pinto, Presidente do ICVS, ao Doutor João Bessa, Coordenador do Domínio de Neurociências, e à Doutora Patrícia Maciel, Diretora do Mestrado em Ciências da Saúde, agradeço pelo apoio institucional.

The work presented in this thesis was performed in the Life and Health Sciences Research Institute (ICVS), University of Minho. Financial support was provided by grants from Prémios Santa Casa Neurociências - Prize Melo e Castro for Spinal Cord Injury Research (MC-04/17); PORTUGAL 2020 Partnership Agreement, through the European Regional Development Fund (ERDF) FEDER, through the Competitiveness Internationalization Operational Programme (POCI), and by National funds, through the Foundation for Science and Technology (FCT), under the scope of the projects POCI-01-0145-FEDER-007038; TUBITAK/0007/2014; PTDC/DTP-FTO/5109/2014; POCI-01-0145-FEDER-029206; POCI-01-0145-FEDER-031392; PTDC/MED-NEU/31417/2017 and NORTE-01-0145-FEDER-029968. ICVS Scientific Microscopy Platform, member of the national infrastructure PPBI - Portuguese Platform of Bioimaging (PPBI-POCI-01-0145-FEDER-022122; by National funds, through the Foundation for Science and Technology (FCT) - project UIDB/50026/2020 and UIDP/50026/2020; and by the projects NORTE-01-0145-FEDER-000013 and NORTE-01-0145-FEDER-000023, supported by Norte Portugal Regional Operational Programme (NORTE 2020), under the PORTUGAL 2020 Partnership Agreement, through the European Regional Development Fund (ERDF).

STATEMENT OF INTEGRITY

I hereby declare having conducted this academic work with integrity. I confirm that I have not used plagiarism or any form of undue use of information or falsification of results along the process leading to its elaboration.

I further declare that I have fully acknowledged the Code of Ethical Conduct of the University of Minho.

RESUMO

A lesão medular traumática é uma condição neurológica que afeta várias funções corporais do paciente. Após a lesão, um conjunto de eventos celulares é iniciado envolvendo respostas imunológicas, rutura vascular e alterações neuronais. Atualmente, não existem tratamentos eficazes na regeneração do tecido e recuperação locomotora. Por este motivo, várias estratégias que visem os mecanismos subjacentes à fisiopatologia da lesão medular ou que promovam a neurorregeneração e a neuroprotecção têm sido exploradas. Terapias que utilizem produtos secretados pelas células estaminais mesenquimais têm revelado ser bastante promissoras no tratamento de lesões medulares. No caso das células estaminais derivadas do tecido adiposo (ASCs), estas demonstraram exercer efeitos benéficos no sistema nervoso central através da secreção de fatores e vesículas extracelulares, que, no conjunto, se designam como secretoma. Apesar do potencial do secretoma das ASCs em contexto de lesões medulares já ser conhecido, a concentração necessária para induzir um efeito terapêutico é desconhecida. Com o fim de clarificar esta questão, este trabalho teve como objetivo analisar a eficácia terapêutica de diferentes concentrações de secretoma das ASCs para o tratamento de lesões medulares. Em estudos *in vitro*, os diferentes tratamentos não pareceram afetar o fenótipo de células da microglia, através da análise da expressão dos genes *IL-6* e *IL-4*. Em murganhos com lesão medular, diferentes concentrações (1x, 25x e 50x) de secretoma de ASCs foram testadas, induzindo uma melhoria da função locomotora dos membros inferiores. Apesar disso, os diferentes tratamentos não levaram a nenhuma alteração significativa da coordenação motora e função sensorial. Por fim, a análise imunohistoquímica para marcadores de inflamação e crescimento axonal não mostrou nenhuma alteração histológica significativa em resposta aos diferentes tratamentos utilizados. No entanto, com o aumento das concentrações de secretoma de ASCs, verificou-se uma possível diminuição da microglia ativada. Esta tendência foi confirmada pela análise Sholl de microglia, onde as células apresentaram uma menor complexidade em animais tratados com secretomas 25x e 50x, indicando uma maior presença de células não ativadas nos mesmos. No geral, os secretomas concentrados a 25x e a 50x parecem modular a inflamação mediada pela microglia ativada, o que pode explicar a recuperação locomotora dos animais tratados com dosagens mais elevadas. Este estudo destaca o potencial dos secretomas 25x e 50x para tratar a lesão medular.

Palavras-chave: Células estaminais derivadas do tecido adiposo; Secretoma; Lesão medular; Neuroinflamação.

ABSTRACT

Traumatic spinal cord injury (SCI) is a neurological condition that leads to impairments of several body functions. Following the injury, a cascade of biological events is initiated involving immunological responses, vascular disruption and neuronal alterations. Currently, treatments for this condition have shown to be inefficient for tissue repair and functional recovery. Thus, different strategies that target the mechanisms underlying the pathophysiology of SCI, promoting neuroregeneration and neuroprotection, have been explored. Considering this, cell free-based therapies employing mesenchymal stem cell (MSC)-secreted products emerge as a novel therapy to treat SCI. MSCs, and among them Adipose tissue-derived Stem Cells (ASCs), have shown to exert beneficial effects on the central nervous system through secreted soluble factors and small extracellular vesicles , commonly referred as secretome. Although the potential of ASC secretome in a SCI context is already known, its therapeutic concentration is still to be determined. In order to bridge this gap, this work aimed to analyze the therapeutic efficacy of different concentrations of ASC secretome for SCI repair. Different secretome concentrations seem to not affect microglial cell phenotype *in vitro*, as analyzed through *IL-6* and *IL-4* gene expression. In SCI mice, different concentrations (1x, 25x and 50x) of ASC secretome were tested, revealing an improvement of the locomotor function of the hindlimbs. In other functional readouts, no major alterations were found, including motor coordination, and sensation, namely perceived pain. Furthermore, immunohistochemistry analysis for several markers of inflammation and axonal sprouting showed that no histological changes occurred in response to different treatments. However, higher concentrations of ASC secretome appeared to induce a reduction of activated microglia. This trend was confirmed by Sholl analysis, where microglial cells from 25x and 50x concentrated secretome-treated animals presented lower complexity, indicating a higher presence of non-activated cells. Overall, 25x and 50x secretomes seem to modulate inflammation mediated by activated microglia, which can partially explain the locomotor recovery of animals treated with higher dosages. This study highlights the potential of 25x and 50x secretomes to treat SCI.

Keywords: Adipose tissue-derived stem cells; Secretome; Spinal cord injury; Neuroinflammation.

TABLE OF CONTENTS

ABBREVIATIONS

A	
ASCs	Adipose tissue-derived stem cells
B	
BB	Beam Balance
BDNF	Brain-derived neurotrophic factor
BM-MSCs	Bone marrow mesenchymal stem cells
BMS	Basso Mouse Scale
BSCB	Blood-spinal cord barrier
C	
cDNA	Complementary DNA
CM	Conditioned medium
CNS	Central nervous system
D	
DAPI	4′,6-Diamidino-2-phenylindole dihydrochloride
DMEM-F12	Dulbecco's Modified Eagle Medium, Nutrient Mixture F12
DNA	Deoxyribonucleic acid
Dpi	Days post-injury
DRG	Dorsal Root Ganglia
E	
EDTA	Ethylenediaminetetraacetic acid
ELISA	Enzyme-linked immunosorbent assay
ESCs	Embryonic stem cells
F	
FBS	Fetal Bovine Serum

FCS	Fetal Calf Serum
G	
GFAP	Glial fibrillary acidic protein
H	
HUCMC	Human umbilical cord matrix cell
I	
Iba1	Ionized calcium binding adaptor molecule 1
IFN-γ	Interferon-gamma
IHC	Immunohistochemistry
IL	Interleukin
iPSCs	Induced pluripotent stem cells
iPSC-NPC	Neural stem cells derived from iPSCs
IV	Intravenous
M	
MEM	Minimum Essential Medium
mRNA	Messenger ribonucleic acid
MSCs	Mesenchymal stem cells
N	
NbA	Neurobasal A
O	
OECs	Olfactory ensheathing cells
OF	Open Field
OPCs	Oligodendrocyte progenitor cells
P	
PBS	Phosphate buffered saline
Pen-Step	Penicillin-Streptomycin

PFA	Paraformaldehyde
R	
RT	Room temperature
qPCR	Quantitative polymerase chain reaction
RT-qPCR	Quantitative reverse transcription-polymerase chain reaction
S	
SCs	Schwann cells
SCI	Spinal cord injury
SD	Standard deviation
SEM	Standard error of the mean
SNT	Simple neurite tracer
T	
TGF-β	Transforming growth factor beta
TNF-α	Tumor necrosis factor alpha
V	
VF	Von Frey

Symbols and units	
°C	Degrees Celsius
h	Hours
kDa	Kilodaltons
%	Percentage
rpm	Rotations per minute
η^2	Eta squared
η^2_p	Partial eta squared

d	Cohen's d
Ca^{2+}	Calcium ion
CO_2	Carbon Dioxide
Mg^{2+}	Magnesium ion
NaCl	Sodium chloride
mM	Millimolar
cm^2	Square centimeter
cm	Centimeter
mm	Millimeter
μm	Micrometer
nm	Nanometer
L	Liter
mL	Milliliter
μL	Microliter
kg	Kilogram
mg	Milligram
μg	Microgram
ng	Nanogram
$\overline{X}$	Mean

LIST OF TABLES

LIST OF FIGURES

Chapter I - INTRODUCTION

1. Nervous System

In humans, a complex network of neural cells, named nervous system, is responsible for perceiving sensations and controlling actions and decisions. These unique abilities of the nervous system are possible due to the presence of two major groups of cells: neurons and glial cells. Neurons are responsible to receive and transmit the information, while glial cells perform several important roles, including nurturing (more specifically astrocytes), insulating axons (oligodendrocytes), among others (Bear et al., 2015). Another specific class of glial cells, microglia, stands out for being the first line of defense against lesions or pathogens invasion. In normal physiological conditions, microglia are in a surveillance mode, protecting the nervous system and maintaining the integrity of the tissue (Okada, 2016). However, when the nervous system is the target of aggression (for example, trauma or infection), microglia are activated (Boche et al., 2013). The conversion of non-activated to activated state of microglia involves a set of morphological and molecular transformations, which include mainly the upregulation of surface molecules, processes shortening, expansion of the soma, acquisition of phagocytosis of the debris, among others (Gomes-Leal, 2012).

1.1. Central Nervous System: Brain and Spinal Cord

The brain is a sophisticated organ composed of three parts (cerebrum, cerebellum and brain stem), which together control body functions and all organs. The cerebrum is in charge of sensing external stimuli and controlling motor function. The cerebellum has a profound impact on motor coordination, posture and balance. Finally, the brainstem is an indispensable structure involved in such fundamental functions, including breathing and consciousness (Bear et al., 2015).

However, how does the brain perceive and respond to an external stimulus in a very precise way? The brain is connected to different levels of the body through a neural bridge called the spinal cord. The latter displays a tube-like shape separated by two heterogeneous regions: 1 – the grey matter, where there is a concentration of interneurons, efferent neurons, afferent neurons, and glial cells; 2 – the white matter, which contains essentially myelinated axons functioning as descending and ascending pathways responsible for conducting nervous signals (Silva et al., 2014).

Thirty-one spinal nerves diverge along the spinal cord with distinct associated responsibilities. In the rostral region of the spinal cord, cervical nerves start to bifurcate for commanding vital functions (breathing and heart rate control) and capturing sensory information from the head, neck and upper limb. Thoracic spinal nerves are the next bundle of divergent fibers responsible for the control of the

chest and abdominal walls. Next, there are lumbar spinal nerves essential for lower limb (hip and leg) movement. Finally, sacral nerves, the most caudal ones, are responsible for bladder and bowel function, followed by coccygeal nerves involved in the skin supply of the coccyx region [Figure 1, (Rupp, 2020; Silva et al., 2014)].

With these pathways, the organ itself conducts the sensory information received by peripheral afferent nerves to the brain and transmits the motor input through efferent nerves (Silva et al., 2014). Knowing this, one can imagine the catastrophic consequences at cellular, molecular and physical level, when this neuronal circuit is destroyed by an injury in the spinal cord.

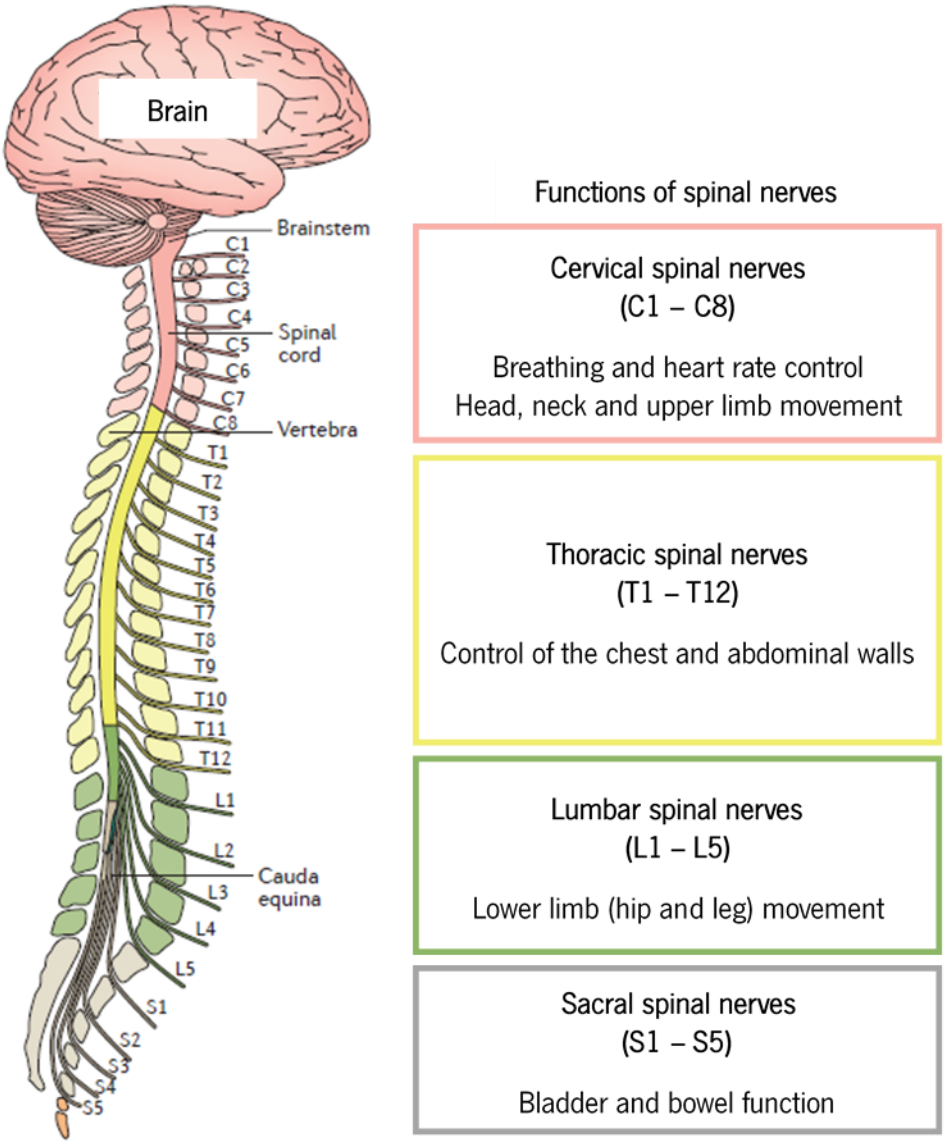

Figure 1. Representation of the central nervous system (brain and spinal cord). Organization of spinal nerves and their functions. Information and image adapted from Ahuja et al. (2017) and Rupp (2020).

1.2. Epidemiological panorama of spinal cord injury: Prevalence, incidence and etiology

An injury in the spinal cord initiates cellular and molecular reactions that may lead to the impairment of motor and sensory functions below the injury site. For this reason, it is a life-changing experience having dramatic consequences in the physical and psychological state of the patient. Around the globe, spinal cord injury (SCI) can vary in terms of etiology, prevalence and incidence. Regarding the etiology, some injury cases can be a result of nontraumatic occurrences (spinal stenosis, infections, tumors and others) (Ho et al., 2007), while the majority is caused by physical trauma derived mainly from falls, vehicle accidents and sports injuries [Figure 2.A, (James et al., 2019)].

The global age-standardised prevalence of traumatic SCI reached 368 per 100 000, giving a total estimation of 27 million people living with this pathology. Concerning the incidence, SCI presented a higher rate in some countries of Middle East region, such as Syria (136 per 100 000), Yemen (42 per 100 000) and Iraq (37 per 100 000). In contrast, some developing regions had a lower incidence, including African territories with the number of cases equal to or less than 9 out of 100 000 people. Among European countries, the incidence of Portugal reached 22 SCI cases per 100 000 [Figure 2.B, (James et al., 2019)].

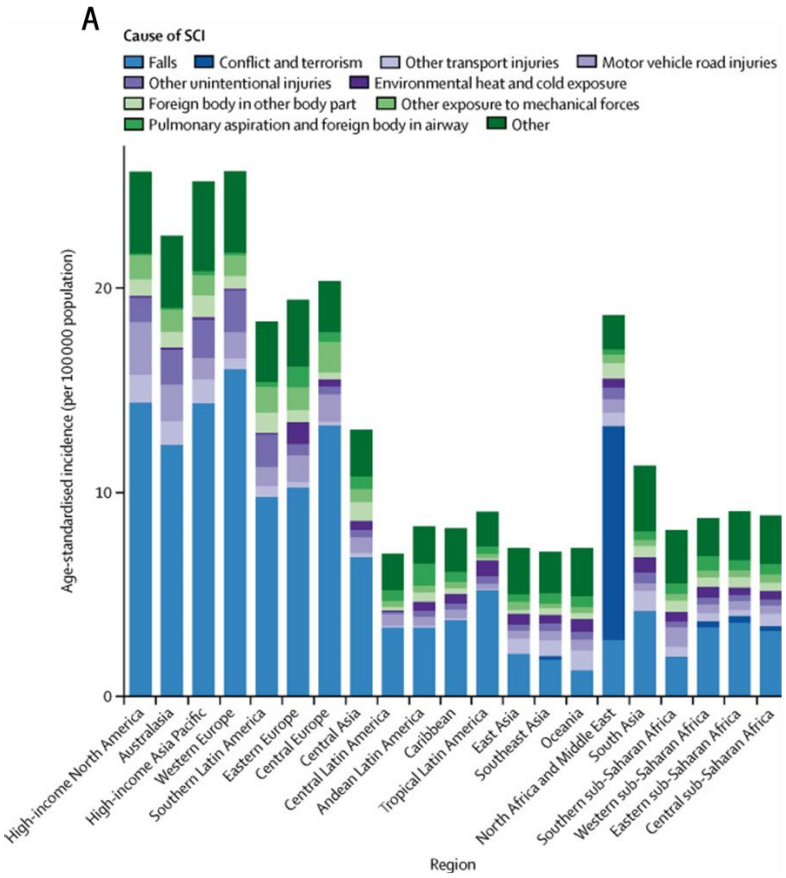

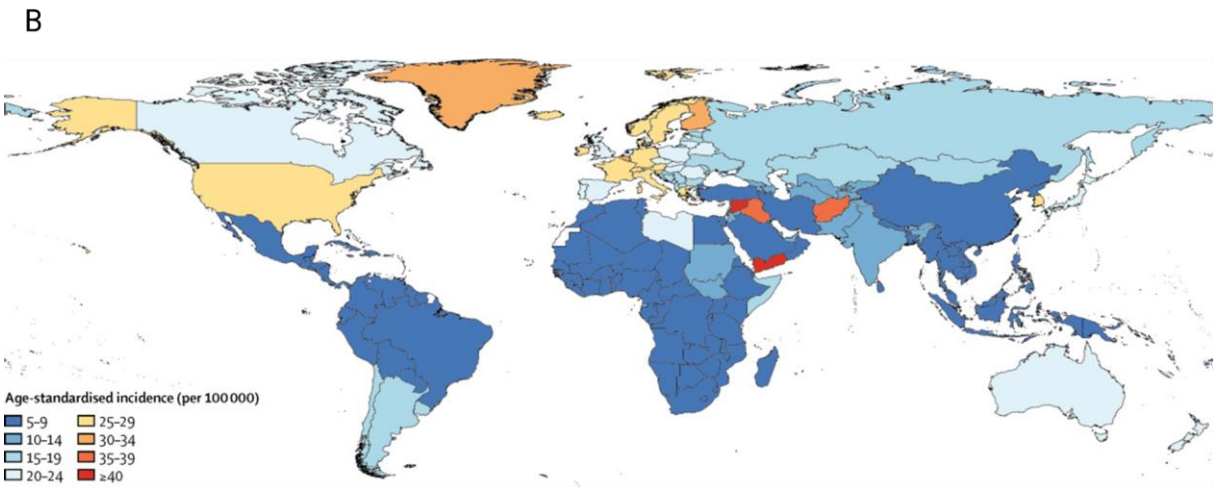

Figure 2 . Epidemiological panorama of SCI. (A) Global incidence of different etiologies of SCI. (B) Representation of a map, in which the countries contain distinct colors that correspond to a specific range of SCI incidence per 100 000 people. The data were standardized according to individuals age and applied to both genders. Both images are adapted from James et al. (2019).

1.3. Pathophysiology of SCI

A traumatic SCI starts with a localized impact with enough force to dislocate the vertebra from the spinal column, which can compress or transect a fragile structure as the spinal cord (Oyinbo, 2011). The primary injury induces neuronal cell damage, disruption of blood vessels and breakage of the blood-spinal cord barrier (BSCB), compromising neuronal communication and vascular supply (Choo et al., 2007; LaPlaca et al., 2007). Consequently, a biological chain reaction, considered as the secondary injury, is activated lasting for days or even weeks (Ahuja et al., 2017). The main occurrences of SCI pathophysiology are mentioned and represented in Figure 3.

In this phase, dramatic modifications occur in the vascular environment, increasing the permeability of the spinal cord to immune cells and cytokines (Pineau & Lacroix, 2007). The combined action of this increased inflammation and BSCB rupture contributes to swelling, necrosis and ischemia, worsening the extent of the existent damage (Ahuja et al., 2017).

A myriad of factors, such as ischemia, overresponsive inflammation and excitotoxicity, culminate in necrosis of neurons and glial cells, in which biological products (adenosine triphosphate, deoxyribonucleic acid [DNA] and potassium) are released. As a result, microglia are activated leading to an exacerbation of neurons and oligodendrocytes death. Additionally, microglia and other phagocytic inflammatory cells release free radicals (for instance, superoxide anion radical and hydrogen peroxide) causing peroxidation of lipids, DNA damage and protein oxidation (Dizdaroglu et al., 2002; Hausmann,

2003). These mechanisms together contribute to extensive cell death in the injury site. With cellular damage and ischemia, action potentials undergo major shifts that lead to dangerous ion levels and excessive release of neurotransmitters, reinforcing neuronal cell death (Faden & Simon, 1988). Initially, the majority of damaged neurons undergo acute axonal degeneration, but over time this process is shifted to Wallerian degeneration, which comprises the deterioration of the distal part of transected axons (Couillard-Despres et al., 2017).

When secondary events start to settle down, SCI evolves to the last stage, the chronic phase, where some processes take place, including glial scar development, the disintegration of grey matter and demyelination of neuronal white matter (Ahuja et al., 2017; Silva et al., 2014). The massive cell death and neurodegeneration create a gap, which is filled with extracellular fluid, connective tissue and macrophages (Norenberg et al., 2004), named cystic cavity. Around the cavity, the glial scar is formed involving astrogliosis (Figure 3), which comprises the increase of astrocyte size and upregulation of specific molecules, such as glial fibrillary acidic protein (GFAP), vimentin and nestin (Barrett et al., 1981; Bignami & Dahl, 1976). Additionally, extracellular matrix-derived molecules (e.g. chondroitin sulfate proteoglycans) secreted by activated microglia, astrocytes and macrophages are accumulated in the perilesional area of the glial scar, creating an inhibitory environment for axonal regeneration, as illustrated in Figure 3 (McKeon et al., 1991). Other cell populations (oligodendrocyte progenitor cells and fibroblasts) migrate to the lesion core, increasing the complexity of the injury-induced environment (Cregg et al., 2014; Norenberg et al., 2004). The multiple interactions of these cell populations give rise to a physical and molecular frontier, the glial scar, that exerts antagonist effects. It protects the structures adjacent to the lesion from the infiltrating immune cells, but it hinders the regeneration of axons for long distances (Cregg et al., 2014).

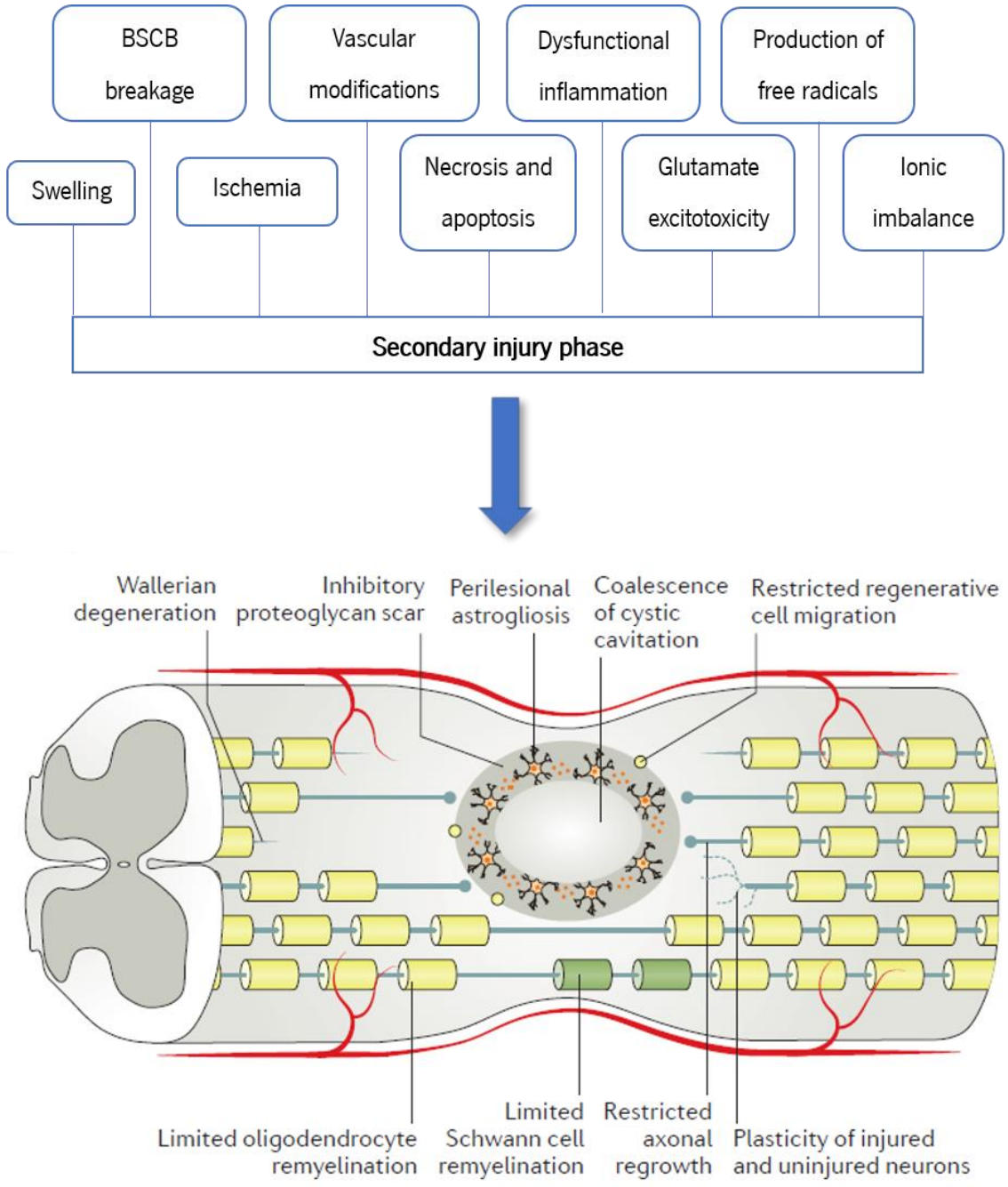

Figure 3. Representation of two different stages of SCI pathophysiology. The scheme above presented various processes that occur in the secondary phase of SCI. The image below is an illustration of an injured spinal cord in a later phase (chronic phase) marked mainly by glial scar development. Information and image adapted from Ahuja et al. (2017).

1.4. The physiological and psychological repercussion of SCI

SCI consequences are not only restricted to motor and sensory perturbations as it can affect autonomic functions (Kumru & Kofler, 2012). In recent years, side effects of autonomic functions have gained more relevance (Hou et al., 2013) for the development of therapeutic strategies, since the latter may target autonomic complications as well as increase patient's life expectancy and quality (Kumru & Kofler, 2012). Besides the nervous system, SCI affects other organs leading to a wide range of autonomic complications, including difficulty to breathe, cardiovascular problems (hypotension and hypertension), loss of bowel and bladder control, muscle and splenic atrophy, sexual dysfunction and a greater vulnerability to infections (Kumru & Kofler, 2012). High-level lesions can lead to the development of autonomic dysreflexia, which is a dangerous condition of hypertension produced by overactivation of sympathetic reflex elicited by a noxious stimulus (Eldahan & Rabchevsky, 2018). At psychological level, patients with SCI face also emotional problems, presenting a higher prevalence of depression, anxiety and post-traumatic stress disorder, and a lower average life satisfaction in comparison to the general population (Post & van Leeuwen, 2012).

1.5. Heterogeneity of SCI

The degree of neurological impairments and prognosis will depend on the level of the damaged spinal cord (Silva et al., 2014). For example, a patient with cervical injury may manifest quadriplegia, whereas a thoracic injury can only cause paraplegia. If the lesion occurs above the fourth vertebrae of the cervical level, the respiratory function can be affected (Ballios et al., 2011). In addition to heterogeneity of the injuries themselves, the type of lesion influences the rearrangement of the cellular network of the cord. For instance, a complete lesion (transection) blocks the passage of neural information between regions above and below the injury, while an incomplete SCI presents spared motor and sensory neurons, allowing a certain degree of neuronal communication (Courtine & Sofroniew, 2019).

1.6. The clinical reality for SCI patients

Following the patient admission to the hospital, it is necessary to carry out a preliminary neurological evaluation supported by the lesion imaging. In order to attenuate the consequences of the injury, a surgical intervention is commonly performed to relieve the pressure exerted in the cord and stabilize the spinal column (Hachem et al., 2017).

In some situations, there are aspects that clearly indicate the need for surgery (decompression and/or stabilization), such as increased neurological damage due to the spinal cord compression and

vertebrae dislocation. However, in cases where these criteria are not met, the application of surgical interventions should be deliberated considering its advantages and disadvantages. When this procedure is not the best option, a conservative treatment, which involves bed rest, is adopted, awaiting the spinal cord recovery (Rath & Balain, 2017). In addition to the intervention itself, the ideal surgical timing has been also an issue of debate. In 2018, Kim and colleagues made a comparison between two groups of SCI patients: the early surgery group, in which the surgery was performed up to 48 hours after injury, and the later surgery group, which was subjected to surgery after 48 hours post-injury. When the patients from both groups were admitted to the hospital, no significant differences in the neurological level of injury existed between them. Nevertheless, 6 months after the surgery, the early surgery group presented a meaningful neurological improvement in comparison to the later surgery group. Hence, the recommendation of the authors is performing the surgery in a period of 48 hours, which appears to allow a better recovery of SCI patients (Kim et al., 2018).

Even after the surgery, the patient still has problems associated with the secondary injury, so pharmacological approaches have been explored to minimize the damage. For instance, the corticosteroid methylprednisolone has been used in SCI aiming to reduce the lesion-derived inflammation and restrict the area of secondary injury to the spinal cord (Russo et al., 2020). Some studies showed *in vitro* and *in vivo* the potential of this drug in different molecular and cellular processes - lipid peroxidation inhibition, BSCB maintenance and inflammation suppression (Hall & Braughler, 1981, 1982; Tator, 1998). Nevertheless, it is advised to use this therapeutic agent as an option and not as a standard treatment due to the severe complications related to its long-term application, such as sepsis and pneumonia (Evaniew et al., 2016; Hugenholtz, 2003). Known for their neuroprotective effects, naloxone, tirilazad and nimodipine were tested in clinical trials, where no proof of enhancement in motor scores was found between groups that received treatment and placebo (Bracken et al., 1997; Bracken et al., 1990; Pointillart et al., 2000; Wilson et al., 2013). In contrast, other therapeutic agents with different mechanisms of action (riluzole and minocycline) have shown to induce an increase in the motor score of SCI patients in phases I and II of clinical trials, respectively (Casha et al., 2012; Grossman et al., 2014; Wilson et al., 2013).

1.7. Research field: *In vitro* and *in vivo* methods to study SCI

No conclusive data support the efficacy of standard treatment protocols (surgery or conventional management) for acute SCI patients. Several pharmacological treatments with anti-inflammatory and neuroprotective action have failed to induce a significant functional recovery (Ahuja et al., 2016). Thus,

research has evolved towards finding suitable and more efficacious treatments for SCI. For that, *in vitro* and *in vivo* models have been used to provide an insight into what can happen in a SCI.

In vitro approaches provide the possibility of controlling environmental variables, which can help to study mechanisms and molecular processes underlying SCI and tissue repair (Boomkamp et al., 2014; Boomkamp et al., 2012; Fisher, 1997; Trotter, 1993). *In vitro* methods comprise cell culture, explants and tissue slices that allow to explore events related to SCI, such as: (a) axonal growth, (b) glial scar formation, and (c) remyelination (McCanney et al., 2017).

a) - *In vitro* assays are crucial for testing the impact of different compounds on neuronal function and axonal growth (Fitch et al., 1999). Among neurite outgrowth assays, Dorsal Root Ganglia (DRG), whether in dissociated cultures (Figure 4.A) or in explant cultures (Figure 4.B), have been commonly used (Ahmed et al., 2006; Deister & Schmidt, 2006; White & Mansfield, 1996). DRG are described as a group of sensory neurons situated dorsally in the intervertebral foramina (Sanes & Yamagata, 1999). The impact of a new drug or growth factor on neurite outgrowth is studied analyzing parameters, such as neurite length, number of intersections and morphology (Ahmed et al., 2006).

b) - To recreate the glial scar, a scratch-wound assay can be established, in which a mechanical lesion is applied in a monolayer of astrocytes (Környei et al., 2000), leading to their activation and proliferation (Pappalardo et al., 2014) (Figure 4.C). This method has been adopted to test the potential of therapies in reducing the glial scar and, consequently, improving the environment for axonal regeneration (Pappalardo et al., 2014).

c) – After a SCI, a process of demyelination occurs exposing the axons to degradation (Guest et al., 2005; Totoiu & Keirstead, 2005). Transplanted Oligodendrocyte Precursor Cells (OPCs) have shown a beneficial impact on the functional recovery of SCI animals due to the ability of these cells to form myelin sheath in demyelinated axons (Groves et al., 1993; Sharp et al., 2010). Thus, a co-culture of OPCs and DRG explants can be used in order to provide information about myelination without the influence of other glial cells (Figure 4.D) (Petersen et al., 2017).

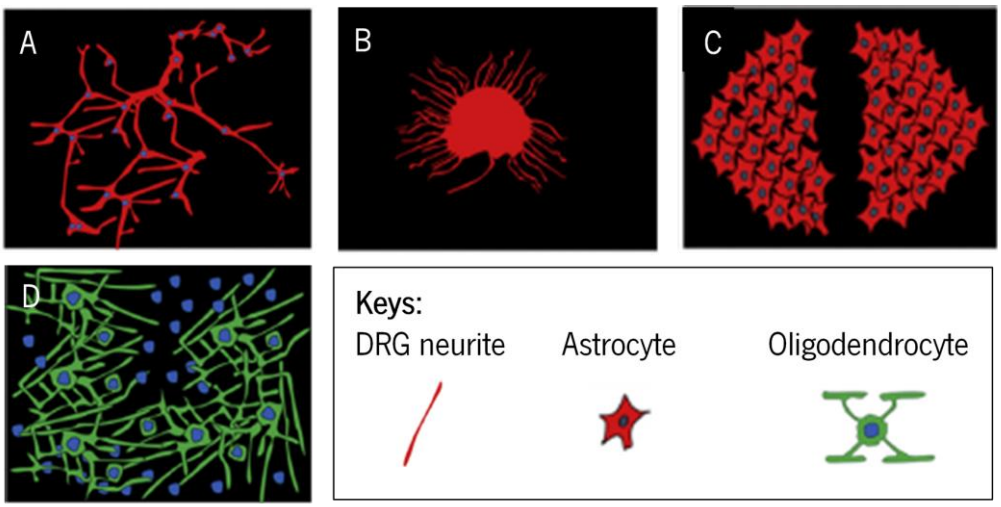

Figure 4. Representation of *in vitro* models to study SCI. A – Dissociated DRG neurons; B – DRG explant; Figures A and B illustrate neurite outgrowth assays, in which neurites are developing from DRG. C – Monolayer of astrocytes representing a scratch-wound assay. D – Co-culture of OPCs and DRG as a tool to study myelination. Images adapted from McCanney et al. (2017).

Regarding the *in vivo* models, animals can simulate a SCI, providing more information about its pathophysiology in a multidimensional environment. For this reason, *in vivo* models display a higher clinical value for testing potential therapies and studying mechanisms involved in the lesion in comparison to *in vitro* models (Nout et al., 2012; Rahimi-Movaghar et al., 2009). Mammals, like cats, pigs and dogs, are an unusual choice as a SCI model due to the requirements of expensive care, and restrictions to ethical authorization (Kundi et al., 2013; Talac et al., 2004). In contrast, SCI rodents are commonly used, once they present several advantages, including the accessibility of ethical approval, easy care and established procedures (Nakae et al., 2011; Talac et al., 2004). In a general way, SCI animal models can be divided into three categories: contusion, compression and transection. These models should be used based on the research question under study, considering the pros and cons that each one exhibits.

In the contusion model, a temporary injury is performed in the exposed spinal cord. A contusion can be produced with the utilization of the following devices: weight-drop device, air gun apparatus and electromagnetic impactor (Alizadeh et al., 2019; Cheriyan et al., 2014). This model can be relevant in the clinical context because this type of lesion occurs frequently in humans, being the most common one (Nobunaga et al., 1999). However, the neurological deficits induced by the lesion can display inconsistency, and also it can be very complicated to discriminate intact tissue from the injured one (Cheriyan et al., 2014; Talac et al., 2004).

In the compression model, the spinal cord can be compressed using forceps, aneurysm clips or balloons (Cheriyan et al., 2014). For the clinical reality, it can be relevant, because it shares many events of SCI pathophysiology with humans (Alizadeh et al., 2019). With this model, it is possible to obtain information about SCI pathophysiology mechanisms and the effectiveness of pharmacological therapies (Sun et al., 2017). Regardless of the tool used to generate the injury, all methods share one main disadvantage that is the lack of control in some variables, including the speed and the amount of applied force (Cheriyan et al., 2014).

Lastly, the third model consists in cutting the spinal cord, being divided into total and partial transections. Despite its easy reproducibility, a complete transection in humans is rare, which makes this model less clinically relevant than the others (Alizadeh et al., 2019; Cheriyan et al., 2014). Nevertheless, it can be quite useful, when the research objective is to evaluate the axonal regeneration and the development of specific therapeutic strategies (for example, biomaterials). Regarding the partial transection, this lesion can be applied in different regions of the spinal cord, producing variants like hemisection, lateral transection or dorsal transection (Alizadeh et al., 2019; Cheriyan et al., 2014). The partial transection model is suitable for studying neural plasticity and grafting, and not so relevant for assessing therapeutic strategies, since it presents a higher degree of spontaneous motor recovery (Alizadeh et al., 2019; Cheriyan et al., 2014).

2. Cell therapy

Neuronal cells (mainly, neurons and oligodendrocytes) damaged by the lesion cannot be substituted by new and functional cells through an endogenous repair pathway (Ahuja & Fehlings, 2016). In this sense, many of the therapeutic strategies involving cell transplantation are being tested to replace cells damaged by the lesion. These treatments aim to contribute to the motor and sensory recovery of SCI patients (Willerth & Sakiyama-Elbert, 2008). A wide range of cells has been explored for SCI regenerative medicine, including glial and stem cells.

2.1. Glial cell therapy

Mature glial cells, namely olfactory ensheathing cells (OECs) and Schwann cells (SCs), might be good candidates for cell therapy against SCI, because they may create a permissive environment for axonal remyelination and regrowth. OECs contribute to the regeneration of peripheral olfactory neurons, directing their growth into the olfactory bulbs in the central nervous system (CNS) (Doucette, 1991).

As shown in the study conducted by Ramón-Cueto and colleagues, the transplantation of OECs boosted axonal regeneration and locomotor function in a complete thoracic transection model (Ramón-Cueto et al., 2000). In line with these results, in another study, OECs and fibroblasts were administered individually into a transection SCI animal model. The results indicated that, in comparison to fibroblasts, OECs survived longer, leading to increased protection of neurons, reduction of immune cell invasion and suppression of immune cell activation in the spinal cord. Consequently, the neuronal microenvironment became more favourable for axonal growth (Khankan et al., 2016).

Regarding SCs, they are responsible for wrapping axons with newly produced myelin. Beyond this role, these cells secrete molecules that promote and support axonal growth (Mirsky et al., 2002; Oudega & Xu, 2006). In an attempt to see these beneficial effects on SCI, SCs were implanted into a moderate contusive rat injury model. SC transplantation led to survival of neurons, increase of axonal regrowth and improvement of hindlimb locomotor function (Takami et al., 2002). In several studies, SC implantation into the cavity of injured animals has shown to stimulate axonal regeneration. However, these cells usually present low survival after transplantation (Bunge & Wood, 2012; Guest et al., 2013; Marquardt et al., 2020). For this reason, Marquardt and co-workers encapsulated SCs in a synthetic hydrogel, injecting it into a contusion SCI model. This combined therapy not only led to decreased inflammation, but also to a substantial improvement of motor function, in particular in the forelimb strength and coordination (Marquardt et al., 2020).

2.2. Stem cell therapy

In the last decades, stem cell-based therapy has also gathered attention in the field of regenerative medicine for SCI (Iwanami et al., 2005; Keirstead et al., 2005; Liu et al., 2000; P. Lu et al., 2012; Zhu et al., 2020). In addition to the replacement of injured cells, stem cells can create a favourable microenvironment for axonal regeneration by modulating the inflammation and stimulating the existent regenerative programs (Ahuja & Fehlings, 2016). Stem cells are pluri- or multipotent cells that are able to give rise to a variety of cell types (Graf, 2002). Another two common features are their remarkable capacity of self-renewing and the high rate proliferative capacity (Watt & Hogan, 2000). Among different types of stem cells, three main options have been the subject of study in a SCI context, such as embryonic stem cells (ESCs), induced pluripotent stem cells (iPSCs) and mesenchymal stem cells (MSCs).

2.2.1. Embryonic stem cells

ESCs are extracted from the inner cell mass of a primordial structure in development (blastocysts), which undergoes the elimination of trophectoderm cells (Smith, 2001). A particular feature of this cell type is its pluripotency nature, meaning that they have the ability to differentiate into the three germ layers, with exception of extraembryonic tissues, including placenta (Conley et al., 2004). Their pluripotency nature makes them a good option to be used as a cell replacement therapy to treat neurological conditions. With this in mind, ESCs have been exploited as a therapy for SCI, once they can be differentiated into neurons and glia replacing the damaged cells, and release immunomodulatory and neuroregenerative factors contributing to functional recovery (Shao et al., 2019; Shroff et al., 2017; Yang et al., 2020). For example, ESCs were induced to obtain OPCs and then transplanted into a SCI model. It was demonstrated that the neurological function of the animals improved, without any evidence of cell transplantation side effects (Liu et al., 2000; Keirstead et al., 2005; Cloutier et al., 2006). In a recent study, Zarei-Kheirabadi et al. used neural stem cells derived from ESCs, encapsulating them in hyaluronic acid-based hydrogel and injecting them into a contusion-lesioned rat. They reported that in groups treated with this combinatorial approach, there was a differentiation of these cells into neuronal and glial cells, accompanied by a reduction of the glial scar and lesion cavity. Additionally, treated animals improved in terms of locomotor function in comparison to vehicle-treated animals (Zarei-Kheirabadi et al., 2020). Despite all these encouraging results, ESC transplantation carries ethical issues regarding their origin and possible risks of tumor development (Mothe & Tator, 2012).

2.2.2. Induced pluripotent stem cells

In 2006, Yamanaka and colleagues developed a ground-breaking work, where differentiated adult cells (fibroblasts) were converted into pluripotent stem cells through the viral delivery of four transcription factors: octamer-binding transcription factor 3/4, sex determining region Y-box 2, proto-oncogene c-Myc and Krüppel-like factor 4 (Takahashi & Yamanaka, 2006). iPSCs arise as an alternative to human ESCs, once the former overcome the ethical problems. Moreover, iPSCs can be obtained from patient cells for autologous transplantation, avoiding cell rejection induced by the immune system (Gazdic et al., 2018). However, to generate iPSCs, it is necessary to reprogram differentiated cells that can contribute to tumor formation (Ben-David & Benvenisty, 2011). After the transplantation of neural stem cells derived from iPSCs (iPSC-NPC) into the spinal cord, results demonstrated the migration of surviving cells and their differentiation into neurons and glial cells in the spinal cord, leading to

locomotor improvements (Fujimoto et al., 2012; Kobayashi et al., 2012; Nutt et al., 2013). In addition to this, it was shown that the injection of iPSC-NPC, either by intraspinal or intrathecal route, induced axonal sprouting, but only the intraspinal delivery of cells exerted immunomodulation reducing astrogliosis (Amemori et al., 2015).

2.2.3. Mesenchymal stem cells

The concept of Mesenchymal Stem Cells refers to multipotent stem cells, which inhabit in almost all tissues (Crisan et al., 2008). The first described MSCs were discovered in the bone marrow by Friedenstein and co-workers (Friedenstein et al., 1970). This is not the only source of MSCs though, since they can be extracted from a variety of tissues, particularly the umbilical cord (Wang et al., 2004), the dental pulp (Gronthos et al., 2000) and the adipose tissue (De Ugarte et al., 2003).

According to the International Society for Cellular Therapy, criteria were established to facilitate MSC identification, such as *in vitro* adherence in a substrate as plastic, the presence of antigen markers on their surface (CD73, CD90 and CD105), the absence of certain proteins (CD45, CD34, CD14, CD11b, CD79a and human leucocyte antigen class II), and the ability to originate osteoblasts, adipocytes and chondroblasts through the differentiation process (Dominici et al., 2006; Horwitz et al., 2005).

Among the alternatives for stem cell therapy, MSCs are very appealing due to a myriad of reasons: accessible isolation from many sources (Lee et al., 2005); small probability of developing tumors (Lu et al., 2006); great proliferation and differentiation capacity (Sekiya et al., 2002); and small immunological responses, induced by implanted allogeneic MSCs (Carrade et al., 2011).

2.2.4. Adipose tissue-derived Mesenchymal Stem Cells

Adipose tissue-derived stem cells (ASCs) can be found in the stromal vascular fraction of subcutaneous adipose tissue (Xu et al., 2003). The determination of ASC location *in situ* has been a challenging task, as no unambiguous marker detects specifically ASCs. However, some studies suggested that ASCs are located in the perivascular zone, which also contains pericytes and endothelial cells (Baer & Geiger, 2012; Lin et al., 2008). Moreover, ASCs share a few surface markers (CD90, CD105, CD73, CD44a, and CD166) with bone marrow-derived mesenchymal stem cells (BM-MSCs) (Bourin et al., 2013).

In comparison to other MSCs (for example, BM-MSCs), ASCs can be collected in a large amount with a surgery involving liposuction. Abundance of ASCs and their easy collection, with little invasive and

almost unpainful techniques, are two factors that make this cell type a good candidate for cell therapy (Baer & Geiger, 2012; Bajek et al., 2015; Zuk et al., 2002).

In regenerative medicine, ASC therapy has revealed to be a good alternative to treat multiple conditions, such as Parkinson's disease, Alzheimer's disease, SCI, heart pathologies and rheumatoid arthritis (Kokai et al., 2014). Zhou et al. analyzed the efficacy of transplantation of human ASCs and BM-MSCs on SCI using a partial transection model. After cellular implantation, there was an increase in the number of blood vessels, an improvement of axonal regeneration, and, in contrast, a reduction in the number of inflammatory cells and lesion cavity area. Also, at the functional level, cell treatment induced an enhancement of locomotor function. Although these modifications were seen in both transplanted cell types, ASCs produced more significant changes than BM-MSCs, suggesting that the former are more suitable for this neurological pathology (Zhou et al., 2013).

Years later, Ohta et al. tested the intravenous infusion of ASCs in a contusion SCI rat model, confirming some of the abovementioned results, including augmentation of locomotor recovery and reduction of lesion cavity area (Ohta et al., 2017). In order to understand if ASC infusion was safe or not, Ra and colleagues injected systemically different doses of ASCs into immunodeficient mice, and the treatments, even with a high cell dose, appeared to not contribute to tumor development or other detrimental events (Ra et al., 2011). Moreover, a human clinical trial in phase I (NCT01274975) was performed involving autologous implantation of ASCs into patients who had been living with traumatic SCI for at least one year. Patients were followed periodically, and, three months later, they did not present any serious side effect resulting from ASC implantation. Animal and human studies supported the fact that ASC infusion is innocuous to both mice and humans (Ra et al., 2011). Besides this, in the human phase I trial, the treated group presented a slight decrease in lesion area, and one patient improved in terms of motor and sensory function. Despite these promising results, this trial presented several limitations, including the absence of a control group and inappropriate sample size to withdraw conclusions concerning the treatment efficacy (Ra et al., 2011). Another human clinical trial (in phase I) (NCT01769872). was created to assess the effectiveness of autologous injection of different ASC doses into SCI patients through multiple routes. Although the trial is finished, results have not yet been published (Silvestro et al., 2020).

At the beginning of stem cell transplantation research, the integration of MSCs followed by their differentiation into tissue-specific cells was a possible explanation for the therapeutic action of these cells. Nevertheless, this hypothesis has not been supported by conclusive data (Jin & Greenberg,

2003; Salgado et al., 2010). Besides that, it has been demonstrated that MSCs do not remain within the human body long enough to have a strong impact (Ide et al., 2010; Toma et al., 2009). Several studies involving cell tracking demonstrated that the survival rate of MSCs was inferior to 1% one week after the systemic injection (Eggenhofer et al., 2012; Lee et al., 2009; Parekkadan & Milwid, 2010; Song et al., 2012; Zhang et al., 2009). When MSCs are injected through the intravenous route, these cells travel around the systemic circulation getting trapped in some organs, namely the lung, where their half-life is 24 hours (Gao et al., 2001; Schrepfer et al., 2007). In order to explain the positive effects of MSCs, another hypothesis was raised, stating that the paracrine mechanisms are responsible for the majority of the benefits obtained from transplanting MSCs (Wei et al., 2009).

3. MSC secretome

In the first decade of the 20th century, Gnecchi and colleagues' work shed light on the hypothesis that MSCs exert their therapeutic effects through the release of bioactive molecules, named as secretome (Gnecchi et al., 2005). The definition of "secretome", described firstly by Tjalsma and colleagues (Tjalsma et al., 2000), was refined by Hathout, referring it as "proteins that are secreted by a cell, tissue or organism at any given time or under certain conditions" (Hathout, 2007).

The soluble portion of MSC secretome comprises a wide range of proteins, including pro- and anti-inflammatory cytokines, growth factors and other molecules with biological properties (Paquet et al., 2015; Pires et al., 2016). In addition to the soluble portion, the secretome is enriched with extracellular vesicles, transporting nucleic acids and proteins. In the vesicular fraction, there are apoptotic bodies, microparticles and exosomes, which are distinct from each other in their source, dimension, markers and density (Beer et al., 2017; Hoogduijn & Lombardo, 2019). Apoptotic bodies with 1 to 5 μm in size are secreted in the cellular apoptosis, and their function has been associated with immunomodulation (György et al., 2011; Raposo & Stoorvogel, 2013; Savill et al., 2002). Particles with dimensions varying between 150 and 1000 nm are called microvesicles, whose secretion is made by the formation of plasma membrane buds (Mathivanan et al., 2010; Raposo & Stoorvogel, 2013). Finally, exosomes refer to vesicles with a smaller dimension (40 - 100 nm) that are secreted through the exocytosis process (Raposo & Stoorvogel, 2013; Yu et al., 2014). An interesting study suggested that, once released by stem cells, exosomes are responsible for delivering bioactive factors (nucleic acids and proteins) that influence the target cell (Eldh et al., 2010), stimulating several mechanisms, such as angiogenesis (Liang et al., 2016), axonal growth (Xin et al., 2012) and immunomodulation

(Lankford et al., 2018). In line with this, our group compared *in vitro* the effect of total ASC secretome with its vesicular and soluble portions on inflammation and axonal growth, using microglial culture and DRG explants, respectively. In comparison to both portions, the total secretome revealed a superior effect on promoting neurite outgrowth and reducing the number of activated microglia. This higher effect of total secretome was confirmed in SCI animal model by showing an improvement of locomotor function (Pinho, 2019).

In the last years, MSC secretome has been proposed as an alternative to cell implantation, once it may be associated with the therapeutic effects of MSCs observed in previous works (Meyerrose et al., 2010). Moreover, problems associated with cell-based approaches, particularly cell survival, can be overcome by secretome-based therapies (Eiró et al., 2014; Vizoso et al., 2017). The use of secretome as a therapeutic strategy provides plenty of advantages, such as: easier assessment of secretome in terms of safety, dosage and potency (Bermudez et al., 2015); the reduction of time and cost necessary for cell culture and expansion, as less cells are needed to obtain similar effects (Mendes-Pinheiro et al., 2018; Vizoso et al., 2017); the chance of modifying cell secretome in order to obtain a desired effect for specific target cells (Vizoso et al., 2017); the utilization of secretome as an "off-the-shelf" product, which means it is available to be applied in acute conditions, obviating the need of high amount of cells for transplantation (Teixeira et al., 2016; Vizoso et al., 2017); lastly, the preservation of the secretome without noxious cryoprotective agents keeping the efficacy of the product (Vizoso et al., 2017).

Evidences have pointed to the fact that the secretome of MSCs from distinct origins may exhibit molecular variability. Intending to explore this topic, our group analyzed and quantified the protein content of the secretome (in the form of conditioned media) from three MSC sources - bone marrow, umbilical cord, and adipose tissue. In this characterization, it was possible to identify 134 (from a total of 451) common proteins present in the secretome of different MSC populations. However, the same analysis also showed that there were important differences and variations between them. Therefore, the secretome from each population can be employed in different neurological conditions (Pires et al., 2016). Knowing this, another work from our group compared the effect of secretomes derived from ASCs, BM-MSCs, and human umbilical cord perivascular cells on neuronal differentiation and axonal growth. Molecules secreted by the different sources exhibited potential in promoting neural differentiation of human neural progenitor cells and neurite outgrowth of DRG explants. However, ASC secretome stood out by showing a greater effect on axonal growth *in vitro* (Assunção-Silva et al., 2018).

3.1. ASC secretome

In paracrine and autocrine pathways of the cell, the secretome plays an important role by mediating effects in several physiological processes (Pinho et al., 2020; Vizoso et al., 2017). ASCs appear to offer a higher clinical value for the treatment of neurological diseases due to the secretion of their factors (Jin & Greenberg, 2003; Salgado et al., 2010; Wei et al., 2009). Thus, it is important to unravel the molecules of the secretome involved in the therapeutic action of ASCs. Bioactive factors secreted by MSCs, in particular ASCs, fall into several categories associated with different processes, such as immunomodulation, vascularization, neuroprotection and neuroregeneration (Figure 5) (Pinho et al., 2020).

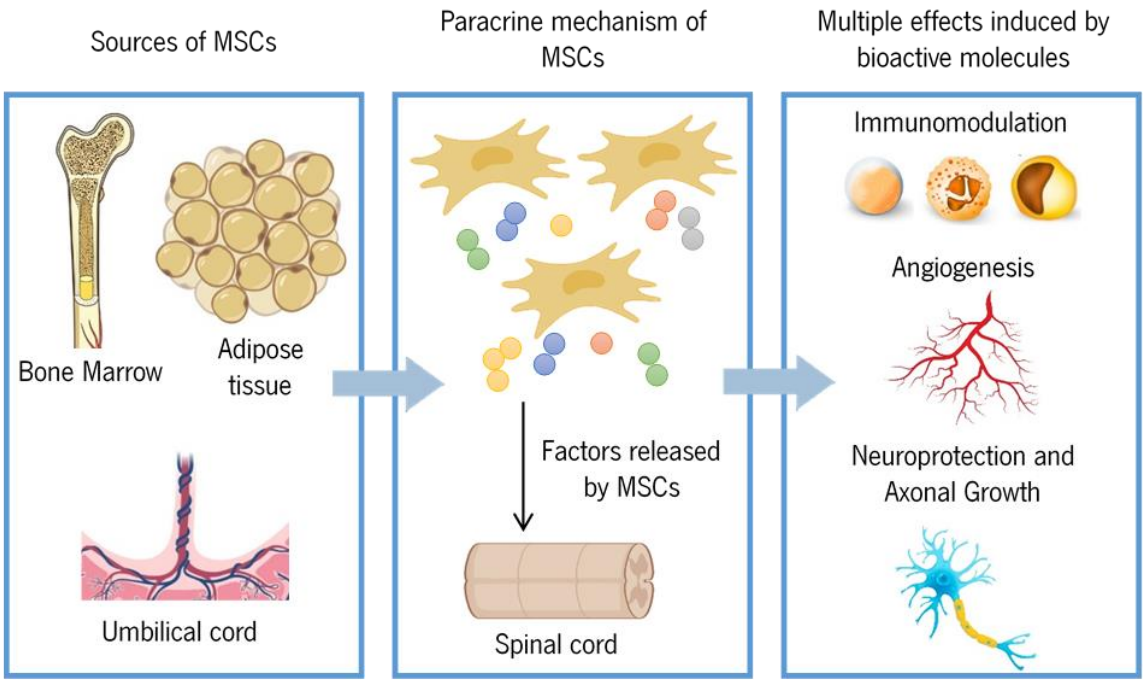

Figure 5. The origin and the effects of MSCs. First rectangle: the main sources of MSCs (bone marrow, adipose tissue and umbilical cord) are represented. Second rectangle: Scheme of paracrine activity of MSCs involving the release of factors that may be applied for spinal cord repair. Third rectangle: After MSC implantation into the injured spinal cord, the secreted bioactive molecules can induce multiple effects, mainly related to immunomodulation, angiogenesis, neuroprotection and axonal regrowth. The scheme was adapted from Cofano et al. (2019).

3.1.1. Immunomodulation

MSCs have shown to suppress cells from innate and adaptive immune systems, affecting their activity, proliferation and function (Fierabracci et al., 2016; Keating, 2012; Vizoso et al., 2017). In 2009, Ivanova-Todorova et al. tested the anti-inflammatory properties of ASCs and BM-MSCs by co-culturing them individually with dendritic cells. There was a decrease of surface markers of dendritic cells and an increase of secretion of interleukin-10 (IL-10, typically an anti-inflammatory cytokine), being more significant when ASCs were present. These results showed that ASCs have a stronger anti-

inflammatory effect than BM-MSCs (Ivanova-Todorova et al., 2009). Furthermore, another study demonstrated that the immunomodulatory factors released by human ASCs [stimulated by interferon-gamma (IFN-γ)] inhibited the proliferation of peripheral blood mononuclear cells, suggesting that cell contact is not necessary to produce an immunosuppressive response (DelaRosa et al., 2009).

Nowadays, the immunomodulatory potential of the secretome has been associated with the existence of immunoregulatory factors (Vizoso et al., 2017). These soluble factors can integrate two groups of cytokines with opposite effects, anti- and pro-inflammatory molecules (Vizoso et al., 2017). The secretion profile of ASCs was characterized, revealing a wide range of immunomodulatory molecules, among them high levels of anti-inflammatory cytokines, namely IL-10 and IL-13, and pro-inflammatory cytokines, including IFN-γ and IL-12 (Blaber et al., 2012). Although each cytokine has been associated with an anti- or pro-inflammatory role, it is important to keep in mind that cytokines seem to be involved in suppression and induction of the inflammation (Kyurkchiev et al., 2014). For instance, IL-6 has shown to exhibit a dual nature (Blaber et al., 2012; Opal & DePalo, 2000), once it has been involved in triggering immune responses and, in contrast, inhibiting the production of pro-inflammatory cytokines (Kyurkchiev et al., 2014).

3.1.2. Angiogenesis

Angiogenesis is a biological event comprising the growth of new vessels from existing ones. It plays a crucial role in the development, growth and healing of the tissue after trauma (Folkman & Shing, 1992; Risau, 1997). Therefore, research has focused on therapeutic strategies that can promote (re)vascularization (Lachmann & Nikol, 2007), since vascular malformation occurs in a wide range of diseases, such as wound healing and atherosclerotic pathologies (Benton and Hagg, 2011; Vizoso et al., 2017). For instance, therapies based on the application of MSCs, namely ASCs, have attracted some interest in chronic wound treatment due to their secretion of pro-angiogenic factors (Kucharzewski et al., 2019; Lombardi et al., 2019; Marfia et al., 2015). An interesting work reported the presence of several regulatory factors in ASC secretome determined by proteomic characterization, using multiplex enzyme-linked immunosorbent assay (ELISA). Factors with angiogenic and antiapoptotic properties were found, mostly vascular endothelial growth factor, hepatocyte growth factor and transforming growth factor-β (Rehman et al., 2004). In *in vitro* experiment, the conditioned media from ASCs (pre-conditioned with hypoxia) revealed pro-angiogenic and anti-apoptotic potential, once it promoted endothelial cell proliferation and avoided cell apoptosis. Then, ASCs were transplanted into an ischemic hindlimb model, augmenting the passage of blood flow to the hindlimb.

All these findings suggested that the synergistic action of angiogenic and anti-apoptotic factors secreted by ASCs can be an important factor for the formation of new vessels (Rehman et al., 2004). Knowing this, ASC secretome can be a good alternative as a therapeutic strategy for SCI, since acting therapeutically on angiogenesis may increase perfusion and restore the BSCB, attenuating the damage caused by the secondary lesion (Ng et al., 2011).

3.1.3. Neuroprotection and neuroregeneration

ASC transplantation has shown to induce functional recovery in different neurological conditions: cerebral ischemia (Kang et al., 2003), SCI (Ryu et al., 2009) and peripheral nerve injury (Wang et al., 2012). Some histological studies revealed the presence of neurons and glial cells that were possibly derived from transplanted ASCs, which could explain the improvement of locomotor function (Kang et al., 2003; Ryu et al., 2009). However, the mechanism of MSC differentiation into cells from other germ layers has been controversial, since cell fusion (with endogenous cells) is more likely to occur rather than differentiation (Alvarez-Dolado et al., 2003; Wurmser & Gage, 2002). It has been increasingly accepted that ASCs exert neuroprotective and neurotrophic effects through a paracrine mechanism. This hypothesis was corroborated by the work of McCoy et al., where administrations of non-differentiated and differentiated ASCs were performed in an animal model of Parkinson's disease. This work revealed that after the injection of both naïve or differentiated cells, the dopaminergic neurons were protected against death induced by 6-hydroxydopamine, indicating that the differentiation of transplanted cells may not be the major factor for the positive effects observed. Furthermore, quantitative polymerase chain reaction (qPCR) was performed to analyze the gene expression of bioactive molecules secreted by ASCs (McCoy et al., 2008). With this analysis, the authors found high amounts of messenger ribonucleic acid (mRNA) for two growth factors, Nerve Growth Factor and Brain-Derived Neurotrophic Factor (BDNF), which contribute to the differentiation of new neurons, as well as the survival of pre-existing neuronal cells (Gu et al., 2009; Li et al., 2009; McCoy et al., 2008). The mRNA for Glial Derived Neurotrophic Factor, which plays a role in the protection and differentiation of specific cells such as dopaminergic neurons, was also detected (Evans & Barker, 2008; McCoy et al., 2008; Sandhu et al., 2009). Moving from Parkinson's disease to SCI, Zhou and co-workers tested the implantation of ASCs or BM-MSCs into SCI rats. As previously mentioned, ASCs demonstrated a higher potential to treat SCI in comparison to BM-MSCs. One-week post-implantation, more than 30% of transplanted ASCs survived in immunosuppressed rats. However, three weeks post-treatment, only a small percentage (1%) of ASCs was found in the spinal cord. Thus,

the authors hypothesized that the improvement of locomotor function observed in animals treated with ASCs may be due to the secretion of factors. In order to explore this hypothesis, qPCR was performed to analyze the expression profile of *BDNF*, showing that ASCs expressed more this neurotrophic factor than BM-MSCs. To complement this result, the authors performed western blot for both cell types revealing higher levels of BDNF in ASCs in comparison to BM-MSCs. Additionally, spinal cord lysates were subjected to ELISA showing that the group treated with ASCs presented a higher expression of BDNF protein, when compared with BM-MSC-treated and non-treated groups. All these results support the hypothesis that ASCs may be contributing to the improvement of locomotor function through the release of BDNF (Zhou et al., 2013).

3.2. Insights about treatments for neurological pathologies

Neurological pathologies, such as Alzheimer's disease, Parkinson's disease or SCI, can be devastating leading to neurodegeneration, as well as structural and functional disturbances of the nervous system. These problems cannot be easily resolved due to the limited neuronal regenerative capacity. In addition, existing therapies can cause undesirable side effects and, even when partially successful, their effects last for a relatively short period of time. Finally, some treatments may present high costs, having an impact in the patient's financial situation. These are the main reasons that lead researchers to replace or complement current treatments, looking for new ways to reduce the morbidity associated with these diseases, in particular SCI (Lindvall & Kokaia, 2006; Salgado et al., 2010; Song et al., 2018).

3.2.1. MSC secretome as a novel approach for SCI repair

In SCI research field, several cell-free based approaches using MSC secretome have been subject of study, since the secretome contains a diversity of factors with immunomodulatory, neuroprotective and neuroregenerative properties, acting in distinct processes of the secondary injury (Cofano et al., 2019). Some groups focused on testing the potential of intravenous delivery of secretome from BM-MSCs in SCI animal models. For instance, the application of this treatment in a contusion rat model exerted a pro-angiogenic effect, increasing the blood vessel diameters. Additionally, the hindlimb function of secretome-treated animals was restored, reaching a higher locomotor score than the control group (Cantinieaux et al., 2013). More recently, Tsai et al. treated the contusion animal model with BM-MSC secretome, demonstrating an improvement of the hindlimb locomotor function accompanied by higher preservation of β-tubulin III-positive nerve fibers (Tsai et al., 2018). Although BM-MSC secretome approach revealed to be very promising in SCI repair, Vader and colleagues

compared the therapeutic efficacy of the secretome from different MSCs, in SCI animals. In this work, two types of MSCs were used, namely BM-MSCs and human umbilical cord matrix cells (HUCMC). In several dimensions, HUCMC secretome appear to be more efficient in comparison to other cell types, decreasing the cavity and lesion volume as well as promoting functional vascularity (Vawda et al., 2020).

Among the diversity of MSC secretome used in regenerative medicine for SCI, ASC secretome is also a valid option to treat this condition, since it displays various beneficial properties. As a demonstration of these properties, Table 1 shows several ASC secretome applications in different pathologies and their respective effects on inflammation, neuroprotection, among others.

In vitro studies have reported the presence of molecules in the ASC secretome responsible for mediating the immunomodulatory, neuroprotective and neuroregenerative effect of these cells (Assunção-Silva et al., 2018; McCoy et al., 2008; Pires et al., 2016). In the context of SCI, these phenomena were demonstrated by our group, which carried out *in vivo* experiments in two SCI animal models. After the intravenous administration of ASC secretome, compression and transection injury animal models exhibited an increase of locomotor recovery (Pinho, 2019; Silva, 2020). It is noteworthy to mention that, in the transection model, the percentage of non-activated microglia was higher in animals treated with ASC secretome, than in control animals (Silva, 2020). All these studies have one common aspect: 100x concentrated secretome was used as the treatment for SCI mice. Nevertheless, a question emerges: What is the concentration of ASC secretome necessary to induce a therapeutic effect on SCI?

The question of secretome concentration has been rarely discussed in the literature. One of the few studies was performed by Egashira and colleagues testing the effect of intracerebroventricular injections of murine ASC secretome in a mice model that mimics ischemic stroke. The authors tested different concentrations of ASC secretome in this pathology revealing that the treatment efficacy varied in a dose-dependent manner. 30x and 100x concentrated ASC secretome revealed to be more effective than 1x secretome, by reducing the infarction volume and brain swelling [Table 1; (Egashira et al., 2012)]. However, thus far, different concentrations of ASC secretome have not been tested in a SCI model. Determining the appropriate dosage of ASC secretome that can induce a positive effect on SCI repair will possibly make this therapy more accessible to patients, by decreasing costs and time of its production and maintenance.

Table 1. Applications of ASC secretome in different neurological pathologies and their respective effects: details about the source of ASCs, the pathology, the cellular pre-treatments (before implantation), the secretome concentration, the treatment dose, the delivery method and time points of the injections. TNF-α – Tumor necrosis factor alpha.

Source	Neurological pathology	Cellular pre-treatment	Concentration factor of the secretome	Delivery route/Dose of the secretome	Time points	Treatment efficacy	Reference
Human ASCs	Traumatic Brain Injury	Hypoxia (5% Oxygen)	Concentrated (Unknown concentration)	Intravenous (100 μL/250g)	Once a day for 7 days post-injury	Improvement of neurological functional; Modulation of neuroinflammation.	(Xu et al., 2020)
Human ASCs	Traumatic Brain Injury	Stimulated with TNF-α and IFN-γ	20x	Intravitreal (1 μL)	Once, 5 minutes post-injury	Mitigation of visual deficits; Downregulation of gene expression associated with microglia activation and inflammatory response.	(Jha et al., 2018)
Human ASCs	Amyotrophic Lateral Sclerosis	None	No concentrated	Intraperitoneally (200 μL)	Once a day for 3 or 7 days after onset	Increased survival time and lifespan after disease onset; Protection of motor neurons and modulation of neuroinflammation.	(Fontanilla et al., 2015)
Rat ASCs	Hypoxic-Ischemic Encephalopathy	None	250x	Intravenous (10 μL)	1 hour before or 24 h post-injury	Protection against hippocampal and cortical volume loss; Amelioration of working and spatial memory deficits.	(Wei et al., 2009)
Human ASCs	Ischemic Stroke	None	10x, 30x and 100x	Intracerebroventricular (2 μL)	1 hour before the MCAO induction	Reduction of the infarct volume after the administration of 30x and 100x conditioned media.	(Egashira et al., 2012)
Mouse ASCs	Alzheimer's	None	No concentrated	Intravenous (100 μL)	Once (at 6 months of age)	Improvement of behaviours associated with depression.	(Yamazaki et al., 2015)

Chapter II - RESEARCH OBJECTIVES

Spinal cord injury is followed by the development of an inhibitory and inflammatory environment decreasing the chances of axonal regeneration. Recently, several studies from our group demonstrated that ASC secretome can induce immunomodulation and tissue regeneration in *in vitro* cell culture and *in vivo* SCI models. However, the appropriate concentration of ASC secretome to obtain a therapeutic effect after SCI still needs to be clarified. Thus, this thesis aimed to bring some insights about the potential of different concentrations of ASC secretome in a SCI context. For that, two main objectives were established:

1. **Assessment of the immunomodulatory properties of different concentrations of ASC secretome in *in vitro* cultures of human microglial cells.**
2. **Evaluation of the therapeutic efficacy of different dosages of ASC secretome in a SCI mouse model.** As an *in vivo* proof-of-concept, the effect of different dosages of ASC secretome at the functional and sensory level was analyzed, using a SCI mouse transection model. Following the *in vivo* experiment, immunohistochemistry analyses of the spinal cord tissues were performed to study the inflammation and neuroregeneration profiles in response to different treatments.

The determination of the therapeutic dosage of ASC secretome can contribute to a reduction of production costs and time, which will be essential for possible application of this treatment into the clinical practice.

Chapter III - MATERIALS AND METHODS

1. ASC culture

Human ASCs were gently provided by Professor Jeffrey Gimble (LaCell LLC, New Orleans, Louisiana, USA). They were collected from human lipoaspirates following the protocol of Dubois et al. (Dubois et al., 2008).

ASCs were thawed and seeded in a T175 flask with ASC medium: Minimum Essential Medium α (α-MEM, Thermo Fisher Scientific), supplemented with sodium bicarbonate (Sigma, 2.2 g/L), 10% fetal bovine serum (FBS, Sigma) and 1% antibiotic solution [penicillin-streptomycin (Pen-Strep), Thermo Fisher Scientific] (Figure 6). Once 80-90% confluence was reached, cells were separated from the flask surface using trypsin-Ethylenediaminetetraacetic acid (trypsin-EDTA, 0.05%, Thermo Fisher Scientific). Afterwards, α-MEM with FBS was added to the cells in order to inhibit trypsin enzymatic activity. The cellular suspension was centrifuged forming a supernatant and a pellet that contained the ASCs. The supernatant was discarded, while the pellet was resuspended with fresh α-MEM and placed in the flask at a density of 4 000 cells/cm^2. ASC culture was maintained at 37 °C and 5% carbon dioxide (CO_2) changing the medium every 2 or 3 days.

2. Collection of secretome

ASCs at passage 6 (P6) were maintained in α-MEM and incubated in the same conditions aforementioned, for 72 hours (h). Afterwards, the medium was removed, and the cells were washed 4 times with phosphate-buffered saline (PBS) without calcium (Ca^{2+}) and magnesium (Mg^{2+}) ions (Thermo Fisher Scientific) (Figure 6). This step is crucial for the removal of FBS-derived proteins and other compounds that can contaminate the conditioned medium (CM). Following the washing step, cells were incubated with Neurobasal A medium (NbA, Thermo Fisher Scientific) with 1% Kanamycin (Thermo Fisher Scientific) to be used in the *in vivo* experiment. For the *in vitro* experiments, cells were incubated with Dulbecco's Modified Eagle Medium: Nutrient Mixture F-12 (DMEM-F12, Thermo Fisher Scientific) with 1% Pen-Strep. The conditioning protocols occurred for 24 h, at 37 °C and 5% CO_2. During this conditioning period, ASCs secreted factors and vesicles to the medium forming the CM, which was collected and centrifuged at 249 g for 5 minutes to separate the supernatant from dead cells and other particles. Finally, the CM was subjected to a freezing step, involving liquid nitrogen, and stored at -80 °C for posterior application.

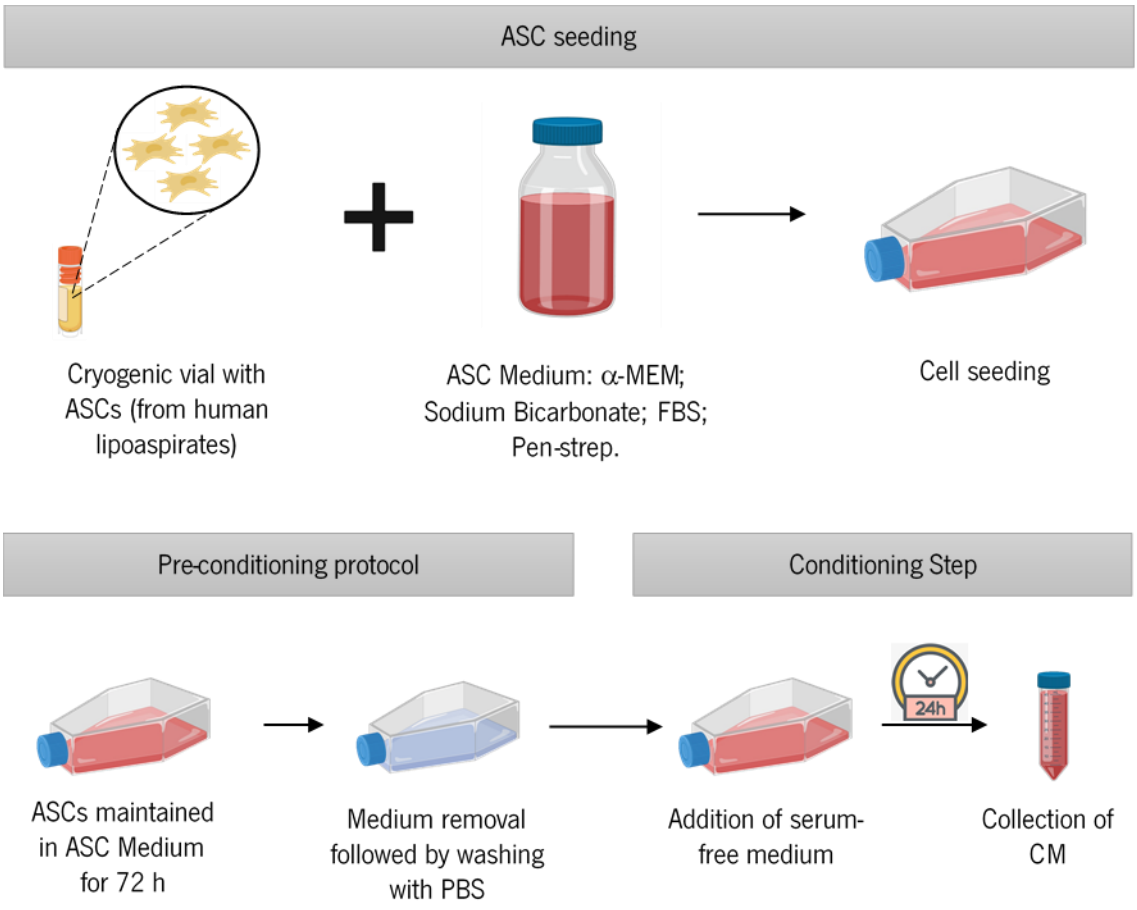

Figure 6. Schematic representation of the conditioning protocol to obtain ASC secretome from cell culture. This protocol started by the incubation of ASCs (passage 6) with ASC medium for 72 h. After this, the medium was removed and, subsequently, PBS was added to wash the cells. Finally, in the conditioning step, the NbA medium was added and, after 24 h, it was collected for posterior experiments.

3. Preparation of secretome

The CM previously collected was concentrated through a centrifugal filtration, by a factor of 100x using a filter with a cut-off of 5 kDa (Vivaspin, GE Healthcare, Figure 7). The fraction of CM with a molecular weight above 5 kDa was collected and further diluted to 1x, 25x and 50x, with the serum-free media, such as DMEM-F12 or NbA. For the negative control group, DMEM-F12 or NbA was used at 100x concentration. Finally, all biological samples were frozen in nitrogen liquid and preserved at -80° C.

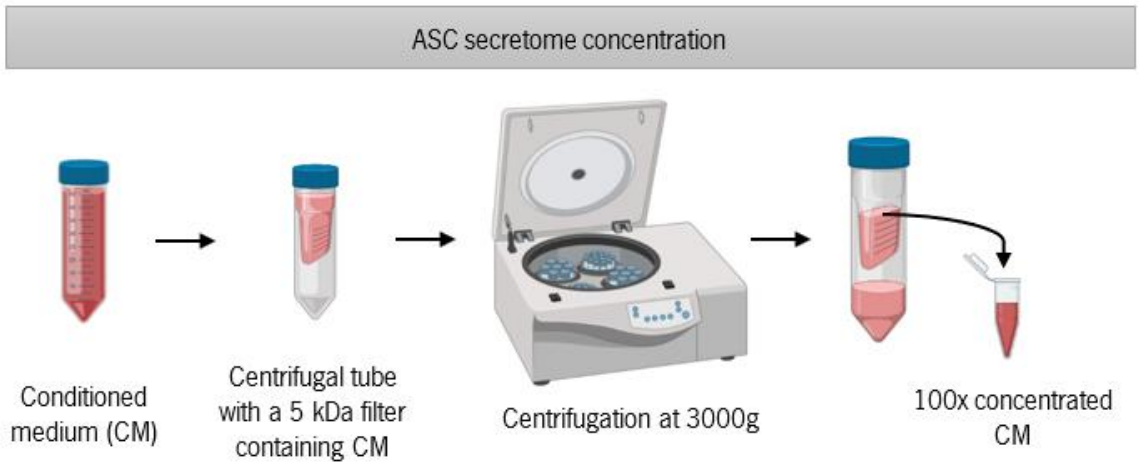

Figure 7. An illustrative scheme of the secretome concentration protocol. This protocol consisted of multiple centrifugations of ASC secretome using a tube with 5 kDa filter. All the secretome samples were concentrated 100x and then diluted to the respective concentration (1x, 25x and 50x).

4. *In vitro* experiment

4.1. Culture of human microglial cells

A human microglial cell line, HMC3, was used for the assessment of the immunomodulatory activity of different concentrations of ASC secretome. HMC3 cells were thawed and cultured in a T75 flask with complete microglia medium containing Dulbecco's Modified Eagle Medium, Nutrient Mixture F-12 (DMEM-F12; Thermo Fisher Scientific) supplemented with L-glutamine (2mM, Thermo Fisher Scientific), 1x non-essential aminoacids (Thermo Fisher Scientific), 10% fetal calf serum (FCS; Biochrom), 1% Pen-Strep (Thermo Fisher Scientific), sodium pyruvate (1mM, Thermo Fisher Scientific) and sodium bicarbonate (1.5 g/L, Sigma). These cells were maintained at 37 °C and 5% CO_2 changing the medium every 2 days. When 80-90% confluence was reached, the cells were washed with PBS without Ca^{2+} and Mg^{2+} and detached with trypsin-EDTA. The centrifugation of cells was performed at 249 g for 5 minutes, forming a pellet that was resuspended in the complete microglia medium.

4.2. Microglia stimulation and treatments

HMC3 cells were seeded in a 12-well plate at a density of 2 x 10^5 cells/cm^2 and maintained in the microglia medium for 24 h. In order to produce a microglial activation response, they were stimulated with IFN-γ (20 ng/mL, Peprotech) and lipopolysaccharides (LPS, 100 ng/mL, Sigma) for 6 hours (Figure 8). Three biological samples of microglial cells were not stimulated to be used as a stimulation negative control. Next, medium removal was proceeded followed by the addition of DMEM-F12 or ASC secretome in different concentrations. Based on the added medium type, 4 experimental groups were

formed: 1 - Treated with 1x concentrated DMEM-F12 (the negative control of the medium); 2 - Treated with 1x secretome; 3 - Treated with 25x secretome; 4 - Treated with 50x secretome. Each group contained three biological samples. Lastly, the incubation of HMC3 cells with the secretome occurred for 24 h (Figure 8).

4.3. RNA Extraction and quantification

After treatments, cell lysis and subsequent extraction of their intracellular contents were performed by applying 100 µL of TripleXTractor (Grisp) per cm^2 in each well, and the extracts were frozen at -80 °C for later use. RNA extraction was carried out according to the company's protocol, starting by mixing the cell lysates with chloroform. The mixture was centrifuged to separate into three phases: 1 – The upper aqueous phase containing RNA; 2 – The interphase containing DNA; 3 – The lower organic phase with proteins and lipids. The upper phase with RNA was transferred to an RNase-free eppendorf tube and mixed with isopropanol, contributing to RNA precipitation. With the centrifugation (13 000 g), the pellet with RNA was formed and then resuspended in the ethanol 70% solution, removing impurities. After another centrifugation step (13 000 g), ethanol was removed, and the RNase-free water (Grisp) was added to dissolve the RNA. RNA quantification was carried out using the NanoDrop 1000 spectrophotometer (ThermoFisher Scientific).

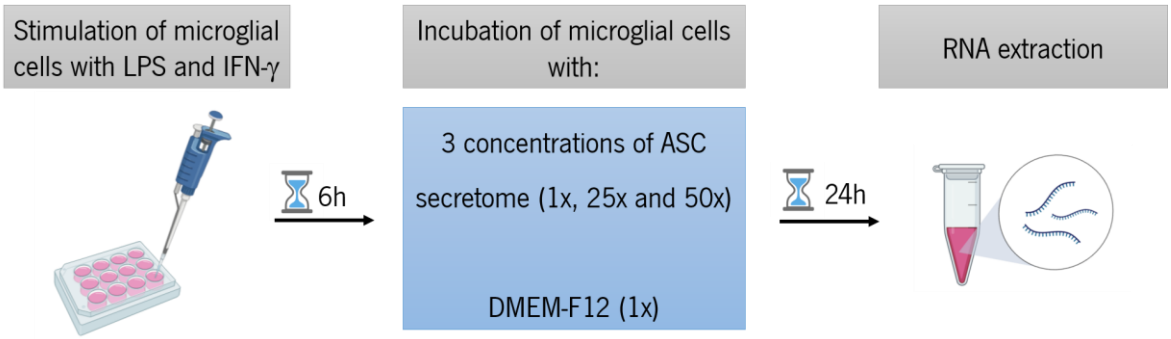

Figure 8. Representative scheme of the *in vitro* experiment of microglia. The first step consisted of 6 h of stimulation of microglial cells (from HMC3 cell line) with LPS (100 ng/µL) and IFN-γ (20 ng/µL). In the second step, microglia were incubated with different mediums [3 concentrations of ASC secretome (1x, 25 and 50x) or DMEM-F12 (1x concentrated)] for 24 h. Finally, the RNA was extracted from microglia following the company's protocol.

4.4. RT-qPCR

Quantitative Reverse Transcription-Polymerase Chain Reaction (RT-qPCR) comprises the reverse transcription step and the qPCR, allowing the amplification and quantification of the target (Nolan et al., 2006). Firstly, the RNA is converted into the complementary DNA (cDNA) template through the

reverse transcription. Secondly, the cDNA obtained is amplified in the presence of a fluorescent dye, which intercalates the double-stranded DNA. Thus, every time the copy number of cDNA increases, the fluorescence signal of the dye increases as well allowing the quantification of the mRNA relative levels (Nolan et al., 2006).

For the synthesis of cDNA, 1 μg of sample was used. Following the instructions of the manufacturer, the synthesis of cDNA from mRNA samples was performed with Xpert cDNA synthesis SuperMix (with gDNA eraser) (Grisp) in the T100 Thermal Cycler (Biorad).

The immunomodulatory properties of ASC secretome were analyzed through the quantification of human *IL-4* and *IL-6* mRNA relative levels. For that, Xpert Fast SYBR Blue (Grisp), together with water and primers of each gene (Table 2), was added to each well of the 96-well plate. Then, RT-qPCR reaction was performed using SYBR Blue dye as a fluorescent signal in the 7500 Real-Time PCR System (ThermoFisher Scientific). The expression levels of *IL-6* and *IL-4* of each experimental condition were normalized to each housekeeping gene (*GAPDH*) and represented as fold expression in comparison to DMEM 1x group. The $2^{-\Delta\Delta CT}$ method was adopted to calculate the fold change expression of *IL-6* and *IL-4*.

Table 2. Forward and reverse sequences of oligonucleotide primers of human *IL-6*, *IL-4* and *GADPH* genes for the RT-qPCR. The sequences are represented in 5'-to-3' direction.

Gene	Forward Sequence (5'→3')	Reverse Sequence (5'→3')
IL-6	CCA CAC AGA CAG CCA CTC ACC T	TTTCACCAGGCAAGTCTCCTCAT
IL-4	GCA GCT GAT CCG ATT CCT GA	TCC AAC GTA CTC TGG TTG GC
GADPH	ACA TCA AGA AGG TGG TGA AGC AGG	AGC TTG ACA AAG TGG TCG TTG AGG

5. *In vivo* experiment

5.1. Animals and housing

The Ethical Subcommittee in Life and Health Sciences (SECVS; ID: 018/2019, University of Minho) gave the authorization for the *in vivo* experiments, which were performed according to the local regulations on animal care and experimentation (European Union Directive 2010/63/EU). C57BL/6J mice (Charles River) were produced and maintained inside of the animal house facilities of the Institute of Life and Health Sciences. Six animals were housed in cages, with 12 hours light/dark cycle and controlled temperature and humidity. Each cage contained soft paper for nesting and unlimited access to water and food. When the age of 12-14 weeks was reached, female C57BL/6J mice were selected for surgery.

5.2. Preparation for surgery

One week prior to the surgery, the animals were handled in order to become familiar with human presence and reduce their stress levels on the surgery day. Additionally, mice were identified with marks in the tail and weighted for the administration of the appropriate doses of anesthetic and analgesic drugs.

5.3. SCI surgery

Twelve weeks old female C57BL/6J mice were prepared for surgery being anesthetized with an intraperitoneal injection of Ketamine (Imalgene, 75 mg/kg, Merial) and Medetomidine hydrochloride (Dormitor, 1 mg/kg, Pfizer). They were also injected with a subcutaneous injection of the analgesic Buprenorphine (Bupaq, 0.1 mg/kg, Richter Pharma AG) to minimize pain during the procedure. As a consequence of anesthesia, animals presented decreased body temperature and loss of the reflex blink. Therefore, mice were placed under a red light to avoid hypothermia, and vaseline was applied to their eyes avoiding eye drying. Following this, the fur of the surgical site located in the dorsal thoracic area was partially shaved and disinfected with chlorhexidine.

The surgery started with a dorsal incision from T2 to T10 thoracic level in the skin and, consequently, the retraction of paravertebral muscles exposing the spinal column. The removal of the laminar arch and spinous processes of thoracic vertebrae (T8 and T9) was performed allowing the visualization of the spinal cord. At T8 level, the spinal cord was completely cut (transection) with microdissection scissor (Figure 9. A).

After the surgery, Vicryl sutures (Johnson and Johnson) were used for skin closure of mice. Atipamezol (Antisedan, 1mg/kg, Orion Corporation) was administered subcutaneously to reverse the anesthetic effect. Then, animals were rehoused in individual new boxes, in pairs, separated by a transparent acrylic wall with small holes on it, avoiding biting of the sutures, but allowing some contact through odor exchanges. Hydrogel and moisturized food were placed on the floor to facilitate access to food and water.

Since the SCI surgery is considered severe, the animals took intense post-operative care in the following 5 days consisting in: administration of a solution containing the analgesic Buprenorphine (0.05 mg/kg, Richter Pharma AG), the antibiotic enrofloxacin (Baytril, 5 mg/kg, Bayer), vitamins (10 mg/kg; Duphalyte, Pfizer) and a saline solution (0.9% sodium chloride, NaCl) twice a day; manual voiding of the bladders, twice a day, due to their lost ability to urinate; moderate heating of their bodies with a red light (in case of hypothermia). Every day, the animal welfare was evaluated in different parameters: body weight, urine and feces condition, behavior, activity, temperature, autophagy, and scar condition. One-week post-surgery, mice were placed together, encouraging socialization as well as decreasing their stress levels.

5.4. Treatments

After the SCI surgery, the animals were randomly divided into 4 groups. Animals of group 1 were administered with vehicle (NbA medium), whereas animals of groups 2, 3 and 4 received secretome of different concentrations, namely 1x, 25x and 50x. With a 26 g needle, 100 µL of secretome or vehicle was injected intravenously into the tail vein of mice, at 10 different time points: half an hour after the injury, 1 and 2 days post-injury and once a week for 7 weeks (Figure 9. B).

5.5. Motor and sensory evaluation

5.5.1. Basso Mouse Scale test

Basso Mouse Scale (BMS) test is a gold standard paradigm designed for the assessment of the locomotor function of SCI mice (Hau & Schapiro, 2013). This test took place in an open arena (Figure 9. C), where mice were placed and evaluated by two trained researchers for 4 minutes (blinded to the treatments). The evaluation of the locomotor function of hindlimbs was made according to an established score table which extends from 0 (no voluntary movement) to 9 (normal plantar stepping with coordination and trunk stability) (Basso et al., 2006). This table attributes a classification to several physical features, comprising ankle movement, plantar and dorsal stepping with weight

support, coordination, rotation of hindlimbs and trunk stability (Annex 1). This test was performed 3 days post-injury and once a week for 7 weeks (Figure 9. B), analyzing the locomotor recovery of each hindlimb. As a criterion of exclusion, every mouse with a score equal or higher to 1 in the first assessment was removed from the analysis, since most likely the transection was not performed correctly.

5.5.2. Open Field test

Gross locomotor function and exploratory activity were evaluated using the Open Field (OF) test (Carter & Shieh, 2015). For the evaluation, mice were placed in the center of the square open field with infrared beams and explored the cage for 5 minutes (Figure 9. C). Infrared beams are connected to a computer that records locomotor aspects of the animal over time, including vertical counts (rearings) and total distance. As depicted in Figure 9. B, this test was performed at week 8 after the surgery.

5.5.3. Gait analysis

Gait analysis was performed to provide more detailed information about a set of kinematic parameters that were not evaluated by the BMS test, including body and tail height (the distance between the body/tail surface and the ground), step angle (the angle of the paw during stepping) and step length. In the last week of the *in vivo* experiment, mice walking was recorded by a camera capturing around 6-7 successive steps in lateral view (Figure 9. C). During the test, mice moved three times to the right and left on the platform. A card with a known size (e.g. card length) was also included in the video track to be used later for software calibration. The kinematic parameters were analyzed with Kinovea analysis software.

5.5.4. Beam Balance

The Beam Balance (BB) test was designed specifically to analyze the motor coordination of animals with motor deficits (Brooks & Dunnett, 2009). The beam balance apparatus consists of two high supports with platforms, a closed box and several beams of different diameters and shapes. The animals were placed on one of the platforms so that they could cross the beam until they reached the closed box, which is considered a safe place for them (Figure 9. C). Before the test, it was necessary to train the animals 3 times on a 12 mm square beam. Seven weeks after injury, mice performed the test, crossing 2 times on each of 4 beams (2 round beams with 10 mm and 28 mm; 2 square beams with 12 mm and 27 mm). While the animals were crossing the beam, they were evaluated and given a score that goes from 1 (corresponding to the incapacity of crossing the beam) to 9 (corresponding

to the ability to traverse the beam normally using both hindlimbs) (Annex 2). These scores were given based on an adapted scale (Carter et al., 2001).

5.5.5. Manual Von Frey test

Manual Von Frey (VF) test is used to test mechanical allodynia, which is the pain resulting from hypersensitivity to an usually harmless stimulus (Deuis et al., 2017). At week 8 of the experiment, this test was performed, immobilizing the animals with a small cage and placing them on a grid through which the filaments placed (Figures 9. B and 9. C). This test consisted of the application of Von Frey filaments of different thicknesses in the rodent paws. In the case of a mouse, 9 filaments of distinct thicknesses, which vary between 0.008 g and 1.4 g, were used. The test started by the perpendicular application of the middle filament of 0.16 g, and then the type of filament was changed gradually based on the mice response to the stimulus. For instance, if the mouse reacted to the stimulus exerted by the filament, the following filament to be applied was of a smaller thickness. If the opposite (non-response to the stimulus) occurred, a thicker filament was applied. The test only finished when the mouse exhibited the same paw reaction five times after the threshold or when the last filament (0.008 g or 1.4 g) was applied. With this test, the pattern of responses of the animal and the last filament were obtained and registered, being used later for the determination of a 50% threshold. In order to calculate the threshold, the formula, $g = \frac{10^{X+k.d}}{10^4}$, was used, where X and k represent respectively the number of the final filament and the defined value that corresponds to the response sequence, while d is the value of average increase from one filament to another (Chaplan et al., 1994).

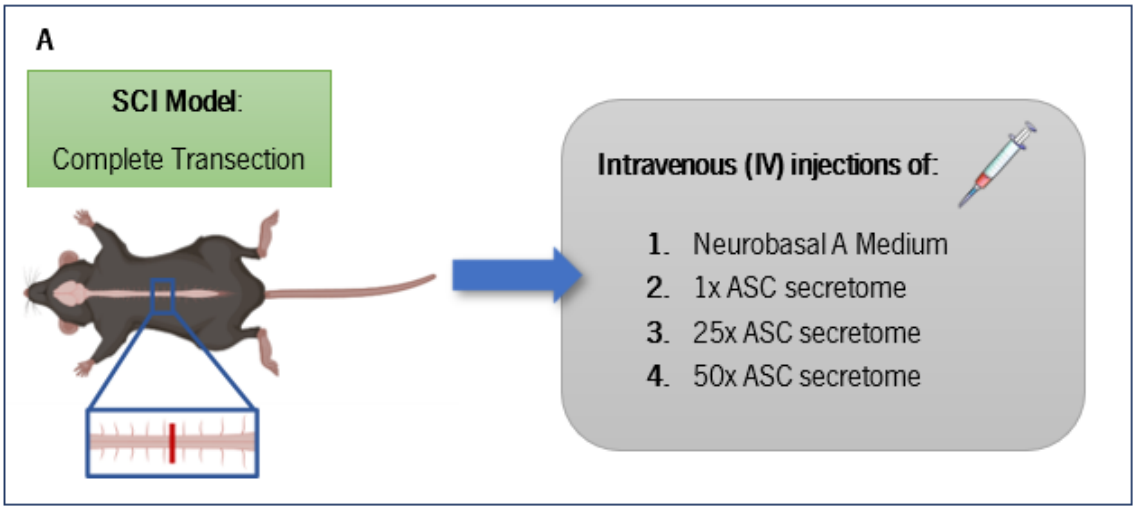

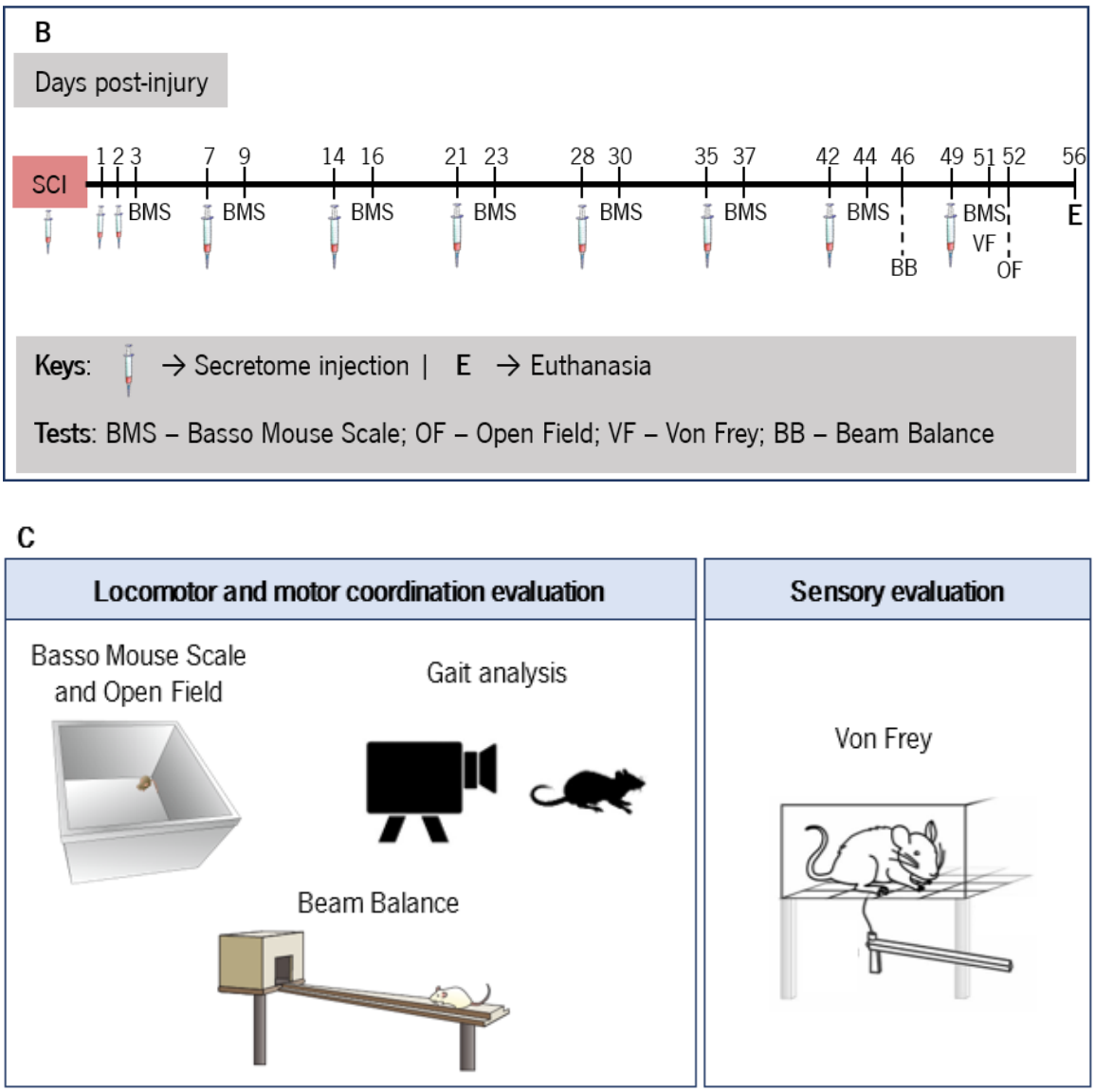

Figure 9. Experimental design for *in vivo* experiment. A. Scheme of spinal cord surgery followed by IV injections: the spinal cord was completely cut (transection) at thoracic level with microdissection scissor. | B. Timeline of the *in vivo* experiment: a total of ten IV injections were administered into the animals, three in the first 2 days after the injury and then once a week. BMS was performed on the third day after the injury and once a week until the eighth week. Other tests (BB, VF and OF) were performed in the last two weeks. | C. Representations of tests that allowed to assess locomotor (left rectangle) and sensory function (right rectangle).

5.6. Euthanasia and collection of the spinal cord

Two months post-injury, mice were euthanized in order to collect their spinal cord for posterior histological analysis. For that, a lethal dose of anaesthetic containing Ketamine (Imalgene, 150 mg/kg, Merial) and Medetomidine hydrochloride (Dormitor, 2 mg/kg, Pfizer) was administered to all animals. After having no response to tail and paws pinching, mice were opened with a ventral incision before the heart stopped. The transcardiac perfusion of mice was processed inserting a syringe with saline solution (0.9% NaCl) into the heart aorta to remove the blood from the circulation, and then with

paraformaldehyde (PFA, 4%). Finally, a dorsal incision was made for the collection of vertebral columns.

6. Cryopreservation protocol and sectioning

After the dissection of vertebral columns, the spinal cords were fixed with PFA (4%) for 24 h at 4 °C. For the tissue fixation, PFA reacts with side groups that contain amines and/or active hydrogen, establishing cross-links with proteins and nucleic acids (Daneshtalab et al., 2010). At the end of this time, the spinal cords were dehydrated in a hypertonic solution (30% sucrose in PBS 1x) to avoid ice crystal formation in the tissue after freezing. When the tissues reached a saturated point, they were removed from sucrose solution and cut in 2 cm fragments centered in the lesion. These spinal cord segments were embedded in a cryoprotective medium (optimal cutting temperature, Sakura Tissue Tek) and frozen in isopentane and liquid nitrogen. Next, the tissue was cut in 20 μm longitudinal sections using a Leica CM 1900 cryostat. Tissue sections were collected with SUPERFROST PLUS® slides (Thermo Fisher Scientific) that can bind electrostatically the frozen tissues to reduce tissue loss. In the end, the samples were stored in the freezer at -20 °C.

7. Immunohistochemistry

Immunostaining of spinal cord sections was performed to study alterations in neuroregeneration (β-tubulin III) and neuroinflammation [Iba1 (Ionized calcium binding adaptor molecule 1) and GFAP]. The first day of the immunohistochemistry (IHC) protocol started by cellular membrane permeabilization, adding a non-ionic detergent (0.2% Triton X-100; Sigma) in PBS over the slides. After this, the tissue sections were washed 3x with a PBS solution at room temperature (RT) for 3 minutes. Before the antibody addition, tissue blocking took place, adding a solution containing 5% FCS and 0.2% Triton X-100 in PBS, over the slides for 30 minutes at RT.

Following the blocking step, spinal cord sections were incubated overnight with primary antibodies, namely rabbit anti-Iba1 (0.5 μg/mL, Fujifilm Wako), rabbit anti-GFAP (14.5 μg/mL, Dako) and rabbit anti-β-tubulin III (4 x 10^{-5} μg/mL, Abcam). On the next day, tissue sections were washed 3x with PBS for 3 minutes, followed by an incubation with a solution containing a secondary antibody labelled with

a specific fluorophore. Alexa Fluor 488 goat anti-rabbit (2 μg/mL, Thermo Fisher Scientific) was conjugated to all primary antibodies used.

After 2 hours of incubation with secondary antibodies, a counterstaining of tissue sections with 4′,6-Diamidino-2-phenylindole dihydrochloride (DAPI, Sigma) occurred for 10 minutes in order to visualize cell nuclei. Next, the slides were washed 3-5x with PBS and mounted in the aqueous reagent Permafluor (Thermo Fisher Scientific) to attenuate fluorescence fading.

7.1. Fluorescence microscopy

After the IHC protocols, spinal cord slice images were obtained with Olympus XM10 camera coupled to a widefield inverted microscope, Olympus IX53, using the Stage Navigator tool of cellSens software (Olympus). In each mouse, the whole spinal cord section was photographed with a 10x objective for Iba-1, GFAP and β-tubulin III.

For microglia process reconstruction, left and right sides of four spinal cord regions (rostral, rostral/epicenter, caudal/epicenter and caudal) were photographed with Olympus FV1000 confocal laser scanning microscope. The photos were taken with a resolution of 800 x 800 pixels and 40x objective.

7.2. Image Analysis:

7.2.1. Quantification of staining area

The photos obtained from the widefield inverted microscope were processed and analyzed to quantify areas marked by the antibody, using the Image J software (NIH). The quantification was performed for the whole spinal cord and individually for 3 different regions (caudal and rostral to the injury, and at the injury epicenter). Firstly, the scale was defined according to the magnification used to photograph the spinal cord section. The images were transformed into RGB color and then to 8-bit grayscale. In order to better define the specific staining of the antibody, some settings were optimized, such as threshold levels and/or image contrast. Afterwards, the processing of the images was performed using the command “make binary”, in which the specific staining was dyed as black and the background as white. Finally, the areas marked in black were measured by using the command “analyze particles”. From this quantification, the values were averaged and normalized by dividing their means with the total area of analysis.

7.2.2. Simple Neurite Tracer - microglia process reconstruction

For the accurate assessment of microglial complexity on the spinal cord, Z-stack confocal pictures of spinal cord slice labelled for Iba-1 underwent microglial processes reconstruction in the FIJI software (NIH). Four microglial cells were selected randomly in 4 spinal cord regions (rostral, rostral/epicenter, caudal/epicenter and caudal), giving a total of sixteen cells per slice. The selection of these cells was performed respecting the exclusion criteria, such as DAPI stained nucleus surrounded by a structure labelled for Iba-1 and absence of truncated processes. The reconstruction of microglial processes was performed using the plugin Simple Neurite Tracer (SNT) as previously described (Tavares et al., 2017). For the reconstruction, the RGB images were firstly converted to 8-bit luminance (Figures 10. A and 10. B) and then, the center of DAPI labelled nuclei was defined as the starting point from which the main paths ramified. After this, the main paths were built through the selection of several points along the microglial process that were joined in a semi-automatic way by the program, respecting the process path. For the Sholl analysis, the center of the nucleus was defined as the starting point and all paths drawn were selected (Figure 10. B). From that focal point, several concentric circles were automatically formed with a radius step size of 4 µm necessary to obtain detailed information on the morphology complexity (Figure 10. C). The number of paths that intersected every sphere of a given radius was calculated.

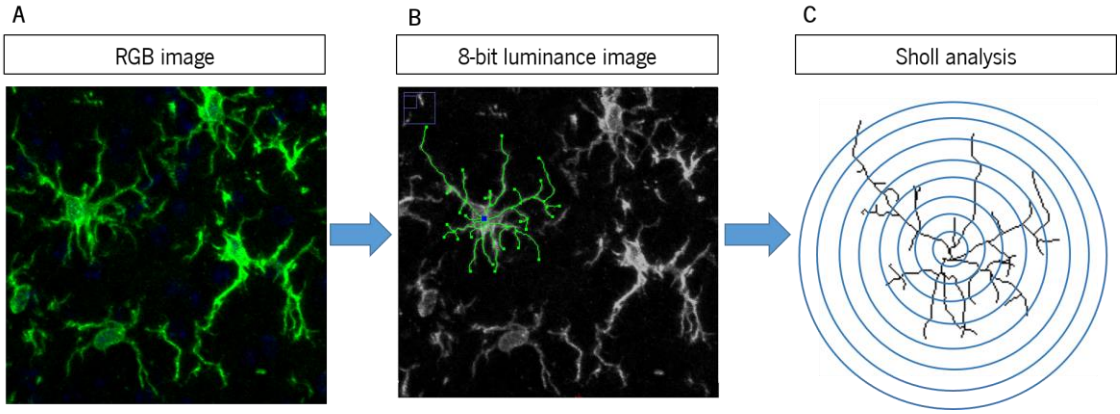

Figure 10. Reconstruction of microglia morphology and Sholl analysis using the plugin SNT. (A) Z-stack confocal picture in the RGB format uploaded to Fiji software. (B) Conversion of RGB to 8-bit luminance image. For Sholl analysis, all traced paths (green) were selected, and the nucleus center was defined as the starting point (blue). (C) Representation of the drawn skeleton with concentric circles originating from the soma with a radius step size of 4 µm.

7.3. Statistical analysis

GraphPad Prism version 8.0.1 for Windows (GraphPad Software) was used to make the statistical analysis. Before applying parametric tests, certain requirements were confirmed, such as homogeneity

of variances and normal distribution. Normal distribution of data was evaluated through the Kolmogorov-Smirnov test, Shapiro-Wilk test, skewness, kurtosis and histogram. Equality of variances and sphericity were evaluated using the Levene's and Mauchly's tests, respectively. Regarding the statistical tests, unpaired t-test was applied to compare mean values between non-stimulated and stimulated groups (both treated with DMEM-F12 1x) in the *in vitro* experiment of microglia. In addition to this, Welch's ANOVA was performed to compare stimulated groups. The comparison of mean values between several groups was accomplished using one-way ANOVA for results from Open Field, Von Frey, Beam Balance, gait analysis and IHC analyses. Two-way repeated measures ANOVA was applied to results of BMS and Sholl analysis of microglia. For multiple comparisons between groups, the Tukey statistical test was used. The calculation of several effect sizes was performed, such as: η^2 (eta squared), η^2_p (partial eta squared) and d (Cohen's d). Statistical significance was considered if p-value ≤ 0.05. All results presented in the tables were expressed as mean ± SD (standard deviation), with 95% confidence interval.

Chapter IV - RESULTS

1. *In vitro* study: The effect of different concentrations of ASC secretome on inflammation

This *in vitro* experiment aimed to elucidate the differential effect of three concentrations of ASC secretome on activated microglia. For that, *in vitro* cultures of a human cell line (HMC3) were firstly stimulated with LPS and IFN-γ and then, incubated with 1x concentrated DMEM (vehicle control) or different concentrations of ASC secretome (1x, 25x and 50x). As a negative control, non-stimulated cells were incubated with 1x concentrated DMEM (NS DMEM 1x). Following this, the expression of inflammation-associated genes, *IL-6* and *IL-4*, was analyzed through RT-qPCR reaction for all experimental conditions. In comparison to NS DMEM 1x group, stimulated DMEM 1x group (S DMEM 1x) seems to present a higher expression of *IL-6* and a lower expression of *IL-4* (Figure 11. A; Table 3). However, different treatments appear to not influence both *IL-6* and *IL-4* expression, when compared to DMEM 1x group (Figure 11. B; Table 4). It is important to highlight that these results are preliminary and, therefore, they must be carefully interpreted, due to the low number of samples per group.

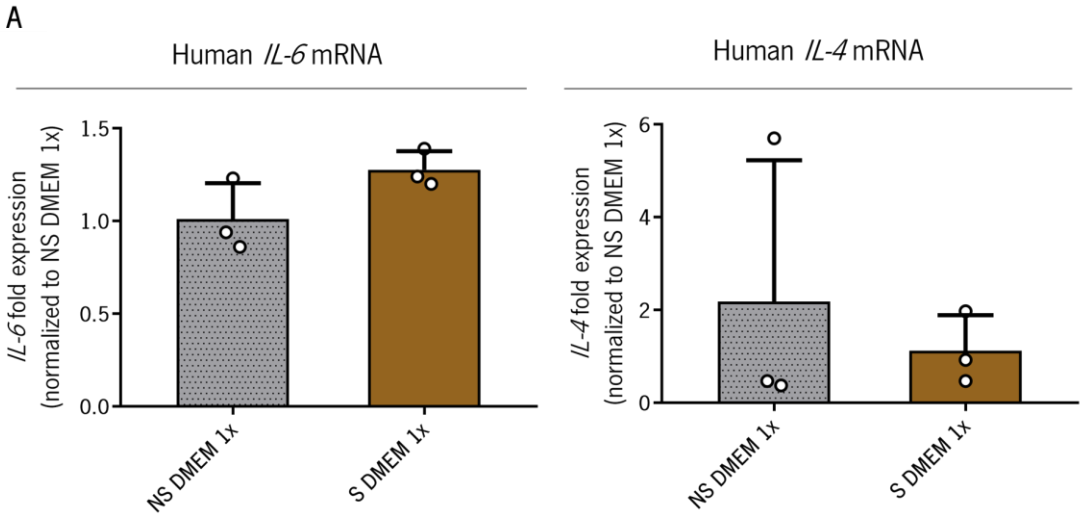

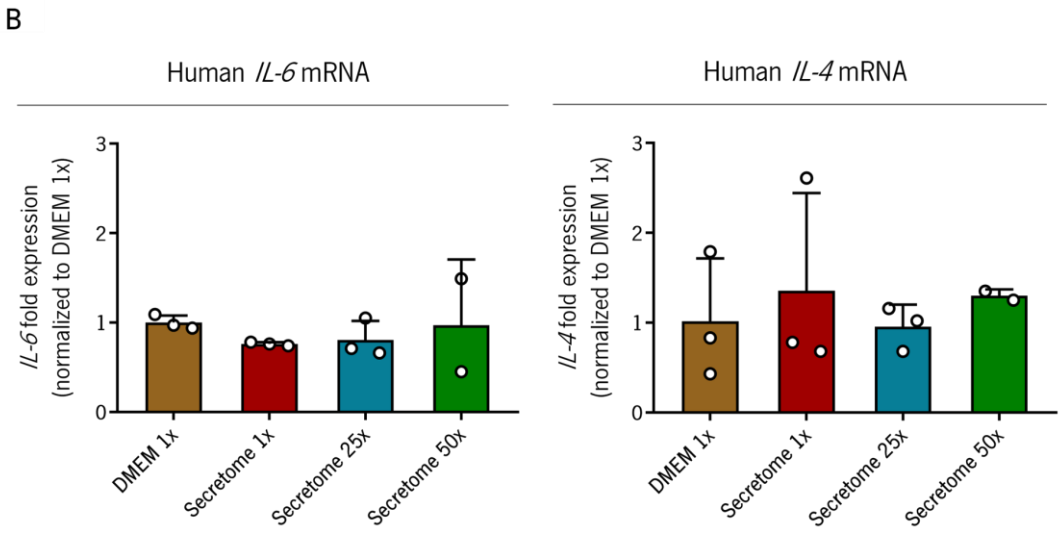

Figure 11. Expression analysis of *IL-6* and *IL-4* genes of human microglia. (A) Non-stimulated and stimulated cells incubated with the vehicle medium, DMEM 1x. (B) Stimulated cells incubated with DMEM 1x or different concentrations of ASC secretome. The genetic expression of both genes in all experimental conditions was normalized to the housekeeping gene, *GAPDH* and represented as fold expression in comparison to the NS DMEM 1x (in panel A) and DMEM 1x (in Panel B) groups. Results are derived from one independent experiment (n=2-3 biological samples/group). Data are represented as mean ± SD.

Table 3. Relative genetic expression of inflammation-associated genes, *IL-6* and *IL-4*, in non-stimulated (NS DMEM 1x) and stimulated (S DMEM 1x) microglial cells. Data are presented as mean ± SD.

Treatments / Gene	NS DMEM 1x	S DMEM 1x	Statistical test, Significance, effect size
IL-6	1.01 ± 0.19	1.28 ± 0.10	t (4) = 2.11 p = 0.10 d = 1.74
IL-4	2.18 ± 3.05	1.12 ± 0.77	t (4) = 0.59 p = 0.59 d = 0.48

Table 4. Relative genetic expression of inflammation-associated genes, *IL-6* and *IL-4*, in microglia previously stimulated with LPS and IFN-γ, and representation of statistical analysis. Data are presented as mean ± SD.

Treatments / Gene	DMEM 1x	Secretome 1x	Secretome 25x	Secretome 50x	Statistical test, significance
IL-6	1.00 ± 0.079	0.76 ± 0.020	0.80 ± 0.21	0.97 ± 0.74	W (3.00, 2.58) = 5.72 p = 0.11
IL-4	1.02 ± 0.70	1.34 ± 1.09	0.95 ± 0.25	1.30 ± 0.070	W (3.00, 3.58) = 1.37 p = 0.38

2. *In vivo* study: The effect of different dosages of ASC secretome on motor and sensory recovery of SCI mice

2.1. BMS test

Following a transection SCI in mice, different ASC secretome concentrations and vehicle were administered intravenously at specific time points. For the evaluation of the locomotor recovery in SCI mice, the BMS test was performed three days post-injury and once a week for seven weeks. In this test, the locomotor function of mice hindlimbs was assessed according to a score table (Annex 1). Three days post-injury, the animals presented limited movement, exhibiting lower limb paralysis. In the following week, SCI mice treated with 25x and 50x secretomes displayed an improvement of hindlimb locomotor function. Nevertheless, statistical differences were only found 16 days after injury, when comparing 25x (p=0.003) and 50x (p=0.031) secretome groups with Neurobasal A group. At the same time, the BMS scores of 25x and 50x secretome groups also differed significantly from the scores of 1x secretome group (p=0.003; p=0.031, respectively). On day 23 after injury, animals treated with 25x concentrated secretome presented a significant locomotor recovery in comparison to the Neurobasal A group (p=0.031). It is noteworthy to mention that the BMS scores of 25x and 50x secretome groups were significantly higher than 1x concentrated secretome on days 23 (p=0.002; p=0.023), 30 (p=0.0006; p=0.002) and 37 (p=0.015; p=0.031) post-injury. Interestingly, the locomotor function of the Neurobasal A group started to improve 16 days after injury, showing a significant locomotor recovery when compared to 1x secretome group on day 30 post-injury (p=0.038). At the end of the experiment, animals treated with 25x and 50x concentrated secretomes reached an

average BMS score of 2.5 and 2.6, respectively, which indicated that they were able to perform plantar placement. At the same time, the other two groups (secretome 1x and neurobasal A) presented average scores of 2 and 1.86, which only reflect the ability to perform extensive ankle movement (Figure 12; Table 5). Additional tables show the variation of BMS scores from the different treatment groups at eight time points and the statistical analysis of these data (Tables 5 and 6).

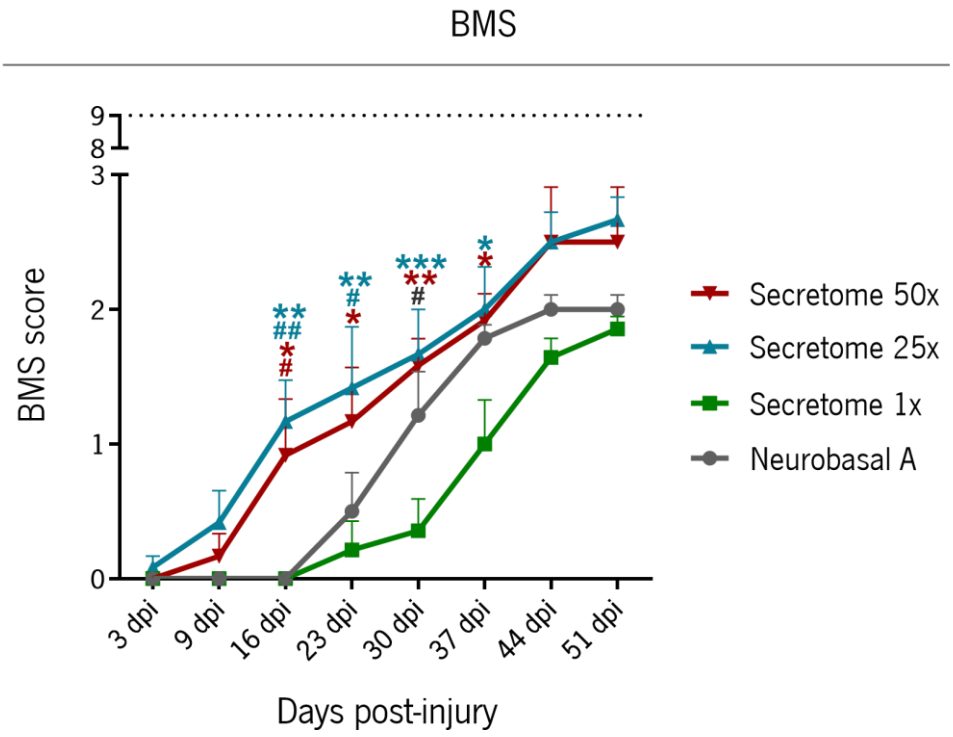

Figure 12. Locomotor recovery of transected animals subjected to several administrations of Neurobasal A or distinct concentrations of ASC secretome (1x, 25x and 50x). Asterisk (*) represents statistical significance for comparisons between secretome groups. Hash sign (#) represents statistical significance for comparisons between Neurobasal A and secretome groups. Blue symbols – Comparisons of 25x secretome with other groups (1x secretome or NbA); Red symbols - Comparisons of 50x secretome with other groups (1x secretome or NbA); Grey symbol – Comparison of NbA with 1x Secretome. dpi – days post-injury. Data are presented as mean ± SEM (standard error of the mean); *one symbol $p \leq 0.05$; **two symbols $p \leq 0.01$; ***three symbols $p \leq 0.001$; n=6-7 animals/group.

Table 5. BMS score variation for all experimental groups over seven weeks. Data are represented as mean ± SD.

TREATMENTS		DAYS POST-INJURY							
		3	9	16	23	30	37	44	51
MEAN ± STANDARD DEVIATION	Neurobasal A	0	0	0	0.50 ± 0.76	1.21 ± 0.86	1.79 ± 0.27	2.00 ± 0.29	2.00 ± 0.29
	Secretome 1x	0	0	0	0.21 ± 0.57	0.36 ± 0.63	1.00 ± 0.87	1.64 ± 0.38	1.86 ± 0.24
	Secretome 25x	0.083 ± 0.20	0.42 ± 0.59	1.17 ± 0.75	1.42 ± 1.11	1.67 ± 0.82	2.00 ± 0.78	2.50 ± 0.55	2.67 ± 0.41
	Secretome 50x	0	0.17 ± 0.41	0.92 ± 1.02	1.17 ± 0.98	1.58 ± 0.49	1.92 ± 0.49	2.50 ± 1.00	2.50 ± 1.00

Table 6. Statistical analysis of locomotor recovery (BMS test) of SCI animals treated with Neurobasal A or different dosages of ASC secretome along seven weeks.

Statistical test, significance, effect size		
Interaction between treatments and time points	Treatments effect	Time points effect
F (21, 154) = 1.63 p = 0.049 η^2_p = 0.18	F (3, 22) = 6.80 p = 0.002 η^2_p = 0.39	F (7, 154) = 81.9 p < 0.0001 η^2_p = 0.79

2.2. OF test

The OF test is designed to measure the total distance traveled and the number of rearings, which can be correlated with locomotor recovery of the animals. The average total distance traveled by animals from groups treated with secretome was not significantly different from the average of the negative control group (Figure 13; Table 7). Additionally, the animals were not able to perform rearings due to the severity of the lesion.

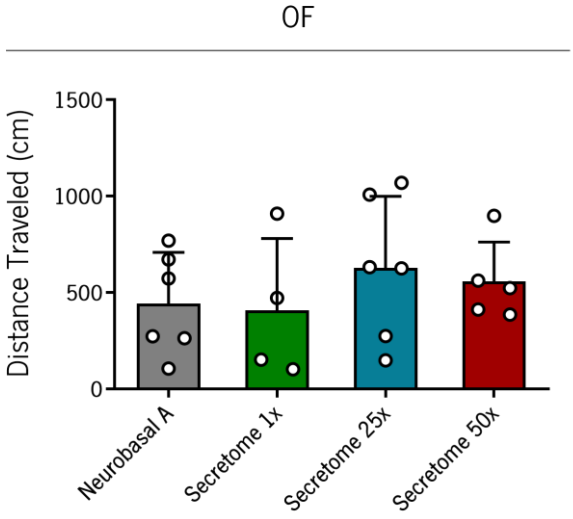

Figure 13. Total distance traveled by SCI mice, recorded in the eighth week of the experiment. Values are shown as mean ± SD; n=4-6 animals/group.

Table 7. Total distance traveled (in cm) by SCI animals in the OF arena and representation of statistical analysis. Data are presented as mean ± SD.

OF - total distance traveled (cm)				
Treatments ($\overline{X}$ ± SD)				
Neurobasal A	Secretome 1x	Secretome 25x	Secretome 50x	Statistical test, significance, effect size
442 ± 265	409 ± 372	627 ± 373	556 ± 205	F (3, 17) = 0.56 p = 0.65 η^2 = 0.089

2.3. BB test

At week 7 of the experiment, the BB test was carried out for the assessment of animal coordination. This evaluation was performed according to a scoring system for the BB presented in Annex 2. Overall, secretome groups did not present any significant improvement in motor coordination (Figure 14). Nevertheless, animals treated with 50x secretome presented an average score of 1.75, which is higher than the score (1.33) exhibited by the Neurobasal A-treated group (Table 8). Despite the absence of statistical differences between groups, two animals from the 50x concentrated secretome group were able to keep the balance for more than five seconds and one animal was able to traverse completely the beam.

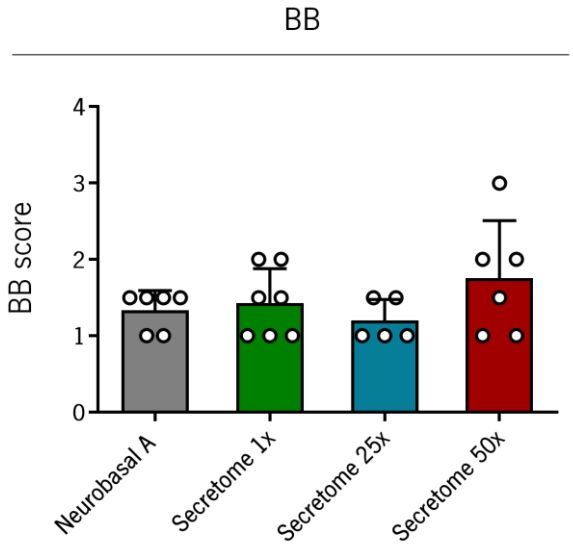

Figure 14. BB scores of SCI mice treated with Neurobasal A or distinct concentrations of secretome, seven weeks after injury. Values are shown as mean ± SD; n=5-7 animals/group.

Table 8. Statistical analysis of BB scores from SCI animals treated with Neurobasal A or distinct concentrations of secretome. Values are shown as mean ± SD.

BB - 27 mm-squared beam				
Treatments ($\overline{X}$ ± SD)				
Neurobasal A	Secretome 1x	Secretome 25x	Secretome 50x	Statistical test, significance, effect size
1.33 ± 0.26	1.43 ± 0.45	1.20 ± 0.27	1.75 ± 0.76	F (3, 20) = 1.32 p = 0.30 η^2 = 0.17

2.4. Gait analysis

To obtain more information about the motor performance of the animals, kinematic parameters were measured being indirectly associated with motor recovery. These parameters include the body and tail height, step angle and step length (Figures 15. A, 15. C and 15. E). Body and tail height of the animals did not change with the administered treatments, having no statistically significant differences between groups (Figures 15. B and 15. D; Table 9). Additionally, step angles of treated mice are very similar in comparison to non-treated animals (Figure 15. F; Table 9). The lack of ability to perform stepping did not allow the measurement of the animals step length. These parameters were analyzed in the left and right sides of the animals (Annex 3), which also revealed no statistical differences

between groups. The graphics illustrated below represent the average values obtained from the analysis of the left and right sides.

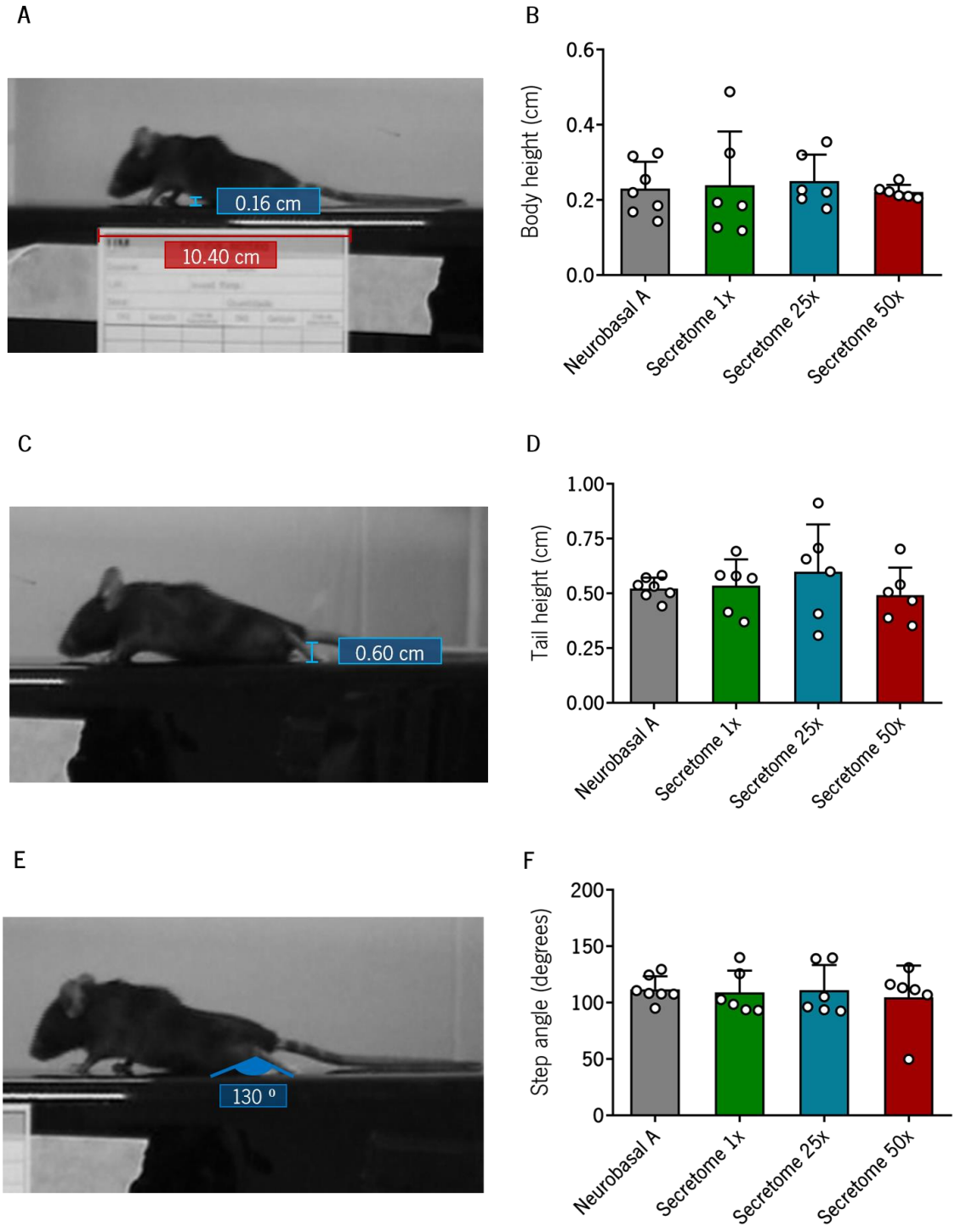

Figure 15. Gait analysis of SCI animals treated with Neurobasal A or different concentrations of ASC secretome. (A) Illustrative image of body height measurement by drawing a line (blue line) between the surface of the animal body and the ground. The red line represents the measure used to calibrate the software. (B) Quantification of the mean animal body height for each group. (C) Illustration of tail height measurement by tracing a line (blue line) between the base of the tail and the ground. (D) Quantification of the animal tail height for each group. (E) Representative image of step angle analysis by measuring the maximum angle performed by the hindpaw during stepping. (F) Quantification of the mean step angle for the different groups. Values are shown as mean ± SD (n=6-7 animals/group).

Table 9. Gait analysis of SCI animals and representation of statistical analysis. Data are represented as mean ± SD.

Motor parameter	Group	Mean ± SD	Statistical test, significance, effect size
Body Height (cm)	Neurobasal A	0.23 ± 0.071	F (3, 21) = 0.119 p = 0.948 η^2 = 0.0168
	Secretome 1x	0.24 ± 0.14	
	Secretome 25x	0.25 ± 0.071	
	Secretome 50x	0.22 ± 0.018	
Tail Height (cm)	Neurobasal A	0.52 ± 0.049	F (3, 21) = 0.63 p = 0.61 η^2 = 0.082
	Secretome 1x	0.54 ± 0.12	
	Secretome 25x	0.60 ± 0.22	
	Secretome 50x	0.49 ± 0.13	
Step angle (degrees)	Neurobasal A	112 ± 11.6	F (3, 21) = 0.145 p = 0.93 η^2 = 0.020
	Secretome 1x	109 ± 19.4	
	Secretome 25x	111 ± 22.4	
	Secretome 50x	105 ± 28.1	

2.5. VF test

In the VF test, paw withdrawals were registered and used to calculate the 50% threshold, providing information about their sensitivity and allodynia. No major statistical differences were found between groups administered with different treatments (Figure 16). However, it is interesting that there is a partial increase of 50% threshold in animals treated with 50x secretome in relation to those treated with Neurobasal A and lower concentrations of secretome (Figure 16; Table 10). This can be a possible indicator of sensory improvement in groups treated with a higher concentration of secretome.

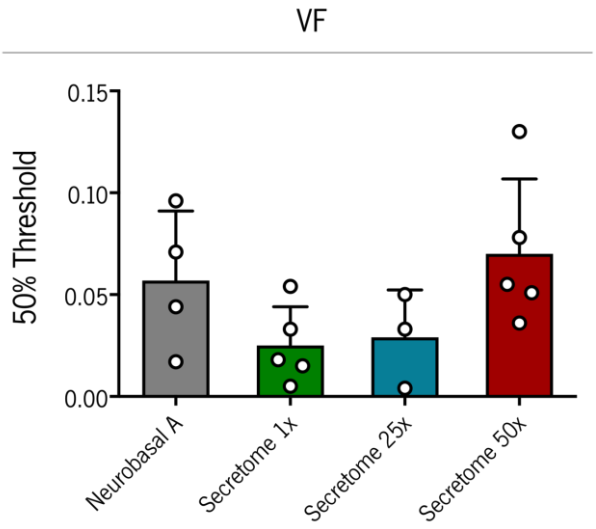

Figure 16. Calculation of the 50% threshold of SCI mice of different treatment groups in the VF test. Data are represented as mean ± SD.

Table 10. Statistical analysis of allodynia in SCI animals with different treatments, at week 8 of the experiment. Data are represented as mean ± SD.

	Groups	Mean ± SD	Statistical test, significance, effect size
50% Threshold	Neurobasal A	0.057 ± 0.034	F (3, 13) = 2.44 p = 0.11 η^2 = 0.36
	Secretome 1x	0.025 ± 0.019	
	Secretome 25x	0.029 ± 0.023	
	Secretome 50x	0.070 ± 0.037	

3. Histological analysis: the effect of different ASC secretome concentrations on the spinal cord tissue

3.1. Immunostaining for Iba1

The immunostaining for Iba1 was performed for the detection of microglia and macrophages present in the spinal cord. In order to address the impact of different treatments on neuroinflammation, two histological analyses were adopted: 1 – Quantification of Iba1 staining area; 2 – Measurement of the areas occupied by non-activated and activated Iba1^{+}cells.

In the quantification of Iba1 staining area, no significant statistical differences were found between treatment groups (Figures 17. A and 17. B; Table 11).

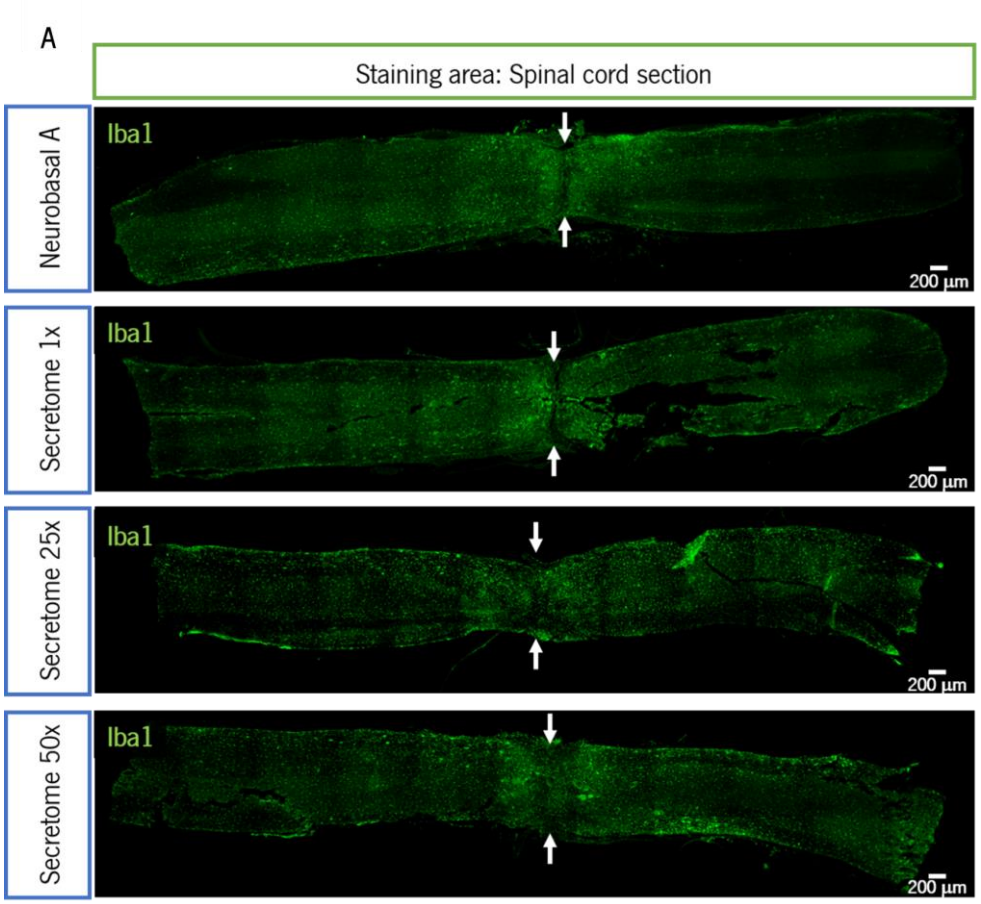

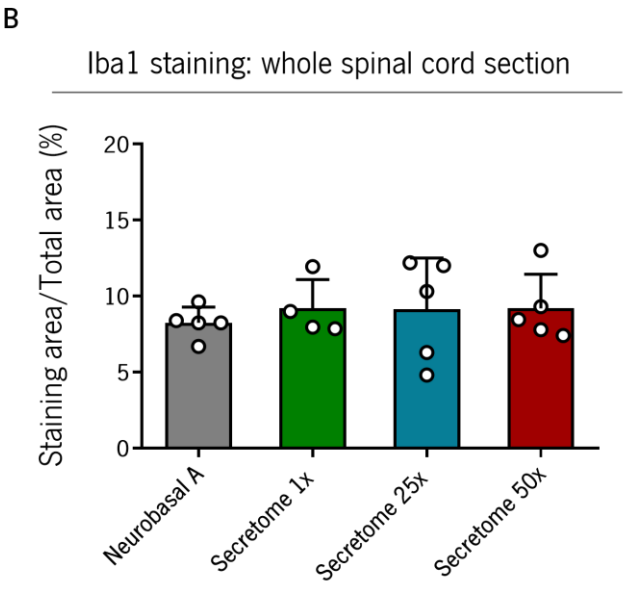

Figure 17. IHC against Iba1 in SCI animals from different treatment groups. (A) Fluorescence microscopy images of spinal cord sections. White arrows indicate the lesion site. Magnification: 100x. Scale: 200 μm. (B) Quantification of the ratio between staining area and total area of the spinal cord section (n=4-5 animals/group) Values are shown in percentage (%) and represented as mean ± SD.

Table 11. Statistical analysis of the results obtained from the quantification of Iba1-stained area. Data are represented as mean ± SD.

	Groups	Mean ± SD	Statistical test, significance, effect size
Iba1 Staining Area (%)	Neurobasal A	8.24 ± 1.04	F (3, 15) = 0.20 p = 0.90 η^2 = 0.31
	Secretome 1x	9.19 ± 1.91	
	Secretome 25x	9.12 ± 3.38	
	Secretome 50x	9.20 ± 2.25	

The second analysis consisted of the measurement of defined areas occupied by activated and non-activated Iba1$^+$ cells. The distinction of two cell states was performed according to the identification of cells that assume a more ramified shape (associated with non-activated microglia) and a more ameboid shape (associated with activated microglia)(Gomes-Leal, 2012; Kolos & Korzhevskii, 2020). Overall, the majority of activated Iba1$^+$ cells was found near the epicenter region of the lesion, while non-activated Iba1$^+$ cells were dispersed throughout regions rostral and caudal to the injury (Figure

18. A). The percentage of activated Iba1⁺ cells is not statistically different between groups. Nevertheless, there is a tendency to diminish the percentage of Iba1⁺ cells with an ameboid morphology as the secretome concentration administered to the animals increases (Figure 18. B; Table 12). The increase in the percentage of activated cells coincides with the decrease in non-activated cells (Figure 18. B).

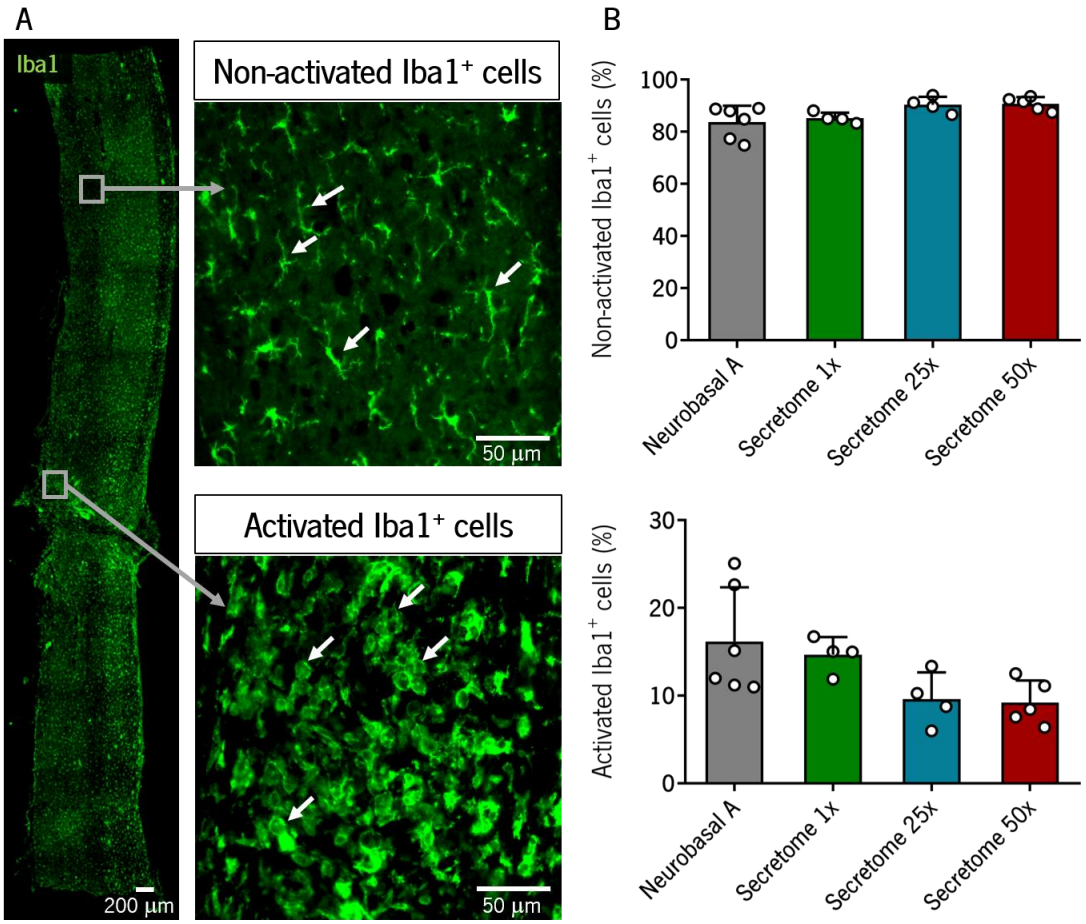

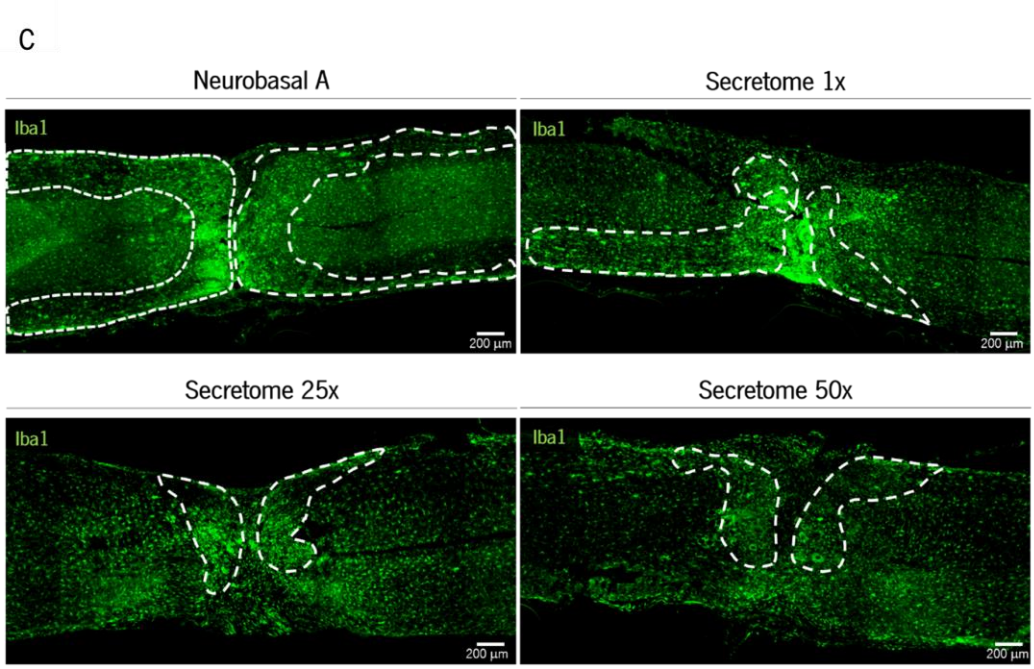

Figure 18. Analysis of defined areas occupied by activated and non-activated Iba1$^+$ cells. (A) Representative amplified images of two regions (grey squares): a region close to the lesion site, mainly occupied by activated Iba1$^+$ cells and another in a region rostral to the injury, mainly occupied by non-activated Iba1$^+$ cells. Scales: 200 and 50 µm. (B) Quantification of areas occupied by non-activated and activated Iba1$^+$ cells (n=4-6 animals/group). Data are represented as mean ± SD. (C) Representative images of areas occupied by activated microglia (dashed lines) in spinal cord sections of different groups. Scale: 200 µm.

Table 12. Statistical analysis of areas occupied by activated and non-activated Iba1$^+$ cells (%). Data are represented as mean ± SD.

	Groups	Mean ± SD	Statistical test, significance, effect size
Area of non-activated Iba1$^+$ cells (%)	Neurobasal A	83.8 ± 6.18	F (3, 15) = 3.65 p = 0.037 η^2 = 0.42
	Secretome 1x	85.3 ± 2.02	
	Secretome 25x	90.4 ± 3.07	
	Secretome 50x	90.8 ± 2.54	
Area of activated Iba1$^+$ cells (%)	Neurobasal A	16.2 ± 6.18	F (3, 15) = 3.65 p = 0.037 η^2 = 0.42
	Secretome 1x	14.7 ± 2.02	
	Secretome 25x	9.6 ± 3.07	
	Secretome 50x	9.2 ± 2.54	

3.2. Sholl analysis

The evaluation of microglial complexity was performed using the plugin SNT from Fiji software. The number of intersections of microglial processes along the radius was superior in mice treated with secretome than in vehicle-treated mice (Figure 19, Tables 13 and 14). Major differences were found in the 25x and 50x secretome groups, when compared to Neurobasal A group at 4 ($p = 0.0006$; $p = 0.005$), 8 ($p = 0.004$; $p = 0.002$) and 16 ($p = 0.014$; $p = 0.022$) micrometers from the soma. At 12 micrometers, only the 50x secretome group differed significantly from the negative control group ($p = 0.037$) (Figure 19.B). The higher number of intersections of 50x and 25x secretome groups can be associated with greater complexity of microglia (Figure 19. A).

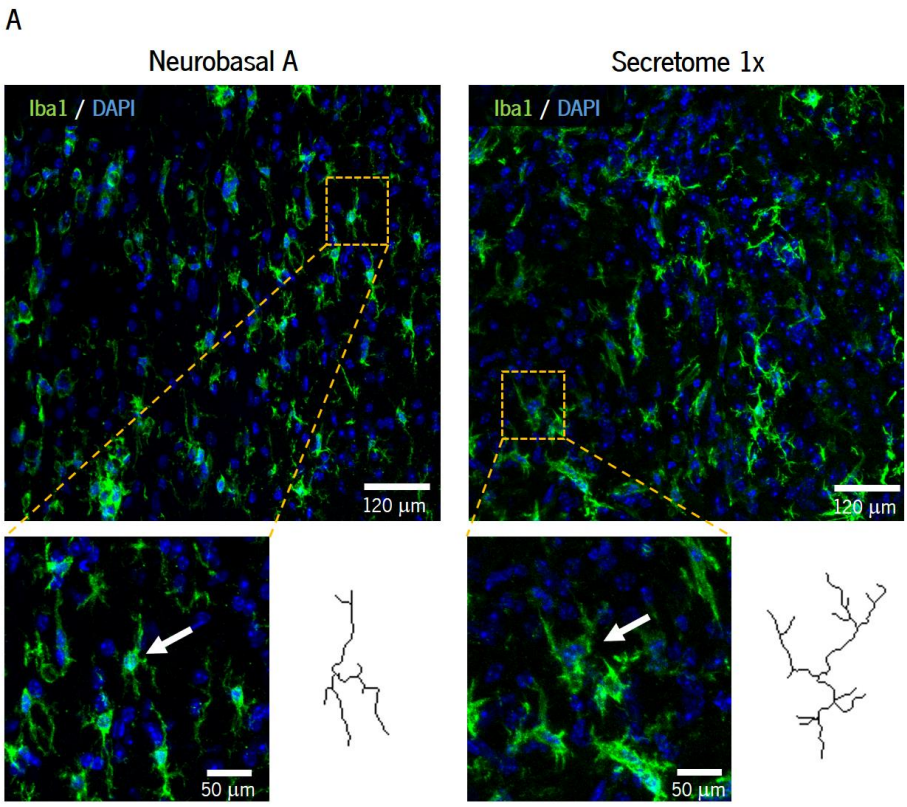

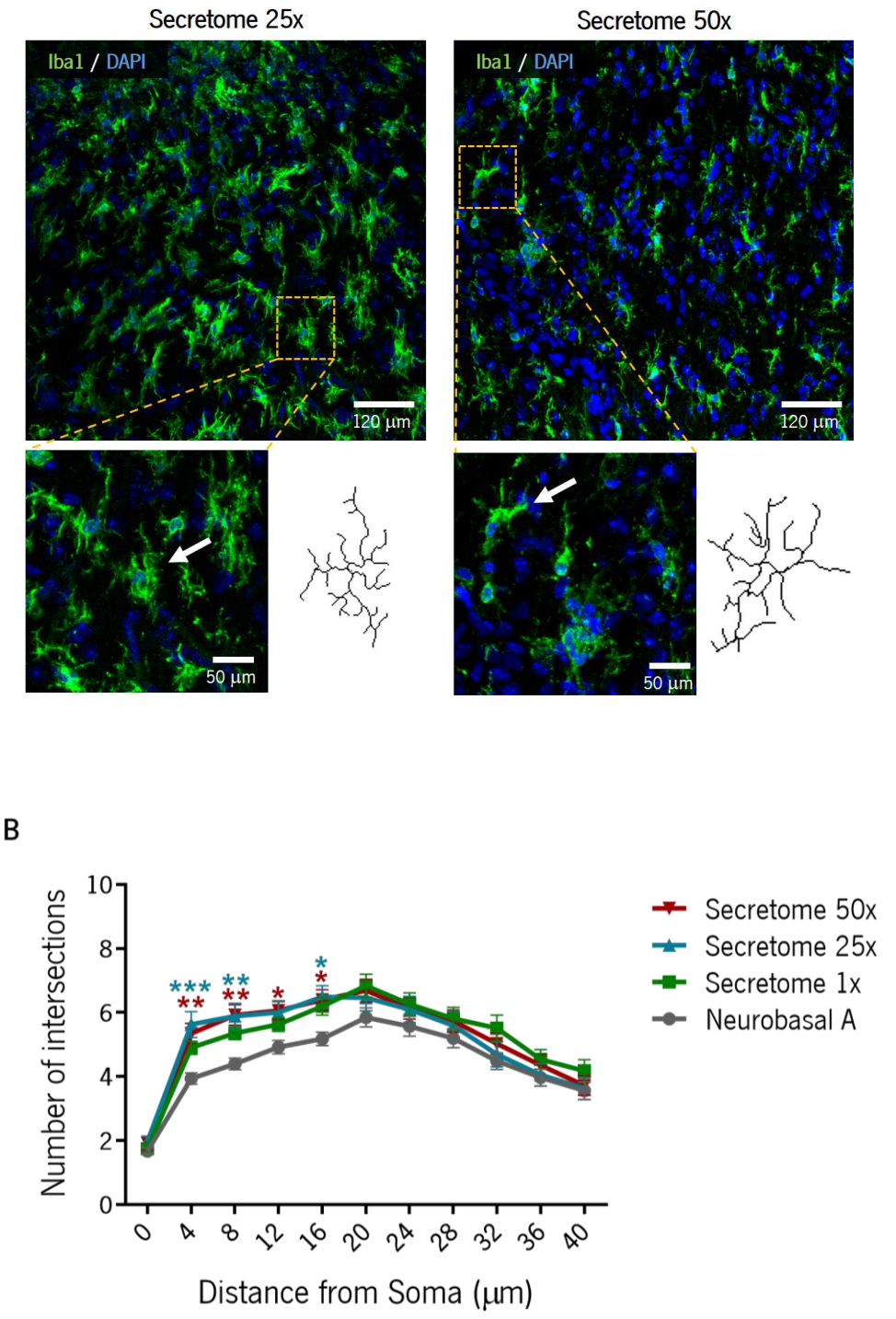

Figure 19. Microglial complexity, as measured by the number of intersections. (A) Confocal Z-stack images of spinal cord areas indicating selected microglia (pointed by the white arrow) for process reconstruction along with representations of traced microglia (in black). The nuclei are stained with DAPI (in blue) and the microglial processes are stained for Iba1 (in green). Magnification: 400x. (B) The number of intersections of the spinal cord microglia from different treatment groups along the radius (radius step size = 4 µm). Blue asterisks – Comparison of 25x secretome with NbA group. Red asterisks – Comparison of 50x secretome with NbA group. Data are presented as mean ± SEM. * $p \leq 0.05$; ** $p \leq 0.01$; *** $p \leq 0.001$; Total number of cells/group: n = 91 (Neurobasal A and Secretome 1x); n = 72 (Secretome 25x); n = 79 (Secretome 50x). These cells were analyzed in three animals per group.

Table 13. Variation in the number of microglial intersections in all experimental groups along the radius. Data are represented as mean ± SD.

Treatments	DISTANCE FROM SOMA (µM)										
	0	4	8	12	16	20	24	28	32	36	40
Neurobasal A	1.68 ± 0.87	3.94 ± 1.67	4.39 ± 1.76	4.93 ± 2.00	5.18 ± 2.00	5.84 ± 2.84	5.57 ± 2.93	5.18 ± 2.84	4.47 ± 2.53	3.96 ± 2.53	3.54 ± 2.69
Secretome 1x	1.75 ± 0.96	4.90 ± 1.97	5.35 ± 1.85	5.63 ± 2.00	6.20 ± 2.63	6.84 ± 3.43	6.26 ± 3.32	5.81 ± 3.34	5.52 ± 3.87	4.54 ± 2.92	4.18 ± 3.37
Secretome 25x	1.97 ± 1.36	5.63 ± 3.41	5.89 ± 3.37	6.00 ± 3.16	6.49 ± 2.97	6.46 ± 3.40	6.10 ± 3.46	5.60 ± 3.68	4.69 ± 3.30	4.06 ± 2.95	3.63 ± 2.86
Secretome 50x	1.92 ± 1.87	5.34 ± 2.87	5.92 ± 2.85	6.06 ± 2.51	6.39 ± 2.87	6.68 ± 3.12	6.14 ± 3.03	5.73 ± 3.05	5.03 ± 2.91	4.35 ± 2.93	3.72 ± 2.73

Table 14. Statistical analysis of microglial intersections along the radius from SCI animals treated with Neurobasal A or different dosages of secretome.

Statistical test, significance, effect size		
Interaction between treatments and distance	Treatments effect	Distance effect
$F(30, 3290) = 2.18$ $p = 0.0002$ $\eta^2_p = 0.019$	$F(3, 329) = 2.68$ $p = 0.047$ $\eta^2_p = 0.036$	$F(10, 3290) = 171$ $p < 0.0001$ $\eta^2_p = 0.34$

3.3. Immunostaining for GFAP

The GFAP staining areas were quantified revealing that the different treatments did not alter protein expression and distribution at the epicenter (Figure 20; Table 15), as well as in rostral and caudal regions to the lesion (Annex 5).

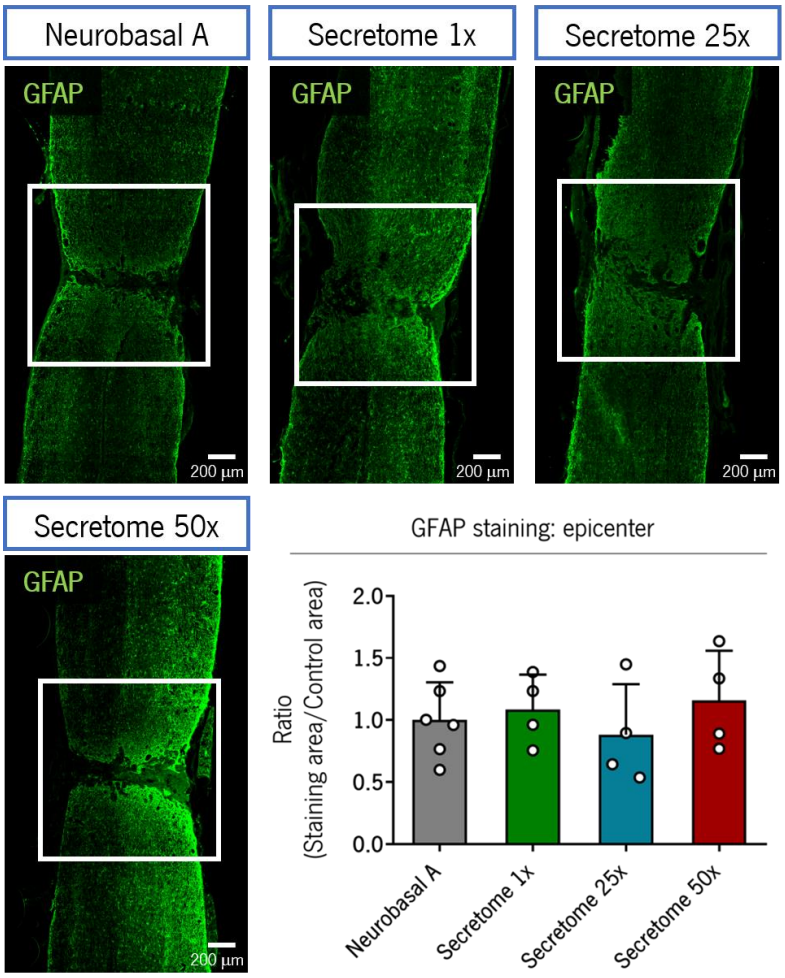

Figure 20. IHC against GFAP in SCI animals from different treatment groups. Representative images of epicenter regions of SCI animals from different treatment groups and quantification of the ratio between the staining area in the epicenter and the average staining area of the negative control group, Neurobasal A. N=4-6 animals/group. White squares indicate the staining areas that were quantified. Magnification: 100x. Scale: 200 µm. Data are represented as mean ± SD.

Table 15. Statistical analysis of GFAP-stained area quantification (ratio to control). Data are represented as mean ± SD.

	Groups	Mean ± SD	Statistical test, significance, effect size
GFAP Staining: epicenter (ratio to control)	Neurobasal A	1.00 ± 0.30	F (3, 14) = 0.47 p = 0.71 η^2 = 0.092
	Secretome 1x	1.09 ± 0.28	
	Secretome 25x	0.88 ± 0.41	
	Secretome 50x	1.16 ± 0.40	

3.4. Immunostaining for β-tubulin III

In order to evaluate the impact of distinct concentrations of ASC secretome on neuronal structures, histological analysis for β-tubulin III was performed for the whole spinal cord tissue (Figure 21) and in each of three regions (epicenter, rostral and caudal to the lesion, Annex 6). In this analysis, the groups did not present any statistical difference among them (Figure 21. B; Table 16).

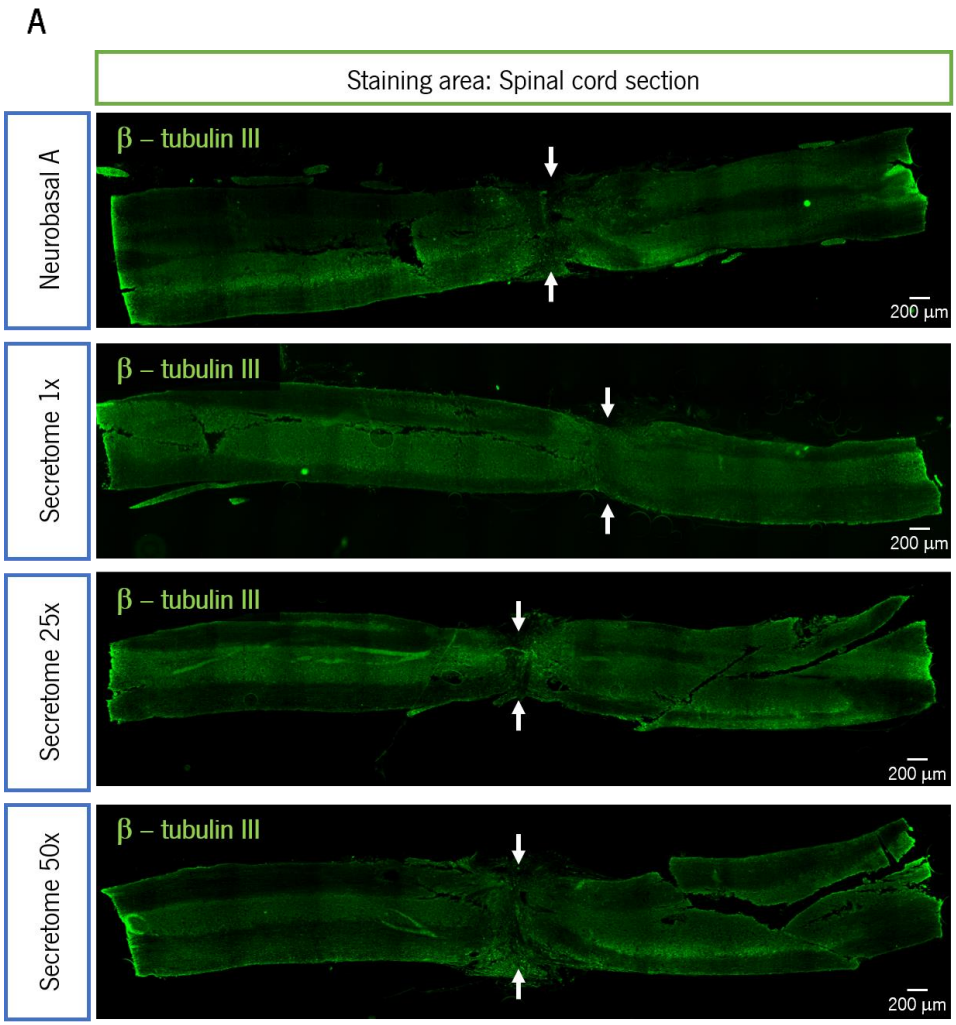

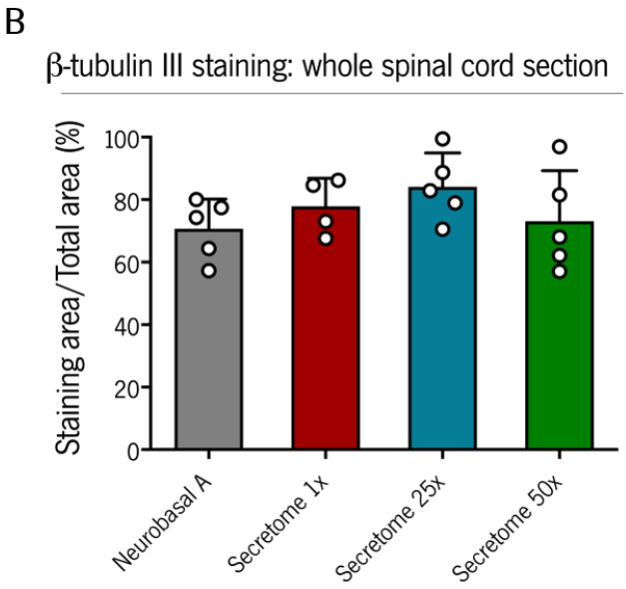

Figure 21. IHC against β-tubulin III in SCI animals from different treatment groups. (A) Fluorescence microscopy images from spinal cord sections. Scale: 200 μm. Magnification: 100x (B) Quantification of the ratio between staining area and total area of the spinal cord section (n=5 animals/group). Values are shown in percentage (%). Data are represented as mean ± SD.

Table 16. Statistical analysis of results obtained from the quantification of β-tubulin III-stained area. Data are represented as mean ± SD.

	Groups	Mean ± SD	Statistical test, significance, effect size
β-tubulin III Staining Area (%)	Neurobasal A	70.7 ± 9.55	F (3, 15) = 1.23 p = 0.34 η^2 = 0.20
	Secretome 1x	77.9 ± 9.01	
	Secretome 25x	84.1 ± 10.83	
	Secretome 50x	73.2 ± 16.18	

Chapter V - DISCUSSION

A traumatic injury in the spinal cord produces a cascade of alterations at the chemical, cellular, immunological and physical levels. Following the injury, the overresponsive inflammation and the abundance of inhibitory molecules in the neuronal environment hinder axonal regeneration (Ahuja & Fehlings, 2016; Silva et al., 2014). In an attempt to diminish the damage created by a SCI, several approaches and treatments have been tested in SCI patients, yet these ones fail to promote tissue regeneration and functional recovery (Silva et al., 2014). MSC secretome-based therapies are emerging as a promising solution for different neurological conditions, including SCI (Pinho et al., 2020). Among secretomes derived from different MSC populations, our group has shown that ASC secretome exerts a superior beneficial effect on DRG explant cultures, promoting higher levels of axonal regeneration, in comparison to bone marrow and umbilical cord derived-MSCs (Assunção-Silva et al., 2018). In addition to this, we have also showed that ASC secretome improves functional recovery following a transection (Silva, 2020) and a mild compression injury (Pinho, 2019), in a SCI mouse model. However, the concentration of ASC secretome necessary to induce a therapeutic effect still needs to be elucidated. In this sense, we designed an *in vivo* experiment, in order to test the minimal concentration of secretome capable of inducing functional recovery and tissue repair in a spinal cord transection mouse model. Furthermore, we explored the anti-inflammatory profile of different ASC secretome doses in a human microglial cell line, subjected to an inflammatory stimulus.

1. Analysis of the effect of different concentrations of ASC secretome on inflammation

In this task, we intended to elucidate if the immunomodulatory properties of ASC secretome vary across different concentrations, through the *in vitro* culture of the human microglial cell line HMC3. The HMC3 cells were previously shown to upregulate the pro-inflammatory gene *IL-6*, in response to a pro-inflammatory stimulus, such as LPS (Lindberg et al., 2005). Also, this cell line was found to express more *IL-4*, which is a known cytokine with anti-inflammatory activity, when infected with a Japanese encephalitis virus (Pareek et al., 2014). Thus, in this work, the expression levels of *IL-6* and *IL-4* genes were chosen as pro- and anti-inflammatory markers of HMC3 cells, respectively.

However, before exploring the effect of ASC secretome, a pilot study was performed to test different stimulation times, using LPS and IFN-γ, and to understand the variation of *IL-6* and *IL-4* expression levels, within 24 hours after stimulation. In this experiment, human microglial cells were stimulated with LPS and IFN-γ for 6 h, 12 h and 24 h. Results revealed that both cytokines seem to be more expressed at six hours of stimulation, in comparison to the non-stimulated group (Annex 7). In accordance with these results, Jašprová and colleagues demonstrated that HMC3 cells expressed

several inflammatory genes, including *IL-6*, after 4 hours of incubation with the pro-inflammatory molecule bilirubin photoproduct (Jašprová et al., 2018). In other time points of stimulation, no major differences were seen. Based on the results of this preliminary assay, the stimulation time of six hours was established for the second assay of the *in vitro* experiment.

In the second assay, microglial cells were subjected to stimulation with LPS and IFN-γ for six hours followed by incubation with DMEM 1x or different concentrations of ASC secretome (1x, 25x and 50x). RT-qPCR reaction was performed measuring the expression levels of *IL-6* and *IL-4* in response to different treatments. When compared to NS DMEM 1x group, S DMEM 1x group appears to express more *IL-6* and less *IL-4*, which might indicate that microglia responded to the applied stimulus by changing gene expression levels. Regarding the genetic impact of ASC secretome, different treatment concentrations did not impact the expression levels of *IL-6* and *IL-4*, after 24 hours of incubation. It is noteworthy to say that the time window to detect changes in cytokine expression levels might be shorter than 24 hours, and in that case the effect of the secretome might not be detected at later time points. Thus, in future studies, shorter periods of treatment should be adopted in order to detect possible early modifications of genetic expression. However, as previously stated, these results need to be interpreted cautiously, due to the low number of biological samples used. Contrarily to what we found, several studies used different concentrations of ASC secretome revealing its anti-inflammatory activity. For example, Guillén et al. incubated M1 and M2 polarized macrophages (with pro- and anti-inflammatory roles, respectively), with non-concentrated ASC secretome for 24 hours. After this, the supernatants were used to measure the protein levels of pro- and anti- inflammatory molecules by ELISA assay. As a result, the treatment contributed to the reduction of the pro-inflammatory mediator TNF-α and, at the same time, an increase of anti-inflammatory cytokines [transforming growth factor beta (TGF-β) and IL-10] released by M1 macrophages. Additionally, the secretion of TGF-β by M2 macrophages was potentiated with secretome treatment. With these results, this study indicates that ASC secretome not only suppressed macrophage activation, but also favored the anti-inflammatory phenotype of macrophage (Guillén et al., 2018). In contrast to this work, we did not observe a similar response in the genetic expression of cytokines in microglia, since both studies applied the inflammatory stimulus to immune cells and used the same time of treatment incubation. However, when comparing both approaches, some technical differences, which can lead to the divergence of these results, should be considered, including the immune cell type analyzed and the measured cytokine levels. To complement this work, another study from Jha et al. incubated a mouse microglial cell line (BV2) with concentrated ASC secretome for 6 hours, and then stimulated the cells with LPS

and IFN-γ for 12 hours. After this, qPCR was performed to measure the expression levels of *IL-1β* and *CD-86* (M1-like microglia markers) and *Arginase 1* (M2-like microglia marker). The levels of *IL-1β* and *CD-86* decreased, while there was a trend for an increase in the M2 marker *Arginase 1*. This result, together with maintenance of ramified morphology of microglia, suggested the anti-inflammatory activity of ASC secretome, which is able to inhibit the M1-like phenotype of microglia (Jha et al., 2018). These results corroborate the ability of ASC secretome to suppress the pro-inflammatory profile of microglia, which was not seen in the preliminary study showed in this thesis. Nevertheless, in Jha and colleagues' work, the microglial cell line was treated before the stimulation, which might modulate the response of the cells to the stimulus. Our group has previously compared the immunomodulatory potential of ASC secretome (total secretome) with its vesicular and proteic fractions separately, using activated and non-activated microglia. When treated with 100x concentrated ASC secretome, the number of activated microglia was smaller in percentage, in comparison to the negative control (Pinho, 2019). These studies suggest that ASC secretome has a promising potential to reduce inflammation, reverting the inflammatory phenotype of immune cells, including microglia. Considering these results, further studies need to be performed to increase the sample size, to optimize gene expression analysis time points and to complement with protein content analysis experiments. Additionally, other markers of M1 and M2-like microglia can be used to obtain a more detailed information regarding the microglial phenotype.

2. *In vivo* evaluation of the potential of different dosages of ASC secretome in a SCI context

As a proof of concept, a transection SCI mouse model was used, since the complete disruption of the spinal cord facilitates the evaluation of treatment efficacy in terms of axonal regeneration and functional recovery (Kwon et al., 2002; Sharif-Alhoseini et al., 2017). Mice were subjected to a SCI surgery, where a complete transection was made at T8 level. Following the injury, the protocol of IV injections of Neurobasal A and ASC secretome (already established by our group) was initiated, consisting in administrations at ten time points: three in the first two days and once a week for seven weeks. During the critical period of recovery from the surgery, 15 animals died, while seven animals were euthanized according to a humane endpoint table. For the assessment of locomotor recovery, Basso Mouse Scale (BMS) was performed every week attributing a specific score to the hindlimb based on the type of movement that the animal was able to perform (Basso et al., 2006). Three days post-injury, animals started with a score of zero indicating complete paralysis. One week later, 25x and 50x

secretome-treated groups improved, while 1x secretome and Neurobasal A groups remained with no movement in the lower limbs. Notably, in comparison to Neurobasal A group, the locomotor function of the hindlimbs of animals from 25x and 50x secretome groups ameliorated, reaching a plateau at 51 days post-injury. At the end of the experiment, 25x and 50x secretome groups had a score equal or greater than 2.5 reflecting the ability of performing the plantar placing of the paw. These results can be supported by the work of Zhou and colleagues, where they demonstrated a significant improvement of locomotor function, when SCI animals were treated with ASCs (Zhou et al., 2020). With the focus on paracrine activity of ASCs, our group showed that the administration of 100x concentrated ASC secretome clearly improved the motor deficits created by a spinal cord transection (Silva, 2020). Interestingly, animals treated with Neurobasal A presented a faster recovery than animals treated with 1x secretome, which might be due to the fact that the negative control was concentrated 100x, accumulating molecules that can potentiate the recovery of the animals. Overall, these data suggest that 25x and 50x concentrations of ASC secretome induced an enhancement of locomotor function of SCI animals.

The open field (OF) test provides information about the traveled distance and number of rearings performed by the animals, both indicators of general locomotor function. Treatment groups did not present any statistical difference in the traveled distance, yet animals treated with 25x and 50x secretomes presented an increase of at least 25% in comparison to the Neurobasal A group. This can further indicate that 25x and 50x secretomes might contribute to a better locomotor performance of SCI mice. The lack of statistical differences between groups can be explained by the dependency of this test on the animal exploratory activity, which in turn is influenced by its motivational state. One of the factors that influences animal motivational state is anxiety, which leads to a freezing behavior and, consequently, reduction of exploratory activity (Sedý et al., 2008). Regarding the number of rearings, animals were not able to perform them due to the severity of the lesion. Animals from 50x secretome group displayed a more homogenous behavior in this test, in comparison to other groups.

The beam balance (BB) test provides information regarding the motor coordination and balance of SCI animals. Four types of beam were used as a bridge for mice to cross until they reached the safe platform: 12 and 27 mm-squared cross section beams; 10 and 28 mm-round diameter beams. In both round and in the 12 mm-square beams, the animals were not able to perform the task. For this reason, only results from the 27 mm-squared beam were used in the analysis. Almost all animals from 1x secretome and Neurobasal A groups fell within five seconds, revealing the absence of balance.

However, some animals treated with 50x secretome displayed a balance for a period superior to 5 seconds or even completely crossed the beam. These data suggest a possible effect of 50x concentrated secretome on improving animals balance and motor coordination. Previously, our group tested the potential of ASC secretome and its proteic and vesicular fraction in a compression SCI model, revealing a significant effect on motor coordination of SCI animals treated with 100x concentrated ASC secretome (Pinho, 2019). This result reinforces the possibility of higher concentrations of ASC secretome being necessary to induce an improvement of motor coordination in SCI animals.

In order to analyze motor parameters that may not be distinguished in the BMS, a gait analysis was performed. For that, mice movements were recorded in their left and right side, and then their body height support, tail height support and step angle were analyzed using the Kinovea software. In all analyzed parameters, the animals from different experimental groups presented similar responses, having no statistical differences between them. These results are in accordance with BMS, where severely injured mice did not show support of their body weight, being only able to perform joint movements or plantar placing of the paws. Without body support, gait analysis was not sensitive enough to discriminate animals with different levels of recovery.

Beyond motor impairments, animals with SCI develop chronic pain, namely neuropathic pain (Gwak et al., 2012). Allodynia (hypersensitivity to an innocuous stimulus) of SCI mice was evaluated through the Von Frey (VF) test. This test consists of the application of a set of monofilaments (Chaplan et al., 1994; Guimarães et al., 2019) with different thicknesses, which do not cause pain in non-injured animals (Detloff et al., 2010). However, animals with allodynia withdraw their paws in response to the filaments (Detloff et al., 2010). The first aspect to note is that all animals seemed to experience pain, since their values of 50% threshold are below 1, which is a threshold for normal animals. In spite of having no significant differences between groups, there is a tendency to increase the 50% threshold values, as the secretome concentration increases. In fact, 50x secretome-treated group exhibited higher mean 50% threshold value in comparison to other groups, meaning that this secretome concentration may be fundamental to induce an improvement of sensory recovery in SCI animals. Nevertheless, these results should be carefully interpreted, since the disadvantage of using paw withdrawal threshold as a measure is that it can be a result of hyperreflexia and not of hypersensitivity (Detloff et al., 2010). The work of Gomes et al. aimed to evaluate the combined therapy of hydrogel, ASCs and OECs in a cervical hemisection SCI model. The interesting point in this work is that the

treatment with only ASCs and OECs was enough to restore partially the sensory function, when compared to the non-treated group, suggesting some potential of both cell types in promoting sensory recovery (Gomes et al., 2020). Supporting the impact of ASC paracrine activity on sensorial perception, Silva and colleagues, by performing the Von Frey test in fully-transected animals, showed that ASC secretome-treated animals displayed a higher response magnitude, in comparison to Neurobasal A (control)-treated mice (Silva, 2020).

3. Histological analysis of neuroinflammation and axonal regeneration

Immunohistochemistry (IHC) analysis of spinal cord sections allowed to analyze structural and cellular modifications of the tissue in response to the different treatments.

Neuroinflammation was assessed through IHC against Iba1 which detects microglia and macrophages present in the CNS (Sasaki et al., 2001). The quantification of total Iba1-stained area revealed no alterations between groups at the histological level, which could indicate that ASC secretome was not acting on the inflammation driven by microglia. Nevertheless, a recent study of Zhou et al. showed that transplantation of ASCs clearly induced a reduction of Iba1-stained area in a contusion SCI mouse model (Zhou et al., 2020). In the quantification of the staining area, no distinction is made between microglia that can assume non-activated and activated phenotypes, exerting distinct effects after SCI. For this reason, a more discriminated analysis was performed measuring the area occupied by activated and non-activated Iba1$^+$ cells that are distinguished by their ameboid and ramified shapes, respectively. Statistically, experimental groups did not differ significantly between them. However, it seems that by increasing secretome concentration, there is a gradual reduction in the area of activated cells. This data probably indicates a modulation of inflammation in highly concentrated secretome conditions, which is consistent with previous results from our group (Silva, 2020). In Silva's work, 100x concentrated ASC secretome significantly induced a reduction of the percentage of Iba1$^+$ activated cells, when compared to the negative control group (Silva, 2020). Therefore, a more sensitive tool, Sholl analysis, was used to detect subtle modifications on microglia morphology through the measurement of the number of intersections along the distance from soma. In the first 16 μm from the soma, the number of microglial intersections was enhanced in groups treated with 25x and 50x secretome groups, in relation to the Neurobasal A group. These data correlate with a higher percentage of ramified Iba1$^+$ cells, which can be associated with higher presence of non-activated microglia. Such results revealed small modifications in the cellular complexity of the microglia that were not detected in the gross quantification of the positive area for Iba1. Altogether, 25x and 50x secretomes appeared

to induce inhibition of microglia activation in SCI animals. Activated microglia released a set of detrimental molecules for neurons, including nitric oxide, superoxide and several cytokines (IL-1, IL-6 and TNF-α), which can provoke neurodegeneration (Kolos & Korzhevskii, 2020). Thus, our hypothesis consists in alleviation of microglial neurotoxic effect on SCI animals mediated by 25x and 50x concentrated secretomes, which could explain the partial locomotor recovery of the animals.

To further explore beyond inflammation in the spinal cord, immunostaining was performed for GFAP, which is highly expressed by astrocytes, providing more information about the glial scar (Silva et al., 2014). The quantification of fluorescence intensity did not show any modification in GFAP staining in the epicenter region in animals treated with different concentrations of secretome, meaning that the treatments appear to not affect significantly the astrocyte population. In another work, western blot analysis of spinal cord lysates revealed an enhancement of GFAP protein levels in contusion SCI animals treated with IV injections of ASCs (Ohta et al., 2017). In the same direction, Zhou et al. transplanted ASCs in a moderate contusion SCI mouse model, demonstrating a higher GFAP staining area by IHC, in ASC-treated group (Zhou et al., 2020). The abundance of astrocytes does not indicate a harmful role in SCI, since in our GFAP staining area quantification, no distinction of astrocytic phenotypes was performed. Following the injury, naïve astrocytes convert into reactive ones, which can present several phenotypes, including A1 and A2 (Okada et al., 2018). When the astrocytes assume an "A1" phenotype, the expression of genes associated with destruction of synapses increases, suggesting that this cell type has "damaging" functions. In contrast, A2 astrocytes produce molecules (including neurotrophic factors and thrombospondins) that boost neuronal survival and synapse formation (Liddelow & Barres, 2017). Days post-injury, reactive astrocytes become glial-scar forming astrocytes (Okada et al., 2018), composing the glial scar which is known to be an obstacle for axonal regeneration. Despite all this knowledge, the role of A1 astrocytes and the glial scar effect still raise controversy. Reactive and glial-scar astrocytes present morphological, molecular and genetic differences, but both overexpress GFAP (Yang et al., 2020). Therefore, it is relevant to understand which type of astrocyte is present in a SCI context, performing a deeper cellular and molecular analysis. In an attempt to fill this gap, Sholl analysis for astrocytes was considered. However, the astrocytic mesh was to dense, precluding the analysis of an isolated astrocyte (Annex 4).

Focusing on neuronal impact of different secretome concentrations, an IHC was carried out for the detection of β-tubulin III, allowing the assessment of neuronal organization, namely axonal growth (Silva et al., 2014). β-tubulin III staining was very similar in all experimental groups, suggesting that

ASC secretome was not inducing neuroregeneration. Contrarily, previous study from our group revealed a significant increase of β-tubulin III$^+$ area in transected mice treated with 100x concentrated ASC secretome in comparison to the Neurobasal A group (Silva, 2020). This indicates that the concentration levels necessary to promote axonal regrowth and regeneration might be higher, than the ones used in this study.

Overall, our results suggest that the beneficial effects are obtained by increasing the concentration of ASC secretome. As demonstrated in this thesis, the 25x and 50x ASC secretomes induced an improvement of the locomotor function of severely injured animals. Histologically, these secretome concentrations also stood out by reducing microglial reactivity. Thus, the 50x secretome revealed to be the ideal concentration to induce immunomodulation and locomotor recovery after SCI.

Previously, Lu and co-workers demonstrated that MSC EVs injected intravenously avoided BSCB disruption, contributing to the enhancement of motor function in SCI animals (Lu et al., 2019). In addition to the vesicular fraction, the total ASC secretome showed to enhance revascularization and improve functional recovery in a stroke model (Cho et al., 2012). Having this in mind, immunomodulation might not be the only mechanism underlying the recovery of the animals, considering the possibility of ASC secretome acting in angiogenesis as well. Therefore, we hypothesized that 50x concentrated secretome contains bioactive factors and vesicles that may act in several processes (for example, immunomodulation and angiogenesis) important for the recovery following the injury. In the future, further studies need to be performed in order to explore the mechanisms of MSC secretome responsible for the motor recovery of injured animals.

Chapter VI - FINAL REMARKS

Following SCI, a patient faces adversities during a long period of rehabilitation. Currently, the available treatments are inefficient to induce axonal regeneration, inflammation reduction and functional recovery in SCI patients. Lately, several studies have shown the positive impact of MSC secretome in SCI. Our group has highlighted ASC secretome as a potential therapy to treat SCI, as it modulates inflammation and improves functional recovery. Despite this, the dosage of ASC secretome necessary to obtain beneficial effects in a SCI context still needed to be explored. Therefore, in this thesis, different concentrations of ASC secretome were tested for the first time in a SCI context.

This study demonstrated that the proposed treatments appeared to have no influence on the *in vitro* microglial phenotype, namely in cytokine gene expression levels. Nevertheless, additional studies are needed in order to confirm these results. Moreover, in an *in vivo* SCI mouse model, we revealed an improvement of hindlimb function of animals in response to higher concentrations of ASC secretome, such as 25x and 50x. Although no major differences were detected in other motor and sensory tests, there is a possibility that 50x concentrated secretome promotes sensory recovery. Therefore, it is relevant to perform complementary paradigms that detect subtle alterations in response to different treatments. In histological studies, the 25x and 50x secretomes seemed to modulate the SCI-derived inflammatory response, by influencing microglial activation state. The 50x concentration demonstrated to be the concentration necessary to exert a beneficial effect on neuroinflammation and locomotor function recovery of the animals. Translating this to research and clinical field can reduce the time and resources spent to obtain the secretome.

BIBLIOGRAPHY

Ahmed, Z., Mazibrada, G., Seabright, R. J., Dent, R. G., Berry, M., & Logan, A. (2006). TACE-induced cleavage of NgR and p75NTR in dorsal root ganglion cultures disinhibits outgrowth and promotes branching of neurites in the presence of inhibitory CNS myelin. *FASEB Journal: Official Publication of the Federation of American Societies for Experimental Biology*, *20*(11), 1939–1941.

Ahuja, C. S., & Fehlings, M. (2016). Concise Review: Bridging the Gap: Novel Neuroregenerative and Neuroprotective Strategies in Spinal Cord Injury. *Stem Cells Translational Medicine*, *5*(7), 914–924.

Ahuja, C. S., Martin, A. R., & Fehlings, M. (2016). Recent advances in managing a spinal cord injury secondary to trauma. *F1000Research*, *5*.

Ahuja, C. S., Wilson, J. R., Nori, S., Kotter, M. R. N., Druschel, C., Curt, A., & Fehlings, M. G. (2017). Traumatic spinal cord injury. *Nature Reviews. Disease Primers*, *3*, 17018.

Alizadeh, A., Dyck, S. M., & Karimi-Abdolrezaee, S. (2019). Traumatic Spinal Cord Injury: An Overview of Pathophysiology, Models and Acute Injury Mechanisms. *Frontiers in Neurology*, *10*.

Alvarez-Dolado, M., Pardal, R., Garcia-Verdugo, J. M., Fike, J. R., Lee, & H. O., Pfeffer. et al. (2003). Fusion of bone-marrow-derived cells with Purkinje neurons, cardiomyocytes and hepatocytes. *Nature*, *425*(6961), 968–973.

Amemori, T., Ruzicka, J., Romanyuk, N., Jhanwar-Uniyal, M., Sykova, E., & Jendelova, P. (2015). Comparison of intraspinal and intrathecal implantation of induced pluripotent stem cell-derived neural precursors for the treatment of spinal cord injury in rats. *Stem Cell Research & Therapy*, *6*.

Assunção-Silva, R. C., Mendes-Pinheiro, B., Patrício, P., Behie, L. A., Teixeira, F. G., Pinto, L., & Salgado, A. J. (2018). Exploiting the impact of the secretome of MSCs isolated from different tissue sources on neuronal differentiation and axonal growth. *Biochimie*, *155*, 83–91.

Baer, P. C., & Geiger, H. (2012). Adipose-Derived Mesenchymal Stromal/Stem Cells: Tissue Localization, Characterization, and Heterogeneity. *Stem Cells International*, *2012*, e812693.

Bajek, A., Gurtowska, N., Gackowska, L., Kubiszewska, I., Bodnar, M., & Marszałek, A. et al. (2015). Does the liposuction method influence the phenotypic characteristic of human adipose-derived stem cells? *Bioscience Reports*, *35*(3).

Ballios, B. G., Baumann, M. D., Cooke, M. J., & Shoichet, M. S. (2011). Chapter 55—Central Nervous System. In A. Atala, R. Lanza, J. A. Thomson, & R. Nerem (Eds.), *Principles of Regenerative Medicine (Second Edition)* (pp. 1023–1046). Academic Press.

Barrett, C. P., Guth, L., Donati, E. J., & Krikorian, J. G. (1981). Astroglial reaction in the gray matter of lumbar segments after midthoracic transection of the adult rat spinal cord. *Experimental Neurology*, *73*(2), 365–377.

Basso, D. M., Fisher, L. C., Anderson, A. J., Jakeman, L. B., Mctigue, D. M., & Popovich, P. G. (2006). Basso Mouse Scale for Locomotion Detects Differences in Recovery after Spinal Cord Injury in Five Common Mouse Strains. *Journal of Neurotrauma*, *23*(5), 635–659.

Bear, M., Connors, B., & Paradiso, M. (2015). *Neuroscience: Exploring the brain* (4th ed.). Wolters Kluwer.

Beer, L., Mildner, M., & Ankersmit, H. J. (2017). Cell secretome based drug substances in regenerative medicine: When regulatory affairs meet basic science. *Annals of Translational Medicine*, *5*(7), 17.

Ben-David, U., & Benvenisty, N. (2011). The tumorigenicity of human embryonic and induced pluripotent stem cells. *Nature Reviews. Cancer*, *11*(4), 268–277.

Benton, R. L., & Hagg, T. (2011). Vascular Pathology as a Potential Therapeutic Target in SCI. *Translational Stroke Research*, *2*(4), 556–574.

Bermudez, M. A., Sendon-Lago, J., Eiro, N., Treviño, M., Gonzalez, F., & Yebra-Pimentel, E. et al. (2015). Corneal epithelial wound healing and bactericidal effect of conditioned medium from human uterine cervical stem cells. *Investigative Ophthalmology & Visual Science*, *56*(2), 983–992.

Bignami, A., & Dahl, D. (1976). The Astroglial Response to Stabbing. Immunofluorescence Studies with Antibodies to Astrocyte-Specific Protein (gfa) in Mammalian and Submammalian Vertebrates. *Neuropathology and Applied Neurobiology*, *2*(2), 99–110.

Blaber, S. P., Webster, R. A., Hill, C. J., Breen, E. J., Kuah, D., Vesey, G., & Herbert, B. R. (2012). Analysis of in vitro secretion profiles from adipose-derived cell populations. *Journal of Translational Medicine*, *10*(1), 172.

Boche, D., Perry, V. H., & Nicoll, J. a. R. (2013). Review: Activation patterns of microglia and their identification in the human brain. *Neuropathology and Applied Neurobiology*, *39*(1), 3–18.

Boomkamp, S. D., McGrath, M. A., Houslay, M. D., & Barnett, S. C. (2014). Epac and the high affinity rolipram binding conformer of PDE4 modulate neurite outgrowth and myelination using an in vitro spinal cord injury model. *British Journal of Pharmacology*, *171*(9), 2385–2398.

Boomkamp, S. D., Riehle, M. O., Wood, J., Olson, M. F., & Barnett, S. C. (2012). The development of a rat in vitro model of spinal cord injury demonstrating the additive effects of Rho and ROCK inhibitors on neurite outgrowth and myelination. *Glia*, *60*(3), 441–456.

Bourin, P., Bunnell, B. A., Casteilla, L., Dominici, M., Katz, A. J., & March, K. L. et al. (2013). Stromal cells from the adipose tissue-derived stromal vascular fraction and culture expanded adipose tissue-derived stromal/stem cells: A joint statement of the International Federation for Adipose Therapeutics and Science (IFATS) and the International Society for Cellular Therapy (ISCT). *Cytotherapy*, *15*(6), 641–648.

Bracken, M. B., Shepard, M. J., Holford, T. R., Leo-Summers, L., Aldrich, E. F., & Fazl, M. et al. (1997). Administration of methylprednisolone for 24 or 48 hours or tirilazad mesylate for 48 hours in the treatment of acute spinal cord injury. Results of the Third National Acute Spinal Cord Injury Randomized Controlled Trial. National Acute Spinal Cord Injury Study. *JAMA*, *277*(20), 1597–1604.

Bracken, M. B., Shepard, M. J., Collins, W. F., Holford, T. R., Young, W., & Baskin, D. S. et al. (1990). A Randomized, Controlled Trial of Methylprednisolone or Naloxone in the Treatment of Acute Spinal-Cord Injury. *New England Journal of Medicine*, *322*(20), 1405–1411.

Brooks, S. P., & Dunnett, S. B. (2009). Tests to assess motor phenotype in mice: A user's guide. *Nature Reviews. Neuroscience*, *10*(7), 519–529.

Bunge, M. B., & Wood, P. M. (2012). Realizing the maximum potential of Schwann cells to promote recovery from spinal cord injury. *Handbook of Clinical Neurology*, *109*, 523–540.

Cantinieaux, D., Quertainmont, R., Blacher, S., Rossi, L., Wanet, T., & Noël, A. et al. (2013). Conditioned Medium from Bone Marrow-Derived Mesenchymal Stem Cells Improves Recovery after Spinal Cord Injury in Rats: An Original Strategy to Avoid Cell Transplantation. *PLOS ONE*, *8*(8), e69515.

Carrade, D. D., Affolter, V. K., Outerbridge, C. A., Watson, J. L., Galuppo, L. D., & Buerchler, S. et al. (2011). Intradermal injections of equine allogeneic umbilical cord-derived mesenchymal stem cells are well tolerated and do not elicit immediate or delayed hypersensitivity reactions. *Cytotherapy*, *13*(10), 1180–1192.

Carter, M., & Shieh, J. (2015). Chapter 2—Animal Behavior. In M. Carter & J. Shieh (Eds.), *Guide to Research Techniques in Neuroscience (Second Edition)* (pp. 39–71). Academic Press.

Carter, R. J., Morton, J., & Dunnett, S. B. (2001). Motor Coordination and Balance in Rodents. *Current Protocols in Neuroscience*, *15*(1), 8.12.1-8.12.14.

Casha, S., Zygun, D., McGowan, M. D., Bains, I., Yong, V. W., & Hurlbert, R. J. (2012). Results of a phase II placebo-controlled randomized trial of minocycline in acute spinal cord injury. *Brain: A Journal of Neurology*, *135*(Pt 4), 1224–1236.

Chaplan, S. R., Bach, F. W., Pogrel, J. W., Chung, J. M., & Yaksh, T. L. (1994). Quantitative assessment of tactile allodynia in the rat paw. *Journal of Neuroscience Methods*, *53*(1), 55–63.

Cheriyan, T., Ryan, D. J., Weinreb, J. H., Cheriyan, J., Paul, J. C., & Lafage, V. et al. (2014). Spinal cord injury models: A review. *Spinal Cord*, *52*(8), 588–595.

Cho, Y. J., Song, H. S., Bhang, S., Lee, S., Kang, B. G., & Lee, J. C. et al. (2012). Therapeutic effects of human adipose stem cell-conditioned medium on stroke. *Journal of Neuroscience Research*, *90*(9), 1794–1802.

Choo, A. M., Liu, J., Lam, C. K., Dvorak, M., Tetzlaff, W., & Oxland, T. R. (2007). Contusion, dislocation, and distraction: Primary hemorrhage and membrane permeability in distinct mechanisms of spinal cord injury. *Journal of Neurosurgery. Spine*, *6*(3), 255–266.

Cloutier, F., Siegenthaler, M. M., Nistor, G., & Keirstead, H. S. (2006). Transplantation of human embryonic stem cell-derived oligodendrocyte progenitors into rat spinal cord injuries does not cause harm. *Regenerative Medicine*, *1*(4), 469–479.

Cofano, F., Boido, M., Monticelli, M., Zenga, F., Ducati, A., Vercelli, A., & Garbossa, D. (2019). Mesenchymal Stem Cells for Spinal Cord Injury: Current Options, Limitations, and Future of Cell Therapy. *International Journal of Molecular Sciences*, *20*(11).

Conley, B. J., Young, J. C., Trounson, A. O., & Mollard, R. (2004). Derivation, propagation and differentiation of human embryonic stem cells. *The International Journal of Biochemistry & Cell Biology*, *36*(4), 555–567.

Couillard-Despres, S., Bieler, L., & Vogl, M. (2017). Pathophysiology of Traumatic Spinal Cord Injury. In N. Weidner, R. Rupp, & K. E. Tansey (Eds.), *Neurological Aspects of Spinal Cord Injury* (pp. 503–528). Springer, Cham.

Courtine, G., & Sofroniew, M. V. (2019). Spinal cord repair: Advances in biology and technology. *Nature Medicine*, *25*(6), 898–908.

Cregg, J. M., DePaul, M. A., Filous, A. R., Lang, B. T., Tran, A., & Silver, J. (2014). Functional regeneration beyond the glial scar. *Experimental Neurology*, *253*, 197–207.

Crisan, M., Yap, S., Casteilla, L., Chen, C.-W., Corselli, M., & Park, T. S. et al. (2008). A perivascular origin for mesenchymal stem cells in multiple human organs. *Cell Stem Cell*, *3*(3), 301–313.

Daneshtalab, N., Doré, J. J. E., & Smeda, J. S. (2010). Troubleshooting tissue specificity and antibody selection: Procedures in immunohistochemical studies. *Journal of Pharmacological and Toxicological Methods*, *61*(2), 127–135.

De Ugarte, D. A., Alfonso, Z., Zuk, P. A., Elbarbary, A., Zhu, M., & Ashjian, P. et al. (2003). Differential expression of stem cell mobilization-associated molecules on multi-lineage cells from adipose tissue and bone marrow. *Immunology Letters*, *89*(2), 267–270.

Deister, C., & Schmidt, C. E. (2006). Optimizing neurotrophic factor combinations for neurite outgrowth. *Journal of Neural Engineering*, *3*(2), 172–179.

DelaRosa, O., Lombardo, E., Beraza, A., Mancheño-Corvo, P., Ramirez, C., & Menta, R. et al. (2009). Requirement of IFN-γ–Mediated Indoleamine 2,3-Dioxygenase Expression in the Modulation of Lymphocyte Proliferation by Human Adipose–Derived Stem Cells. *Tissue Engineering Part A*, *15*(10), 2795–2806.

Detloff, M. R., Clark, L. M., Hutchinson, K. J., Kloos, A. D., Fisher, L. C., & Basso, D. M. (2010). Validity of acute and chronic tactile sensory testing after spinal cord injury in rats. *Experimental Neurology*, *225*(2), 366–376.

Deuis, J. R., Dvorakova, L. S., & Vetter, I. (2017). Methods Used to Evaluate Pain Behaviors in Rodents. *Frontiers in Molecular Neuroscience*, *10*.

Dizdaroglu, M., Jaruga, P., Birincioglu, M., & Rodriguez, H. (2002). Free radical-induced damage to DNA: Mechanisms and measurement. *Free Radical Biology & Medicine*, *32*(11), 1102–1115.

Dominici, M., Le Blanc, K., Mueller, I., Slaper-Cortenbach, I., Marini, F., & Krause, D. et al. (2006). Minimal criteria for defining multipotent mesenchymal stromal cells. The International Society for Cellular Therapy position statement. *Cytotherapy*, *8*(4), 315–317.

Doucette, R. (1991). PNS-CNS transitional zone of the first cranial nerve. *The Journal of Comparative Neurology*, *312*(3), 451–466.

Dubois, S. G., Floyd, E. Z., Zvonic, S., Kilroy, G., Wu, X., & Carling, S. et al. (2008). Isolation of human adipose-derived stem cells from biopsies and liposuction specimens. *Methods in Molecular Biology*, *449*, 69–79.

Egashira, Y., Sugitani, S., Suzuki, Y., Mishiro, K., Tsuruma, K., & Shimazawa, M. et al. (2012). The conditioned medium of murine and human adipose-derived stem cells exerts neuroprotective effects against experimental stroke model. *Brain Research*, *1461*, 87–95.

Eggenhofer, E., Benseler, V., Kroemer, A., Popp, F., Geissler, E., & Schlitt, H. et al. (2012). Mesenchymal stem cells are short-lived and do not migrate beyond the lungs after intravenous infusion. *Frontiers in Immunology*, *3*.

Eiró, N., Sendon-Lago, J., Seoane, S., Bermúdez, M. A., Lamelas, M. L., & Garcia-Caballero, T. et al. (2014). Potential therapeutic effect of the secretome from human uterine cervical stem cells against both cancer and stromal cells compared with adipose tissue stem cells. *Oncotarget*, *5*(21), 10692–10708.

Eldahan, K. C., & Rabchevsky, A. G. (2018). Autonomic Dysreflexia after Spinal Cord Injury: Systemic Pathophysiology and Methods of Management. *Autonomic Neuroscience : Basic & Clinical*, *209*, 59–70.

Eldh, M., Ekström, K., Valadi, H., Sjöstrand, M., Olsson, B., Jernås, M., & Lötvall, J. (2010). Exosomes Communicate Protective Messages during Oxidative Stress; Possible Role of Exosomal Shuttle RNA. *PLOS ONE*, *5*(12), e15353.

Evaniew, N., Belley-Côté, E. P., Fallah, N., Noonan, V. K., Rivers, C. S., & Dvorak, M. F. (2016). Methylprednisolone for the Treatment of Patients with Acute Spinal Cord Injuries: A Systematic Review and Meta-Analysis. *Journal of Neurotrauma*, *33*(5), 468–481.

Evans, J. R., & Barker, R. A. (2008). Neurotrophic factors as a therapeutic target for Parkinson's disease. *Expert Opinion on Therapeutic Targets*, *12*(4), 437–447.

Faden, A. I., & Simon, R. P. (1988). A potential role for excitotoxins in the pathophysiology of spinal cord injury. *Annals of Neurology*, *23*(6), 623–626.

Fierabracci, A., Fattore, A. D., Muraca, M., Delfino, D. V., & Muraca, M. (2016). The Use of Mesenchymal Stem Cells for the Treatment of Autoimmunity: From Animals Models to Human Disease. *Current Drug Targets*, *17*(2), 229–238.

Fisher, L. J. (1997). Neural precursor cells: Applications for the study and repair of the central nervous system. *Neurobiology of Disease*, *4*(1), 1–22.

Fitch, M. T., Doller, C., Combs, C. K., Landreth, G. E., & Silver, J. (1999). Cellular and molecular mechanisms of glial scarring and progressive cavitation: In vivo and in vitro analysis of inflammation-induced secondary injury after CNS trauma. *The Journal of Neuroscience: The Official Journal of the Society for Neuroscience*, *19*(19), 8182–8198.

Folkman, J., & Shing, Y. (1992). Angiogenesis. *The Journal of Biological Chemistry*, *267*(16), 10931–10934.

Fontanilla, C. V., Gu, H., Liu, Q., Zhu, T. Z., Zhou, C., Johnstone, B. H., & March, K. L. et al. (2015). Adipose-derived Stem Cell Conditioned Media Extends Survival time of a mouse model of Amyotrophic Lateral Sclerosis. *Scientific Reports*, *5*(1), 1–11.

Friedenstein, A. J., Chailakhjan, R. K., & Lalykina, K. S. (1970). The development of fibroblast colonies in monolayer cultures of guinea-pig bone marrow and spleen cells. *Cell and Tissue Kinetics*, *3*(4), 393–403.

Fujimoto, Y., Abematsu, M., Falk, A., Tsujimura, K., Sanosaka, T., & Juliandi, B. et al. (2012). Treatment of a mouse model of spinal cord injury by transplantation of human induced pluripotent stem cell-derived long-term self-renewing neuroepithelial-like stem cells. *Stem Cells*, *30*(6), 1163–1173.

Gao, J., Dennis, J. E., Muzic, R. F., Lundberg, M., & Caplan, A. I. (2001). The dynamic in vivo distribution of bone marrow-derived mesenchymal stem cells after infusion. *Cells, Tissues, Organs*, *169*(1), 12–20.

Gazdic, M., Volarevic, V., Harrell, C. R., Fellabaum, C., Jovicic, N., Arsenijevic, N., & Stojkovic, M. (2018). Stem Cells Therapy for Spinal Cord Injury. *International Journal of Molecular Sciences*, *19*(4).

Gnecchi, M., He, H., Liang, O. D., Melo, L. G., Morello, F., & Mu, H. et al. (2005). Paracrine action accounts for marked protection of ischemic heart by Akt-modified mesenchymal stem cells. *Nature Medicine*, *11*(4), 367–368.

Gomes, E. D., Ghosh, B., Lima, R., Goulão, M., Moreira-Gomes, T., & Martins-Macedo, J. et al. (2020). Combination of a Gellan Gum-Based Hydrogel With Cell Therapy for the Treatment of Cervical Spinal Cord Injury. *Frontiers in Bioengineering and Biotechnology*, *8*.

Gomes-Leal, W. (2012). Microglial physiopathology: How to explain the dual role of microglia after acute neural disorders? *Brain and Behavior*, *2*(3), 345–356.

Graf, T. (2002). Differentiation plasticity of hematopoietic cells. *Blood*, *99*(9), 3089–3101.

Gronthos, S., Mankani, M., Brahim, J., Robey, P. G., & Shi, S. (2000). Postnatal human dental pulp stem cells (DPSCs) in vitro and in vivo. *Proceedings of the National Academy of Sciences*, *97*(25), 13625–13630.

Grossman, R. G., Fehlings, M. G., Frankowski, R. F., Burau, K. D., Chow, D. S. L., & Tator, C. et al. (2014). A prospective, multicenter, phase I matched-comparison group trial of safety, pharmacokinetics, and preliminary efficacy of riluzole in patients with traumatic spinal cord injury. *Journal of Neurotrauma*, *31*(3), 239–255.

Groves, A. K., Barnett, S. C., Franklin, R. J., Crang, A. J., Mayer, M., Blakemore, W. F., & Noble, M. (1993). Repair of demyelinated lesions by transplantation of purified O-2A progenitor cells. *Nature*, *362*(6419), 453–455.

Gu, H., Long, D., Song, C., & Li, X. (2009). Recombinant human NGF-loaded microspheres promote survival of basal forebrain cholinergic neurons and improve memory impairments of spatial learning in the rat model of Alzheimer's disease with fimbria-fornix lesion. *Neuroscience Letters*, *453*(3), 204–209.

Guest, J. D., Hiester, E. D., & Bunge, R. P. (2005). Demyelination and Schwann cell responses adjacent to injury epicenter cavities following chronic human spinal cord injury. *Experimental Neurology*, *192*(2), 384–393.

Guest, J., Santamaria, A. J., & Benavides, F. D. (2013). Clinical translation of autologous Schwann cell transplantation for the treatment of spinal cord injury. *Current Opinion in Organ Transplantation*, *18*(6), 682–689.

Guillén, M. I., Platas, J., Pérez del Caz, M. D., Mirabet, V., & Alcaraz, M. J. (2018). Paracrine Anti-inflammatory Effects of Adipose Tissue-Derived Mesenchymal Stem Cells in Human Monocytes. *Frontiers in Physiology*, *9*, 661.

Guimarães, M. R., Soares, A. R., Cunha, A. M., Esteves, M., Borges, S., & Magalhães, R. et al. (2019). Evidence for lack of direct causality between pain and affective disturbances in a rat peripheral neuropathy model. *Genes, Brain and Behavior*, *18*(6), e12542.

Gwak, Y. S., Kang, J., Unabia, G. C., & Hulsebosch, Claire. E. (2012). Spatial and Temporal Activation of Spinal Glial Cells: Role of Gliopathy in Central Neuropathic Pain Following Spinal Cord Injury in Rats. *Experimental Neurology*, *234*(2), 362–372.

György, B., Szabó, T. G., Pásztói, M., Pál, Z., Misják, P., & Aradi, B. et al. (2011). Membrane vesicles, current state-of-the-art: Emerging role of extracellular vesicles. *Cellular and Molecular Life Sciences*, *68*(16), 2667–2688.

Hachem, L. D., Ahuja, C. S., & Fehlings, M. G. (2017). Assessment and management of acute spinal cord injury: From point of injury to rehabilitation. *The Journal of Spinal Cord Medicine*, *40*(6), 665–675.

Hall, E. D., & Braughler, J. M. (1981). Acute effects of intravenous glucocorticoid pretreatment on the in vitro peroxidation of cat spinal cord tissue. *Experimental Neurology*, *73*(1), 321–324.

Hall, E. D., & Braughler, J. M. (1982). Effects of intravenous methylprednisolone on spinal cord lipid peroxidation and (Na+ + K+)-ATPase activity: Dose-response analysis during 1st hour after contusion injury in the cat. *Journal of Neurosurgery*, *57*(2), 247–253.

Hathout, Y. (2007). Approaches to the study of the cell secretome. *Expert Review of Proteomics*, *4*(2), 239–248.

Hau, J., & Schapiro, S. J. (2013). *Handbook of Laboratory Animal Science, Volume III: Animal Models* (3rd ed.). CRC Press.

Hausmann, O. N. (2003). Post-traumatic inflammation following spinal cord injury. *Spinal Cord*, *41*(7), 369–378.

Ho, C. H., Wuermser, L.-A., Priebe, M. M., Chiodo, A. E., Scelza, W. M., & Kirshblum, S. C. (2007). Spinal Cord Injury Medicine. 1. Epidemiology and Classification. *Archives of Physical Medicine and Rehabilitation*, *88*(3), S49–S54.

Hoogduijn, M. J., & Lombardo, E. (2019). Mesenchymal Stromal Cells Anno 2019: Dawn of the Therapeutic Era? Concise Review. *STEM CELLS Translational Medicine*, *8*(11), 1126–1134.

Horwitz, E. M., Le Blanc, K., Dominici, M., Mueller, I., Slaper-Cortenbach, I., & Marini, F. C. et al. (2005). Clarification of the nomenclature for MSC: The International Society for Cellular Therapy position statement. *Cytotherapy*, *7*(5), 393–395.

Hou, S., Lu, P., & Blesch, A. (2013). Characterization of supraspinal vasomotor pathways and autonomic dysreflexia after spinal cord injury in F344 rats. *Autonomic Neuroscience: Basic & Clinical*, *176*(1–2), 54–63.

Hugenholtz, H. (2003). Methylprednisolone for acute spinal cord injury: Not a standard of care. *CMAJ: Canadian Medical Association Journal*, *168*(9), 1145–1146.

Ide, C., Nakai, Y., Nakano, N., Seo, T.-B., Yamada, Y., & Endo, K. et al. (2010). Bone marrow stromal cell transplantation for treatment of sub-acute spinal cord injury in the rat. *Brain Research*, *1332*, 32–47.

Ivanova-Todorova, E., Bochev, I., Mourdjeva, M., Dimitrov, R., Bukarev, D., & Kyurkchiev, S. et al. (2009). Adipose tissue-derived mesenchymal stem cells are more potent suppressors of dendritic cells differentiation compared to bone marrow-derived mesenchymal stem cells. *Immunology Letters*, *126*(1), 37–42.

Iwanami, A., Kaneko, S., Nakamura, M., Kanemura, Y., Mori, H., & Kobayashi, S. et al. (2005). Transplantation of human neural stem cells for spinal cord injury in primates. *Journal of Neuroscience Research*, *80*(2), 182–190.

James, S. L., Theadom, A., Ellenbogen, R. G., Bannick, M. S., Montjoy-Venning, W., & Lucchesi, L. R. et al. (2019). Global, regional, and national burden of traumatic brain injury and spinal cord injury, 1990–2016: A systematic analysis for the Global Burden of Disease Study 2016. *The Lancet Neurology*, *18*(1), 56–87.

Jašprová, J., Dal Ben, M., Hurný, D., Hwang, S., Žížalová, K., & Kotek, J. et al. (2018). Neuro-inflammatory effects of photodegradative products of bilirubin. *Scientific Reports*, *8*.

Jha, K. A., Pentecost, M., Lenin, R., Klaic, L., Elshaer, S. L., & Gentry, J. et al. (2018). Concentrated Conditioned Media from Adipose Tissue Derived Mesenchymal Stem Cells Mitigates Visual Deficits and Retinal Inflammation Following Mild Traumatic Brain Injury. *International Journal of Molecular Sciences*, *19*(7).

Jin, K., & Greenberg, D. A. (2003). Tales of transdifferentiation. *Experimental Neurology*, *183*(2), 255–257.

Kang, S. K., Lee, D. H., Bae, Y. C., Kim, H. K., Baik, S. Y., & Jung, J. S. (2003). Improvement of neurological deficits by intracerebral transplantation of human adipose tissue-derived stromal cells after cerebral ischemia in rats. *Experimental Neurology*, *183*(2), 355–366.

Keating, A. (2012). Mesenchymal Stromal Cells: New Directions. *Cell Stem Cell*, *10*(6), 709–716.

Keirstead, H. S., Nistor, G., Bernal, G., Totoiu, M., Cloutier, F., Sharp, K., & Steward, O. (2005). Human Embryonic Stem Cell-Derived Oligodendrocyte Progenitor Cell Transplants Remyelinate and Restore Locomotion after Spinal Cord Injury. *The Journal of Neuroscience*, *25*(19), 4694–4705.

Khankan, R. R., Griffis, K. G., Haggerty-Skeans, J. R., Zhong, H., Roy, R. R., Edgerton, V. R., & Phelps, P. E. (2016). Olfactory Ensheathing Cell Transplantation after a Complete Spinal Cord Transection Mediates Neuroprotective and Immunomodulatory Mechanisms to Facilitate Regeneration. *The Journal of Neuroscience: The Official Journal of the Society for Neuroscience*, *36*(23), 6269–6286.

Kim, M., Hong, S. K., Jeon, S. R., Roh, S. W., & Lee, S. (2018). Early (≤48 Hours) versus Late (>48 Hours) Surgery in Spinal Cord Injury: Treatment Outcomes and Risk Factors for Spinal Cord Injury. *World Neurosurgery*, *118*, e513–e525.

Kobayashi, Y., Okada, Y., Itakura, G., Iwai, H., Nishimura, S., & Yasuda, A. et al. (2012). Pre-evaluated safe human iPSC-derived neural stem cells promote functional recovery after spinal cord injury in common marmoset without tumorigenicity. *PloS One*, *7*(12), e52787.

Kokai, L. E., Marra, K., & Rubin, J. P. (2014). Adipose stem cells: Biology and clinical applications for tissue repair and regeneration. *Translational Research*, *163*(4), 399–408.

Kolos, E. A., & Korzhevskii, D. E. (2020). Spinal Cord Microglia in Health and Disease. *Acta Naturae*, *12*(1), 4–17.

Környei, Z., Czirók, A., Vicsek, T., & Madarász, E. (2000). Proliferative and migratory responses of astrocytes to in vitro injury. *Journal of Neuroscience Research*, *61*(4), 421–429.

Kucharzewski, M., Rojczyk, E., Wilemska-Kucharzewska, K., Wilk, R., Hudecki, J., & Los, M. J. (2019). Novel trends in application of stem cells in skin wound healing. *European Journal of Pharmacology*, *843*, 307–315.

Kumru, H., & Kofler, M. (2012). Effect of spinal cord injury and of intrathecal baclofen on brainstem reflexes. *Clinical Neurophysiology: Official Journal of the International Federation of Clinical Neurophysiology*, *123*(1), 45–53.

Kundi, S., Bicknell, R., & Ahmed, Z. (2013). Spinal Cord Injury: Current Mammalian Models. *Neuroscience International*, *4*(1), 1–12.

Kwon, B. K., Oxland, T. R., & Tetzlaff, W. (2002). Animal models used in spinal cord regeneration research. *Spine*, *27*(14), 1504–1510.

Kyurkchiev, D., Bochev, I., Ivanova-Todorova, E., Mourdjeva, M., Oreshkova, T., Belemezova, K., & Kyurkchiev, S. (2014). Secretion of immunoregulatory cytokines by mesenchymal stem cells. *World Journal of Stem Cells*, *6*(5), 552–570.

Lachmann, N., & Nikol, S. (2007). Therapeutic angiogenesis for peripheral artery disease: Stem cell therapy. *VASA. Zeitschrift Fur Gefasskrankheiten*, *36*(4), 241–251.

Lankford, K. L., Arroyo, E. J., Nazimek, K., Bryniarski, K., Askenase, P. W., & Kocsis, J. D. (2018). Intravenously delivered mesenchymal stem cell-derived exosomes target M2-type macrophages in the injured spinal cord. *PloS One*, *13*(1), e0190358.

LaPlaca, M. C., Simon, C. M., Prado, G. R., & Cullen, D. K. (2007). CNS injury biomechanics and experimental models. *Progress in Brain Research*, *161*, 13–26.

Lee, M. W., Yang, M. S., Park, J. S., Kim, H. C., Kim, Y. J., & Choi, J. (2005). Isolation of mesenchymal stem cells from cryopreserved human umbilical cord blood. *International Journal of Hematology*, *81*(2), 126–130.

Lee, R. H., Pulin, A. A., Seo, M. J., Kota, D. J., Ylostalo, J., & Larson, B. L. et al. (2009). Intravenous hMSCs Improve Myocardial Infarction in Mice because Cells Embolized in Lung Are Activated to Secrete the Anti-inflammatory Protein TSG-6. *Cell Stem Cell*, *5*(1), 54–63.

Li, T., Jiang, L., Zhang, X., & Chen, H. (2009). In-vitro effects of brain-derived neurotrophic factor on neural progenitor/stem cells from rat hippocampus. *Neuroreport*, *20*(3), 295–300.

Liang, X., Zhang, L., Wang, S., Han, Q., & Zhao, R. C. (2016). Exosomes secreted by mesenchymal stem cells promote endothelial cell angiogenesis by transferring miR-125a. *Journal of Cell Science*, *129*(11), 2182–2189.

Liddelow, S. A., & Barres, B. A. (2017). Reactive Astrocytes: Production, Function, and Therapeutic Potential. *Immunity*, *46*(6), 957–967.

Lin, G., Garcia, M., Ning, H., Banie, L., Guo, Y.-L., Lue, T. F., & Lin, C.-S. (2008). Defining stem and progenitor cells within adipose tissue. *Stem Cells and Development*, *17*(6), 1053–1063.

Lindberg, C., Crisby, M., Winblad, B., & Schultzberg, M. (2005). Effects of statins on microglia. *Journal of Neuroscience Research*, *82*(1), 10–19.

Lindvall, O., & Kokaia, Z. (2006). Stem cells for the treatment of neurological disorders. *Nature*, *441*(7097), 1094–1096.

Liu, S., Qu, Y., Stewart, T. J., Howard, M. J., Chakrabortty, S., Holekamp, T. F., & McDonald, J. W. (2000). Embryonic stem cells differentiate into oligodendrocytes and myelinate in culture and after spinal cord transplantation. *Proceedings of the National Academy of Sciences*, *97*(11), 6126–6131.

Lombardi, F., Palumbo, P., Augello, F. R., Cifone, M. G., Cinque, B., & Giuliani, M. (2019). Secretome of Adipose Tissue-Derived Stem Cells (ASCs) as a Novel Trend in Chronic Non-Healing Wounds: An Overview of Experimental In Vitro and In Vivo Studies and Methodological Variables. *International Journal of Molecular Sciences*, *20*(15).

Lu, L.-L., Liu, Y.-J., Yang, S.-G., Zhao, Q.-J., Wang, X., & Gong, W. et al. (2006). Isolation and characterization of human umbilical cord mesenchymal stem cells with hematopoiesis-supportive function and other potentials. *Haematologica*, *91*(8), 1017–1026.

Lu, P., Wang, Y., Graham, L., McHale, K., Gao, M., & Wu, D. et al. (2012). Long-Distance Growth and Connectivity of Neural Stem Cells after Severe Spinal Cord Injury. *Cell*, *150*(6), 1264–1273.

Lu, Y., Zhou, Y., Zhang, R., Wen, L., Wu, K., & Li, Y. et al. (2019). Bone Mesenchymal Stem Cell-Derived Extracellular Vesicles Promote Recovery Following Spinal Cord Injury via Improvement of the Integrity of the Blood-Spinal Cord Barrier. *Frontiers in Neuroscience*, *13*.

Marfia, G., Navone, S. E., Vito, C. D., Ughi, N., Tabano, S., & Miozzo, M. et al. (2015). Mesenchymal stem cells: Potential for therapy and treatment of chronic non-healing skin wounds. *Organogenesis*, *11*(4), 183–206.

Marquardt, L. M., Doulames, V. M., Wang, A. T., Dubbin, K., Suhar, R. A., & Kratochvil, M. J. et al. (2020). Designer, injectable gels to prevent transplanted Schwann cell loss during spinal cord injury therapy. *Science Advances*, *6*(14), eaaz1039.

Mathivanan, S., Ji, H., & Simpson, R. J. (2010). Exosomes: Extracellular organelles important in intercellular communication. *Journal of Proteomics*, *73*(10), 1907–1920.

McCanney, G. A., Whitehead, M. J., McGrath, M. A., Lindsay, S. L., & Barnett, S. C. (2017). Neural cell cultures to study spinal cord injury. *Drug Discovery Today: Disease Models*, *25–26*, 11–20.

McCoy, M. K., Martinez, T. N., Ruhn, K. A., Wrage, P. C., Keefer, E. W., & Botterman, B. R. et al. (2008). Autologous transplants of Adipose-Derived Adult Stromal (ADAS) afford dopaminergic neuroprotection in a model of Parkinson's disease. *Experimental Neurology*, *210*(1), 14–29.

McKeon, R. J., Schreiber, R. C., Rudge, J. S., & Silver, J. (1991). Reduction of neurite outgrowth in a model of glial scarring following CNS injury is correlated with the expression of inhibitory molecules on reactive astrocytes. *The Journal of Neuroscience: The Official Journal of the Society for Neuroscience*, *11*(11), 3398–3411.

Mendes-Pinheiro, B., Teixeira, F. G., Anjo, S. I., Manadas, B., Behie, L. A., & Salgado, A. J. (2018). Secretome of Undifferentiated Neural Progenitor Cells Induces Histological and Motor Improvements in a Rat Model of Parkinson's Disease. *Stem Cells Translational Medicine*, *7*(11), 829–838.

Meyerrose, T., Olson, S., Pontow, S., Kalomoiris, S., Jung, Y., & Annett, G. et al. (2010). Mesenchymal stem cells for the sustained in vivo delivery of bioactive factors. *Advanced Drug Delivery Reviews*, *62*(12), 1167–1174.

Mirsky, R., Jessen, K. R., Brennan, A., Parkinson, D., Dong, Z., & Meier, C. et al. (2002). Schwann cells as regulators of nerve development. *Journal of Physiology-Paris*, *96*(1), 17–24.

Mothe, A. J., & Tator, C. H. (2012). Advances in stem cell therapy for spinal cord injury. *The Journal of Clinical Investigation*, *122*(11), 3824–3834.

Nakae, A., Nakai, K., Yano, K., Hosokawa, K., Shibata, M., & Mashimo, T. (2011). The Animal Model of Spinal Cord Injury as an Experimental Pain Model. *Journal of Biomedicine and Biotechnology*, *2011*, 939023.

Ng, M. T. L., Stammers, A. T., & Kwon, B. K. (2011). Vascular Disruption and the Role of Angiogenic Proteins After Spinal Cord Injury. *Translational Stroke Research*, *2*(4), 474–491.

Nobunaga, A. I., Go, B. K., & Karunas, R. B. (1999). Recent demographic and injury trends in people served by the Model Spinal Cord Injury Care Systems. *Archives of Physical Medicine and Rehabilitation*, *80*(11), 1372–1382.

Nolan, T., Hands, R. E., & Bustin, S. A. (2006). Quantification of mRNA using real-time RT-PCR. *Nature Protocols*, *1*(3), 1559–1582.

Norenberg, M. D., Smith, J., & Marcillo, A. (2004). The pathology of human spinal cord injury: Defining the problems. *Journal of Neurotrauma*, *21*(4), 429–440.

Nout, Y. S., Rosenzweig, E. S., Brock, J. H., Strand, S. C., Moseanko, R., & Hawbecker, S. et al. (2012). Animal Models of Neurologic Disorders: A Nonhuman Primate Model of Spinal Cord Injury. *Neurotherapeutics*, *9*(2), 380–392.

Nutt, S. E., Chang, E.-A., Suhr, S. T., Schlosser, L. O., Mondello, S. E., & Moritz, C. T. et al. (2013). Caudalized human iPSC-derived neural progenitor cells produce neurons and glia but fail to restore function in an early chronic spinal cord injury model. *Experimental Neurology*, *248*, 491–503.

Ohta, Y., Hamaguchi, A., Ootaki, M., Watanabe, M., Takeba, Y., & Iiri, T. et al. (2017). Intravenous infusion of adipose-derived stem/stromal cells improves functional recovery of rats with spinal cord injury. *Cytotherapy*, *19*(7), 839–848.

Okada, S. (2016). The pathophysiological role of acute inflammation after spinal cord injury. *Inflammation and Regeneration*, *36*(1), 20.

Okada, S., Hara, M., Kobayakawa, K., Matsumoto, Y., & Nakashima, Y. (2018). Astrocyte reactivity and astrogliosis after spinal cord injury. *Neuroscience Research*, *126*, 39–43.

Opal, S. M., & DePalo, V. A. (2000). Anti-inflammatory cytokines. *Chest*, *117*(4), 1162–1172.

Oudega, M., & Xu, X.-M. (2006). Schwann Cell Transplantation for Repair of the Adult Spinal Cord. *Journal of Neurotrauma*, *23*(3–4), 453–467.

Oyinbo, C. A. (2011). Secondary injury mechanisms in traumatic spinal cord injury: A nugget of this multiply cascade. *Acta Neurobiologiae Experimentalis*, *71*(2), 281–299.

Pappalardo, L. W., Samad, O. A., Black, J. A., & Waxman, S. G. (2014). Voltage-gated sodium channel Nav 1.5 contributes to astrogliosis in an in vitro model of glial injury via reverse Na+ /Ca2+ exchange. *Glia*, *62*(7), 1162–1175.

Paquet, J., Deschepper, M., Moya, A., Logeart-Avramoglou, D., Boisson-Vidal, C., & Petite, H. (2015). Oxygen Tension Regulates Human Mesenchymal Stem Cell Paracrine Functions. *Stem Cells Translational Medicine*, *4*(7), 809–821.

Pareek, S., Roy, S., Kumari, B., Jain, P., Banerjee, A., & Vrati, S. (2014). MiR-155 induction in microglial cells suppresses Japanese encephalitis virus replication and negatively modulates innate immune responses. *Journal of Neuroinflammation*, *11*(1), 97.

Parekkadan, B., & Milwid, J. M. (2010). Mesenchymal Stem Cells as Therapeutics. *Annual Review of Biomedical Engineering*, *12*(1), 87–117.

Petersen, M. A., Ryu, J. K., Chang, K.-J., Etxeberria, A., Bardehle, S., & Mendiola, A. S. et al. (2017). Fibrinogen Activates BMP Signaling in Oligodendrocyte Progenitor Cells and Inhibits Remyelination after Vascular Damage. *Neuron*, *96*(5), 1003-1012.e7.

Pineau, I., & Lacroix, S. (2007). Proinflammatory cytokine synthesis in the injured mouse spinal cord: Multiphasic expression pattern and identification of the cell types involved. *The Journal of Comparative Neurology*, *500*(2), 267–285.

Pinho, A. (2019). *Impact of the proteic and vesicular secretome of adipose tissue derived stem cells in spinal cord injury* [Master thesis]. University of Minho.

Pinho, A. G., Cibrão, J. R., Silva, N. A., Monteiro, S., & Salgado, A. J. (2020). Cell Secretome: Basic Insights and Therapeutic Opportunities for CNS Disorders. *Pharmaceuticals*, *13*(2), 31.

Pires, A. O., Mendes-Pinheiro, B., Teixeira, F. G., Anjo, S. I., Ribeiro-Samy, S., & Gomes, E. D. et al. (2016). Unveiling the Differences of Secretome of Human Bone Marrow Mesenchymal Stem Cells, Adipose Tissue-Derived Stem Cells, and Human Umbilical Cord Perivascular Cells: A Proteomic Analysis. *Stem Cells and Development*, *25*(14), 1073–1083.

Pointillart, V., Petitjean, M. E., Wiart, L., Vital, J. M., Lassié, P., Thicoipé, M., & Dabadie, P. (2000). Pharmacological therapy of spinal cord injury during the acute phase. *Spinal Cord*, *38*(2), 71–76.

Post, M. W. M., & van Leeuwen, C. M. C. (2012). Psychosocial issues in spinal cord injury: A review. *Spinal Cord*, *50*(5), 382–389.

Ra, J. C., Shin, I. S., Kim, S. H., Kang, S. K., Kang, B. C., & Lee, H. Y. et al. (2011). Safety of Intravenous Infusion of Human Adipose Tissue-Derived Mesenchymal Stem Cells in Animals and Humans. *Stem Cells and Development*, *20*(8), 1297–1308.

Rahimi-Movaghar, V., Rasouli, M. R., Smith, H., & Vaccaro, A. R. (2009). An evidence-based review of spinal cord injury decompression in experimental animals and human studies. *Handbook of Spinal Cord Injuries: Types, Treatments and Prognosis*, 635–664.

Ramón-Cueto, A., Cordero, M. I., Santos-Benito, F. F., & Avila, J. (2000). Functional Recovery of Paraplegic Rats and Motor Axon Regeneration in Their Spinal Cords by Olfactory Ensheathing Glia. *Neuron*, *25*(2), 425–435.

Raposo, G., & Stoorvogel, W. (2013). Extracellular vesicles: Exosomes, microvesicles, and friends. *Journal of Cell Biology*, *200*(4), 373–383.

Rath, N., & Balain, B. (2017). Spinal cord injury—The role of surgical treatment for neurological improvement. *Journal of Clinical Orthopaedics and Trauma*, *8*(2), 99–102.

Rehman, J., Traktuev, D., Li, J., Merfeld-Clauss, S., Temm-Grove, C. J., & Bovenkerk, J. E. et al. (2004). Secretion of angiogenic and antiapoptotic factors by human adipose stromal cells. *Circulation*, *109*(10), 1292–1298.

Risau, W. (1997). Mechanisms of angiogenesis. *Nature*, *386*(6626), 671–674.

Rupp, R. (2020). Chapter 6—Spinal cord lesions. In N. F. Ramsey & J. del R. Millán (Eds.), *Handbook of Clinical Neurology* (Vol. 168, pp. 51–65). Elsevier.

Russo, G. S., Mangan, J. J., Galetta, M. S., Boody, B., Bronson, W., & Segar, A. et al. (2020). Update on Spinal Cord Injury Management. *Clinical Spine Surgery*, *33*(7), 258–264.

Ryu, H. H., Lim, J. H., Byeon, Y. E., Park, J. R., Seo, M. S., & Lee, Y. W. et al. (2009). Functional recovery and neural differentiation after transplantation of allogenic adipose-derived stem cells in a canine model of acute spinal cord injury. *Journal of Veterinary Science*, *10*(4), 273–284.

Salgado, A. J. B. O. G., Reis, R. L. G., Sousa, N. J. C., & Gimble, J. M. (2010). Adipose tissue derived stem cells secretome: Soluble factors and their roles in regenerative medicine. *Current Stem Cell Research & Therapy*, *5*(2), 103–110.

Sandhu, J. K., Gardaneh, M., Iwasiow, R., Lanthier, P., Gangaraju, S., & Ribecco-Lutkiewicz, M. et al. (2009). Astrocyte-secreted GDNF and glutathione antioxidant system protect neurons against 6OHDA cytotoxicity. *Neurobiology of Disease*, *33*(3), 405–414.

Sanes, J. R., & Yamagata, M. (1999). Formation of lamina-specific synaptic connections. *Current Opinion in Neurobiology*, *9*(1), 79–87.

Sasaki, Y., Ohsawa, K., Kanazawa, H., Kohsaka, S., & Imai, Y. (2001). Iba1 Is an Actin-Cross-Linking Protein in Macrophages/Microglia. *Biochemical and Biophysical Research Communications*, *286*(2), 292–297.

Savill, J., Dransfield, I., Gregory, C., & Haslett, C. (2002). A blast from the past: Clearance of apoptotic cells regulates immune responses. *Nature Reviews. Immunology*, *2*(12), 965–975.

Schrepfer, S., Deuse, T., Reichenspurner, H., Fischbein, M. P., Robbins, R. C., & Pelletier, M. P. (2007). Stem cell transplantation: The lung barrier. *Transplantation Proceedings*, *39*(2), 573–576.

Sekiya, I., Larson, B. L., Smith, J. R., Pochampally, R., Cui, J.-G., & Prockop, D. J. (2002). Expansion of human adult stem cells from bone marrow stroma: Conditions that maximize the yields of early progenitors and evaluate their quality. *Stem Cells*, *20*(6), 530–541.

Shao, A., Tu, S., Lu, J., & Zhang, J. (2019). Crosstalk between stem cell and spinal cord injury: Pathophysiology and treatment strategies. *Stem Cell Research & Therapy*, *10*(1), 238.

Sharif-Alhoseini, M., Khormali, M., Rezaei, M., Safdarian, M., Hajighadery, A., & Khalatbari, M. M. et al. (2017). Animal models of spinal cord injury: A systematic review. *Spinal Cord*, *55*(8), 714–721.

Sharp, J., Frame, J., Siegenthaler, M., Nistor, G., & Keirstead, H. S. (2010). Human Embryonic Stem Cell-Derived Oligodendrocyte Progenitor Cell Transplants Improve Recovery after Cervical Spinal Cord Injury. *Stem Cells*, *28*(1), 152–163.

Shroff, G., Titus, J. D., & Shroff, R. (2017). A review of the emerging potential therapy for neurological disorders: Human embryonic stem cell therapy. *American Journal of Stem Cells*, *6*(1), 1.

Silva, N. A., Sousa, N., Reis, R. L., & Salgado, A. J. (2014). From basics to clinical: A comprehensive review on spinal cord injury. *Progress in Neurobiology*, *114*, 25–57.

Silva, R. (2020). *The secretome of Mesenchymal Stem Cells as a cell-free based therapy for Spinal Cord Injury* [Doctoral Thesis]. University of Minho.

Silvestro, S., Bramanti, P., Trubiani, O., & Mazzon, E. (2020). Stem Cells Therapy for Spinal Cord Injury: An Overview of Clinical Trials. *International Journal of Molecular Sciences*, *21*(2).

Smith, A. G. (2001). Embryo-Derived Stem Cells: Of Mice and Men. *Annual Review of Cell and Developmental Biology*, *17*(1), 435–462.

Song, C.-G., Zhang, Y.-Z., Wu, H.-N., Cao, X.-L., Guo, C.-J., & Li, Y.-Q. et al. (2018). Stem cells: A promising candidate to treat neurological disorders. *Neural Regeneration Research*, *13*(7), 1294–1304.

Song, Y. S., Lee, H. J., Doo, S. H., Lee, S. J., Lim, I., Chang, K.-T., & Kim, S. U. (2012). Mesenchymal Stem Cells Overexpressing Hepatocyte Growth Factor (HGF) Inhibit Collagen Deposit and Improve Bladder Function in Rat Model of Bladder Outlet Obstruction. *Cell Transplantation*, *21*(8), 1641–1650.

Sun, G., Chen, Y., Zhou, Z., Yang, S., Zhong, C., & Li, Z. (2017). A progressive compression model of thoracic spinal cord injury in mice: Function assessment and pathological changes in spinal cord. *Neural Regeneration Research*, *12*(8), 1365–1374.

Takahashi, K., & Yamanaka, S. (2006). Induction of Pluripotent Stem Cells from Mouse Embryonic and Adult Fibroblast Cultures by Defined Factors. *Cell*, *126*(4), 663–676.

Takami, T., Oudega, M., Bates, M. L., Wood, P. M., Kleitman, N., & Bunge, M. B. (2002). Schwann cell but not olfactory ensheathing glia transplants improve hindlimb locomotor performance in the moderately contused adult rat thoracic spinal cord. *The Journal of Neuroscience: The Official Journal of the Society for Neuroscience*, *22*(15), 6670–6681.

Talac, R., Friedman, J. A., Moore, M. J., Lu, L., Jabbari, E., & Windebank, A. J. et al. (2004). Animal models of spinal cord injury for evaluation of tissue engineering treatment strategies. *Biomaterials*, *25*(9), 1505–1510.

Tator, C. H. (1998). Biology of Neurological Recovery and Functional Restoration after Spinal Cord Injury. *Neurosurgery*, *42*(4), 696–706.

Tavares, G., Martins, M., Correia, J. S., Sardinha, V. M., Guerra-Gomes, S., & das Neves, S. P. et al. (2017). Employing an open-source tool to assess astrocyte tridimensional structure. *Brain Structure & Function*, *222*(4), 1989–1999.

Teixeira, F. G., Panchalingam, K. M., Assunção-Silva, R., Serra, S. C., Mendes-Pinheiro, B., & Patrício, P. et al. (2016). Modulation of the Mesenchymal Stem Cell Secretome Using Computer-Controlled Bioreactors: Impact on Neuronal Cell Proliferation, Survival and Differentiation. *Scientific Reports*, *6*.

Tjalsma, H., Bolhuis, A., Jongbloed, J. D. H., Bron, S., & Dijl, J. M. van. (2000). Signal Peptide-Dependent Protein Transport in Bacillus subtilis: A Genome-Based Survey of the Secretome. *Microbiology and Molecular Biology Reviews*, *64*(3), 515–547.

Toma, C., Wagner, W. R., Bowry, S., Schwartz, A., & Villanueva, F. (2009). Fate Of Culture-Expanded Mesenchymal Stem Cells in The Microvasculature. *Circulation Research*, *104*(3), 398–402.

Totoiu, M. O., & Keirstead, H. S. (2005). Spinal cord injury is accompanied by chronic progressive demyelination. *The Journal of Comparative Neurology*, *486*(4), 373–383.

Trotter, J. (1993). The development of myelin-forming glia: Studies with primary cell cultures and immortalized cell lines. *Perspectives on Developmental Neurobiology*, *1*(3), 149–154.

Tsai, M.-J., Liou, D.-Y., Lin, Y.-R., Weng, C.-F., Huang, M.-C., & Huang, W.-C. et al. (2018). Attenuating Spinal Cord Injury by Conditioned Medium from Bone Marrow Mesenchymal Stem Cells. *Journal of Clinical Medicine*, *8*(1), 23.

Vawda, R., Badner, A., Hong, J., Mikhail, M., Dragas, R., & Xhima, K. et al. (2020). Harnessing the Secretome of Mesenchymal Stromal Cells for Traumatic Spinal Cord Injury: Multi-cell Comparison and Assessment of In Vivo Efficacy. *Stem Cells and Development*.

Vizoso, F., Eiro, N., Cid, S., Schneider, J., & Perez-Fernandez, R. (2017). Mesenchymal Stem Cell Secretome: Toward Cell-Free Therapeutic Strategies in Regenerative Medicine. *International Journal of Molecular Sciences*, *18*(9), 1852.

Wang, H.-S., Hung, S.-C., Peng, S.-T., Huang, C.-C., Wei, H.-M., & Guo, Y.-J. et al. (2004). Mesenchymal Stem Cells in the Wharton's Jelly of the Human Umbilical Cord. *STEM CELLS*, *22*(7), 1330–1337.

Wang, Y., Zhao, Z., Ren, Z., Zhao, B., Zhang, L., Chen, J., & Xu, W. et al. (2012). Recellularized nerve allografts with differentiated mesenchymal stem cells promote peripheral nerve regeneration. *Neuroscience Letters*, *514*(1), 96–101.

Watt, F. M., & Hogan, B. L. (2000). Out of Eden: Stem Cells and Their Niches. *Science*, *287*(5457), 1427–1430.

Wei, X., Du, Z., Zhao, L., Feng, D., Wei, G., & He, Y. et al. (2009). IFATS Collection: The Conditioned Media of Adipose Stromal Cells Protect Against Hypoxia-Ischemia-Induced Brain Damage in Neonatal Rats. *Stem Cells*, *27*(2), 478–488.

White, D. M., & Mansfield, K. (1996). Vasoactive intestinal polypeptide and neuropeptide Y act indirectly to increase neurite outgrowth of dissociated dorsal root ganglion cells. *Neuroscience*, *73*(3), 881–887.

Willerth, S. M., & Sakiyama-Elbert, S. E. (2008). Cell Therapy for Spinal Cord Regeneration. *Advanced Drug Delivery Reviews*, *60*(2), 263–276.

Wilson, J. R., Forgione, N., & Fehlings, M. G. (2013). Emerging therapies for acute traumatic spinal cord injury. *CMAJ : Canadian Medical Association Journal*, *185*(6), 485–492.

Wurmser, A. E., & Gage, F. H. (2002). Cell fusion causes confusion. *Nature*, *416*(6880), 485–487.

Xin, H., Li, Y., Buller, B., Katakowski, M., Zhang, Y., & Wang, X. et al. (2012). Exosome-mediated transfer of miR-133b from multipotent mesenchymal stromal cells to neural cells contributes to neurite outgrowth. *Stem Cells*, *30*(7), 1556–1564.

Xu, C., Diao, Y.-F., Wang, J., Liang, J., Xu, H.-H., Zhao, M.-L., & Zheng, B. et al. (2020). Intravenously Infusing the Secretome of Adipose-Derived Mesenchymal Stem Cells Ameliorates Neuroinflammation and Neurological Functioning After Traumatic Brain Injury. *Stem Cells and Development*, *29*(4), 222–234.

Xu, H., Barnes, G. T., Yang, Q., Tan, G., Yang, D., & Chou, C. J. et al. (2003). Chronic inflammation in fat plays a crucial role in the development of obesity-related insulin resistance. *The Journal of Clinical Investigation*, *112*(12), 1821–1830.

Yamazaki, H., Jin, Y., Tsuchiya, A., Kanno, T., & Nishizaki, T. (2015). Adipose-derived stem cell-conditioned medium ameliorates antidepression-related behaviors in the mouse model of Alzheimer's disease. *Neuroscience Letters*, *609*, 53–57.

Yang, B., Zhang, F., Cheng, F., Ying, L., Wang, C., & Shi, K. et al. (2020). Strategies and prospects of effective neural circuits reconstruction after spinal cord injury. *Cell Death & Disease*, *11*(6), 1–14.

Yang, T., Dai, Y., Chen, G., & Cui, S. (2020). Dissecting the Dual Role of the Glial Scar and Scar-Forming Astrocytes in Spinal Cord Injury. *Frontiers in Cellular Neuroscience*, *14*.

Yu, B., Zhang, X., & Li, X. (2014). Exosomes Derived from Mesenchymal Stem Cells. *International Journal of Molecular Sciences*, *15*(3), 4142–4157.

Zarei-Kheirabadi, M., Sadrosadat, H., Mohammadshirazi, A., Jaberi, R., Sorouri, F., Khayyatan, F., & Kiani, S. (2020). Human embryonic stem cell-derived neural stem cells encapsulated in hyaluronic acid promotes regeneration in a contusion spinal cord injured rat. *International Journal of Biological Macromolecules*, *148*, 1118–1129.

Zhang, H., Cheng, H., Cai, Y., Ma, X., Liu, W., & Yan, Z. et al. (2009). Comparison of adult neurospheres derived from different origins for treatment of rat spinal cord injury. *Neuroscience Letters*, *458*(3), 116–121.

Zhou, Z., Chen, Y., Zhang, H., Min, S., Yu, B., He, B., & Jin, A. (2013). Comparison of mesenchymal stromal cells from human bone marrow and adipose tissue for the treatment of spinal cord injury. *Cytotherapy*, *15*(4), 434–448.

Zhou, Z., Tian, X., Mo, B., Xu, H., Zhang, L., & Huang, L. et al. (2020). Adipose mesenchymal stem cell transplantation alleviates spinal cord injury-induced neuroinflammation partly by suppressing the Jagged1/Notch pathway. *Stem Cell Research & Therapy*, *11*(1), 212.

Zhu, S., Chen, M., Deng, L., Zhang, J., Ni, W., & Wang, X. et al. (2020). The repair and autophagy mechanisms of hypoxia-regulated bFGF-modified primary embryonic neural stem cells in spinal cord injury. *STEM CELLS Translational Medicine*, *9*(5), 603–619.

Zuk, P. A., Zhu, M., Ashjian, P., De Ugarte, D. A., Huang, J. I., & Mizuno, H. et al. (2002). Human Adipose Tissue Is a Source of Multipotent Stem Cells. *Molecular Biology of the Cell*, *13*(12), 4279–4295.

ANNEXES

Annex 1. Scoring system for the BMS (Basso et al., 2006).

Score	
0	No ankle movement
1	Slight ankle movement
2	Extensive ankle movement
3	Plantar placing of the paw with or without weight support -OR- Occasional, frequent or consistent dorsal stepping but no plantar stepping
4	Occasional plantar stepping
5	Frequent or consistent plantar stepping, no coordination -OR- Frequent or consistent plantar stepping, *some* coordination, paws *rotated* at initial contact and lift off (R/R)
6	Frequent or consistent plantar stepping, *some* coordination, paws *parallel* at initial contact (P/R, P/P) -OR- Frequent or consistent plantar stepping, *mostly* coordinated, paws *rotated* at initial contact and lift off (R/R)
7	Frequent or consistent plantar stepping, *mostly* coordinated, paws *parallel* at initial contact and *rotated* at lift off (P/R) -OR- Frequent or consistent plantar stepping, *mostly* coordinated, paws *parallel* at initial contact and lift off (P/P), and *severe* trunk instability
8	Frequent or consistent plantar stepping, *mostly* coordinated, paws *parallel* at initial contact and lift off (P/P), and *mild* trunk instability -OR- Frequent or consistent plantar stepping, *mostly* coordinated, paws *parallel* at initial contact and lift off (P/P), and *normal* trunk stability and tail *down or up & down*
9	Frequent or consistent plantar stepping, *mostly* coordinated, paws *parallel* at initial contact and lift off (P/P), and *normal* trunk stability and tail *always* up.

Slight: Moves less than half of the ankle joint excursion.
Extensive: Moves more than half of the ankle joint excursion.
Plantar placing: Paw is actively placed with both the thumb and the last toe of the paw touching the ground.
Weight support: (dorsal or plantar): The hindquarters must be elevated enough that the hind end near the base of the tail is raised off of the surface and the knees do not touch the ground during the step cycle.
Stepping: (dorsal or plantar): Weight support at lift off, forward limb advancement and re-establishment of weight support at initial contact.
Occasional: Stepping less than or equal to half of the time moving forward.
Frequent: Stepping more than half the time moving forward.
Consistent: Plantar stepping all of the time moving forward with less than 5 missed steps (due to medial placement at initial contact, butt down, knee down, skiing, scoliosis, spasms or dragging) or dorsal steps.
Coordination: For every forelimb step a hindlimb step is taken and the hindlimbs alternate during an assessable pass. For a pass to be assessable, a mouse must move at a consistent speed and a distance of at least 3 body lengths. Short or halting bouts are not assessable for coordination. At least 3 assessable passes must occur in order to evaluate coordination. If less than 3 passes occur then the mouse is scored as having no coordination.
Some coordination: Of all assessable passes (a minimum of 3), most of them are *not* coordinated.
Most coordination: Of all assessable passes (a minimum of 3), most of them *are* coordinated.
Paw position: *Digits* of the paw are parallel to the body (P), turned out away from the body (external rotation: E) or turned inward toward midline (internal rotation; I).
Severe trunk instability: Severe trunk instability occurs in two ways.

(1) The hindquarters show severe postural deficits such as extreme lean, pronounced waddle and/or near collapse of the hindquarters predominantly during the test.

or

(2) Five or more of any of the following *events* stop stepping of one or both hindlimbs
- Haunch hit: the side of hindquarters rapidly contacts the ground
- Spasms: sustained muscle contraction of the hindlimb which appears to immobilize the limb in a flexed or extended position
- Scoliosis: lateral deviation of the spinal column to appear "C" shaped instead of straight

Mild trunk instability: Less than 5 events listed above and some sway in the hindquarters. Mild trunk instability is scored when the pelvis and haunches predominantly dip, rock, or tilt from side-to-side (tilt). If the tail is up, the swaying of the pelvis and/or haunches produces side-to-side movements of the distal third of the tail which also indicates mild trunk instability (side tail).
Normal trunk stability: No lean or sway of the trunk, and the distal third of the tail is steady and unwavering during locomotion. No severe postural deficits or events and less than 5 instances of mild instability.

Annex 2. Scoring table for the BB (Carter et al., 2001).

Score	Performance on the beam
7	Traverses beam normally with both affected paws on horizontal beam surface, neither paw ever grasps the side surface, and there are no more than two footslips; toe placement style is the same as preinjury.
6	Traverses beam successfully and uses affected limbs to aid >50% of steps along beam.
5	Traverses beam successfully but uses affected limbs in <50% of steps along beam.
4	Traverses beam and, at least once, places affected limbs on horizontal beam surface.
3	Traverses beam by dragging affected hindlimbs.
2	Unable to traverse beam but places affected limbs on horizontal beam surface and maintains balance for ≥5 sec.
1	Unable to traverse beam; cannot place affected limbs on horizontal beam surface.

[a]Adapted from the method of Feeney et al. (1982) used to evaluate unilateral lesions of sensory cortex in rats.

Annex 3. Gait analysis of left and right sides of SCI animals treated with Neurobasal A and different concentrations of secretome. Data are represented as mean ± SD.

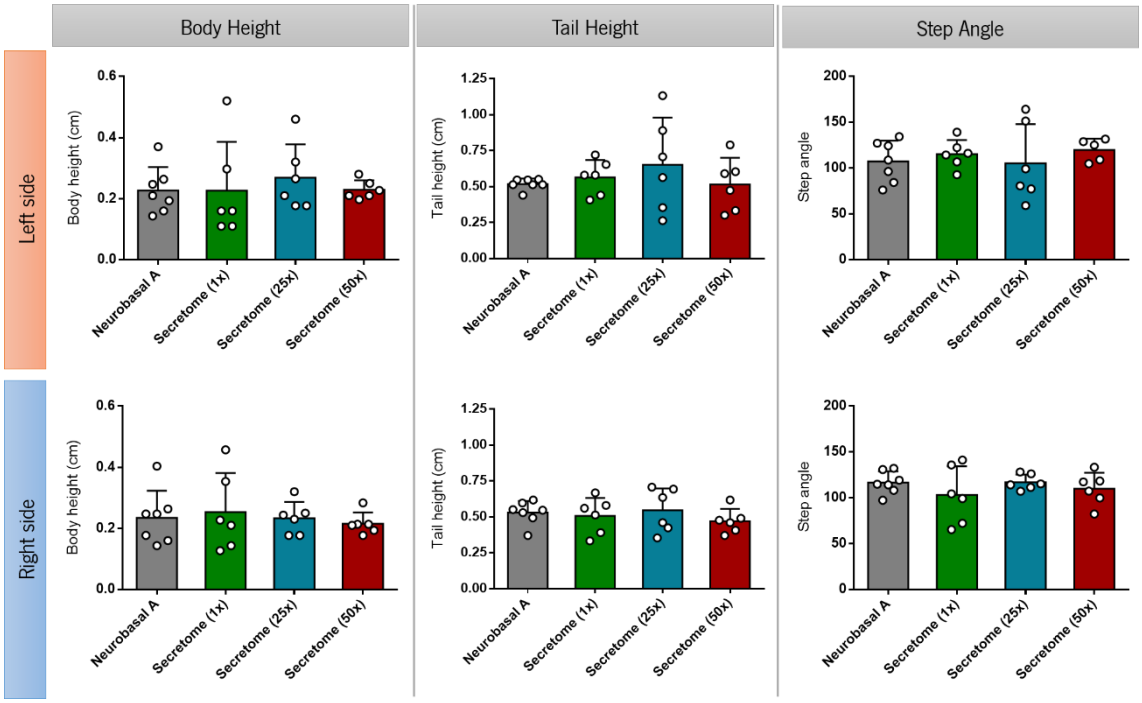

Annex 4. Confocal Z-stack images of GFAP staining area, in the rostral (A) and epicenter regions of the lesion (B). Nuclei are stained with DAPI (in blue) and the astrocytic processes (GFAP) are stained in green. Magnification: 400x. Scale bar: 120 μm.

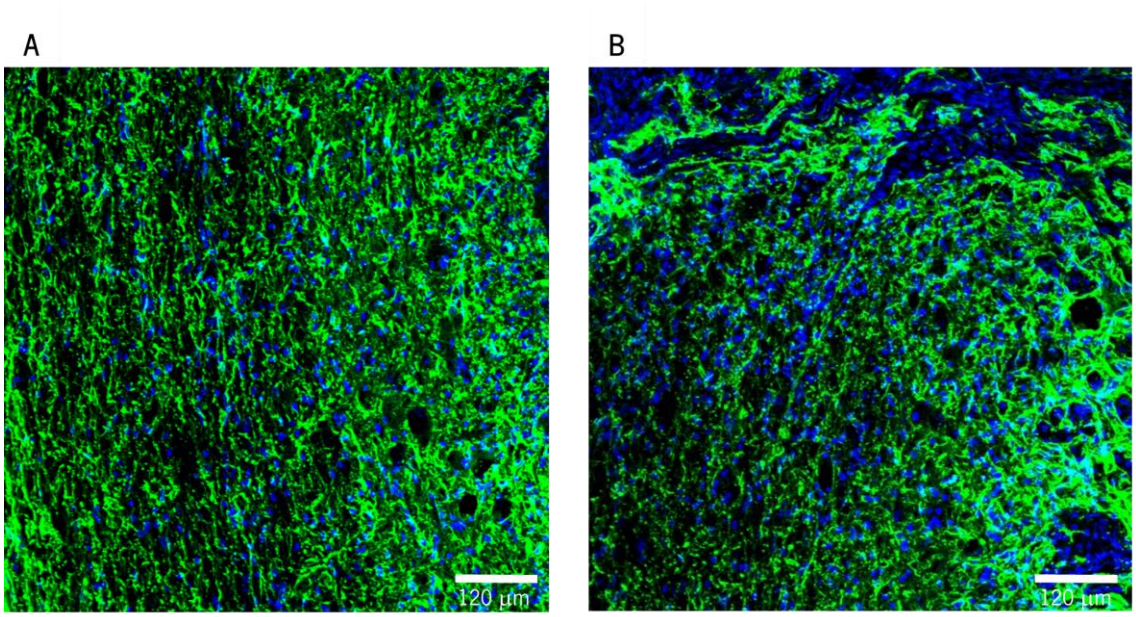

Annex 5. Quantification of GFAP staining area of SCI animals treated with Neurobasal A and different concentrations of secretome. Data are represented as mean ± SD.

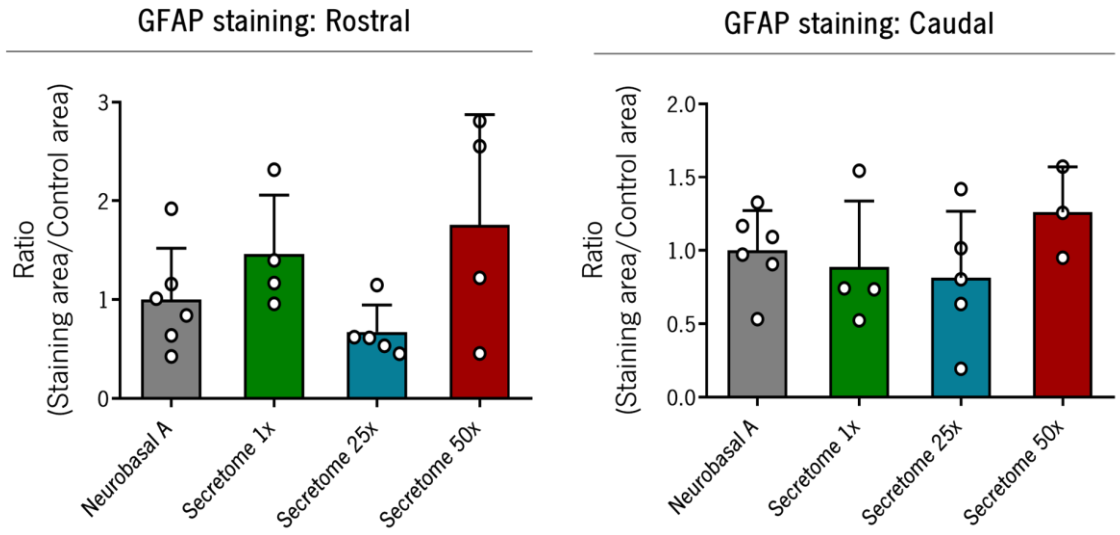

Annex 6. Quantification of β-tubulin III staining area of SCI animals treated with Neurobasal A and different concentrations of secretome. Data are represented as mean ± SD.

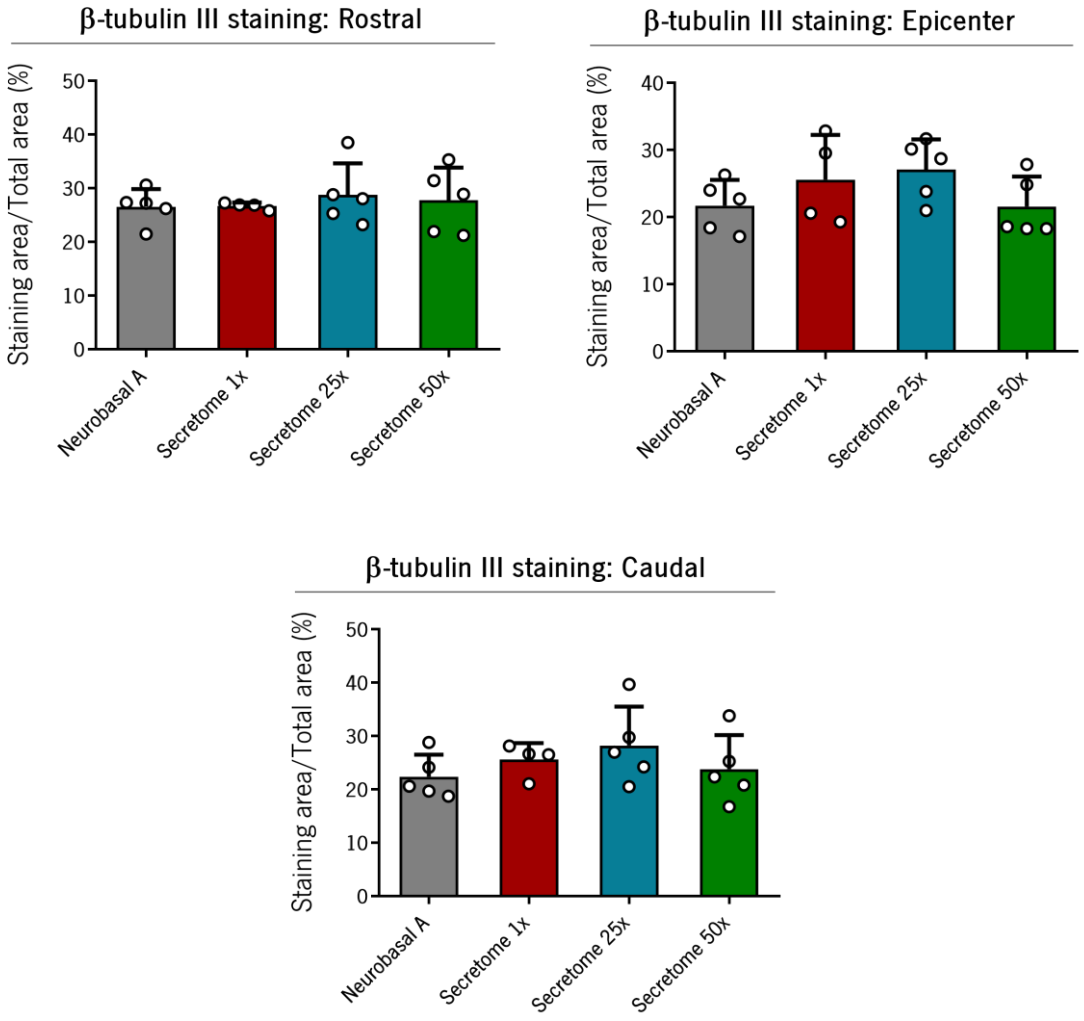

Annex 7. Expression analysis of *IL-6* and *IL-4* genes from human microglia in response to LPS and IFN-γ stimulation, at different times (6h, 12h and 24h). The genetic expression of both genes was normalized to the housekeeping gene *GAPDH* and represented as fold expression in comparison to the respective non-stimulated group. Results are derived from one independent experiment (n=3 biological samples/group). Data are represented as mean ± SD.